STEADY-STATE VISUAL EVOKED POTENTIALS AND THEIR APPLICATION TO BRAIN-COMPUTER INTERFACES

BY

JAMES J.S. NORTON

DISSERTATION

Submitted in partial fulfillment of the requirements
for the degree of Doctor of Philosophy in Neuroscience
in the Graduate College of the
University of Illinois at Urbana-Champaign, 2017

Urbana, Illinois

Doctoral Committee:

Associate Professor Timothy Bretl, Chair
Professor Kara Federmeier
Associate Professor Diane Beck
Professor Minh Doh

ABSTRACT

This dissertation presents five contributions to the design of steady-state visual evoked potential (SSVEP)-based brain-computer interfaces (BCIs). First, a new method—based on visual stimulation during sleep—for investigating the neural mechanisms of SSVEPs. Second, a comparison of performance—in terms of accuracy, latency, bitrate, and engagement—between children and adults when using an SSVEP-based BCI. Third, a gel-less epidermal electronic system electrode for use in SSVEP-based BCIs that adheres to the skin through van der Waals forces. Fourth, a potential application for SSVEP-based BCIs in individuals without disabilities. Fifth, an adaptive user interface for SSVEP-based BCI text-entry that nearly doubles the performance of existing systems. Following the description of these contributions, potential directions for future research are also discussed. These contributions each move a step towards the long-term goal of developing SSVEP-based BCIs that are useful outside of the research laboratory for either those with or without disabilities.

To my wife, Stephanie Dockins, for coming back to Illinois in order to move forward with life. To my parents, John and Penelope Norton, for giving me everything I have ever needed to succeed.

ACKNOWLEDGMENTS

It takes a village. It is not a small village either. For the past seven years, I have received love and support from my family, friends, and colleagues. Support that has made the difference between giving up and pushing through.

Stephanie, a short written thank you feels rather insufficient after everything you have done. Whether it has been work weekends, or nights in the Beckman, or a last minute review of a paper you have provided me with the endless support that I have needed. I am forever grateful. Thank you and I love you.

Mom and Dad, thank you for giving me the tools that I needed to succeed. Thank you for providing me with a loving place to grow up, an environment in which exploration was celebrated, and the encouragement to "follow my bliss". Mom, thank you for collaborating on ideas, reading my papers, and most of all for listening. Dad, thank you for encouraging me to finish, believing in me, and helping me with whatever random problem I had for you.

To the rest of my family, especially Matt, Amanda, Claire, Pat, Trish, Deb, Jan, Steve, Tom, Cassandra, and the family that has passed on and is dearly missed, thank you for supporting my dreams.

Professor Bretl, thank you for teaching me how to be a scientist. Considering how we started, I look at the work we are generating now and the ideas we exchange and marvel at how far I (and we) have come. Thank you for teaching me how to be critical of my own work, to write, and to not be satisfied with an incomplete paper.

Carney, thanks for showing me how to live between fields. Thank you for giving me a home with the senior design team, for demonstrating the power of endless positivity, and for teaching me how to connect great minds from every possible field.

Sam Beshers, I am not the only NSP student to say this...I wouldn't have

made it without you. Thank you for being my advocate, professional mentor, friend, and (R2R) teammate.

To my committee with special thanks to Professor Federmeier, thank you for your support of my research, critical feedback on my direction, and advice for how to be a better scientist. Professor Makela, thank you for leading by example and for giving me sage advice whenever asked. Professor Jones, thank you for helping me believe I could live between fields.

To Stephen Umunna, to quote Drake, "we started from the bottom now we here". For the past seven years, we have grown together. From those early days where we had no idea what we were doing, to ideas about sleeping in the laboratory that led to a whole new research direction, to our current morning discussions as colleagues and friends, thank you for being my mentee, friend, and colleague.

Jessica, thank you for being my closest collaborator in the lab. You brought a new perspective to coding, mentoring, organizing, that made me a better scientist. Thank for continuing to support me and be my colleague in your free time.

To the BCI lab, thanks for getting my Ph.D. moving. Thank you Stephen, Kevin, and Majewski for being the test subjects as I learned how to be a mentor. To the inseparable Nisha and Sasi, thank you for adding a bit of organization to our chaos. Finally, to the last cohort including Mythri thanks for helping me across the finish line.

To my fellow graduate students Aadeel and Trucci, thank you for doing this with me. They say not all who wander are lost...I'm not sure that saying always applied to us. Now, however, as the last of us to find his way across the finish line, I can say that we aren't lost anymore.

To Erik, Dave, and Sarah thank you for being my colleagues and friends. Thank you for being the kind and supportive engineers who introduced me to a whole new world of signals and analyses. To Danielle, for being in a whole new world with me and trying to enjoy the experience.

To "The Cliff", thank you for taking your time to collaborate with three random graduate students on a wrist band. I can honestly say that our IDEAS was one of my favorite parts of graduate school.

Hong, thank you for taking a chance with me. Thank you for supporting those overnight experiments in the lab, for building new devices after we broke them, and for reminding me to laugh after a long day in the lab.

To Abdullah and Dennis, thank you for being my mentors in the Bretl Lab. For supporting my research whether it was showing me how to write a research paper or teaching me about simple circuits, I was always grateful for your expertise.

To the Wolfe Pack, thanks for listening to me refine my talks semester after semester. Thanks for answering random questions, for empathizing with me, and for generally being a wonderful collection of scientists and engineers. Thanks especially to Andy for your wisdom, kindness, and friendship. To our honorary group member Katy, thanks for reminding me to eat well, laugh, and not be too serious.

To Claudia Lutz, thanks for being my running buddy, co-editor of Neuronews with me, and for being willing to apply those crazy science writer skills to my occasional manuscript.

Special thanks to the senior design team, Jacob, Jackson, Katherine, Luke, Cara, Gary, and everyone else for taking a neuroscientist into your midst for four semesters and for making me feel like a part of the team.

Thank you to the Graduate College, NSF, and NIH for the funding that made my graduate work possible and to all of the administrative staff, especially Linda Meccoli, Stephanie Pregent, and Jana Lenz, who put up with my late paperwork.

Finally, a special note to my Nana, I know you would be proud.

TABLE OF CONTENTS

CHAPTER 1 INTRODUCTION 1
1.1 A Bit of History 2
1.2 SSVEP-based BCIs 4
1.3 Design of SSVEP-based BCIs 5
1.4 Organization of Dissertation 9

CHAPTER 2 THE ELICITATION OF STEADY-STATE VISUAL EVOKED POTENTIALS DURING SLEEP 11
2.1 Abstract 11
2.2 Introduction 11
2.3 Method 16
2.4 Results 20
2.5 Discussion 26
2.6 Conclusion 35
2.7 Acknowledgement 35
2.8 Supplemental Information 36

CHAPTER 3 THE PERFORMANCE OF 9-11 YEAR OLD CHILDREN USING AN SSVEP-BASED BCI FOR TARGET SELECTION 49
3.1 Abstract 49
3.2 Introduction 50
3.3 Method 54
3.4 Results 57
3.5 Discussion 64
3.6 Classification of the Predicted Target 67
3.7 Supplemental Information 69

CHAPTER 4 SOFT, CURVED ELECTRODE SYSTEMS CAPABLE OF INTEGRATION ON THE AURICLE AS A PERSISTENT BRAIN-COMPUTER INTERFACE 71
4.1 Abstract 71
4.2 Introduction 72
4.3 Materials and Method 74
4.4 Results and Discussion 76

CHAPTER 5 "OK BRAIN": A COMPARISON OF SPEECH, TOUCH, AND SSVEP-BASED BCI INPUTS FOR HEAD-MOUNTED DISPLAYS 86
5.1 Abstract 86
5.2 Introduction 87
5.3 Method 89
5.4 Results 95
5.5 Discussion 99
5.6 Acknowledgments 102

CHAPTER 6 AN SSVEP-BASED BRAIN-COMPUTER INTERFACE FOR TEXT SPELLING WITH ADAPTIVE QUERIES THAT MAXIMIZE INFORMATION GAIN RATES 103
6.1 Abstract 103
6.2 Introduction 104
6.3 Design of Our Speller 107
6.4 Method 113
6.5 Results 118
6.6 Discussion 123
6.7 Conclusion 125
6.8 Derivation of Language Model Update Rule 126
6.9 Derivation of Information Gain Rate 127

CHAPTER 7 CONCLUSION 128
7.1 Future Work 129

REFERENCES 132

CHAPTER 1

INTRODUCTION

In 1973, Jacques J. Vidal [195] noted that the long-term potential of BCIs is to, "elevate the computer to a genuine prosthetic of the brain." Yet, some 40 years after this first BCI publication:

- There is, arguably, not a single proven application for electroencephalography (EEG)-based BCIs for people without disabilities outside of the laboratory.
- The only application of EEG-based BCIs for those with disabilities is to enable communication between those with locked-in syndrome (LIS) and the outside world [174, 96, 175].

Given—Vidal's original sentiments, the more than 1000 publications related to their development as of 2010 [74], and the limited number of applications—clearly the potential for BCIs is high, but the actual design and implementation of these systems is a challenge.

One explanation for the lack of successful BCIs is that researchers are too narrowly focused on improving only one component (see Section 1.3.1) of a BCI system [209]. Wolpaw and Wolpaw [209] suggest that the long-term success of BCI development, and ultimately the field of brain-computer interfacing, depend on designing systems that are useful. Even though Wolpaw and Wolpaw [209] argue that the field should be focusing on useful BCIs for those with disabilities, this too could be viewed as being too narrowly focused. By focusing solely on those with physical disabilities, we overlook the considerable opportunities to design BCIs for those without disabilities [4].

In order to design a useful BCI for those with or without disabilities, it is important to consider what brain signal will be used to control the BCI (*paradigm*), the design of the individual parts of the BCI (*components*), and the planned BCI use (*application*). We have chosen to design BCIs that use

SSVEPs, the brain's response to flashing lights. Instead of focusing on the design of a single BCI component, we address challenges in the design of multiple components. The long-term goal is to develop a BCI that is useful outside of the research laboratory for either those with or without disabilities.

The remainder of the introduction is organized into four sections. In Section 1.1, we provide a brief history of electroencephalography (EEG), SSVEPs, and BCIs. In Section 1.2, we introduce SSVEP-based BCIs. In Section 1.3, we describe the design of SSVEP-based BCI and the challenges associated with the design of each of the components of an SSVEP-based BCI. Finally, in Section 1.4, we describe the organization of this dissertation.

1.1 A Bit of History

The history of BCIs begins with one man's 40 year search for "psychic energy." In 1892, a young German named Hans Berger was thrown from his horse during a German military exercise. He narrowly escaped death. On the exact same day, Berger received a telegraph from his family, the first one they ever sent. His sister had an "ominous feeling" [133] about the day and insisted her father contact Hans. Reflecting on what had happened (described in more detail by Millet [133, 15]), Berger concluded that he and his sister had communicated telepathically. The incident, combined with an education in medicine, led Berger to spend his career searching for measurable signs of psychic energy. In a way, he succeeded. In 1924, working with a young patient undergoing brain surgery [44], Berger successfully recorded the electrical signals generated in the brain. While searching for proof of telepathy, Berger proved that the human brain generates measurable electrical activity, extending earlier work in animals by Caton [34]. After spending five years confirming his results, Berger reported his findings and techniques in a 1929 article "*Über das elektrenkephalogramm des menschen*" or "On the electroencephalogram of man" [16]. Not only had Hans Berger [16] discovered the electrical signals generated by the brain, he also published the first use of EEG in human beings.

Many scientists were skeptical of Berger's findings and methods. Five

years later Edgar Adrian[1] and Brian Matthews[2] replicated Berger's findings, bringing them wide-spread acceptance. Using the moving-iron oscillograph of Matthew's own design (a recent photo can be seen in Figure 1.1; [127]) and electrodes made of "copper gauze wrapped in lint and soaked in warm saline" [44], Adrian and Matthews recorded EEG from their own scalps[3] [1, 47, 44].

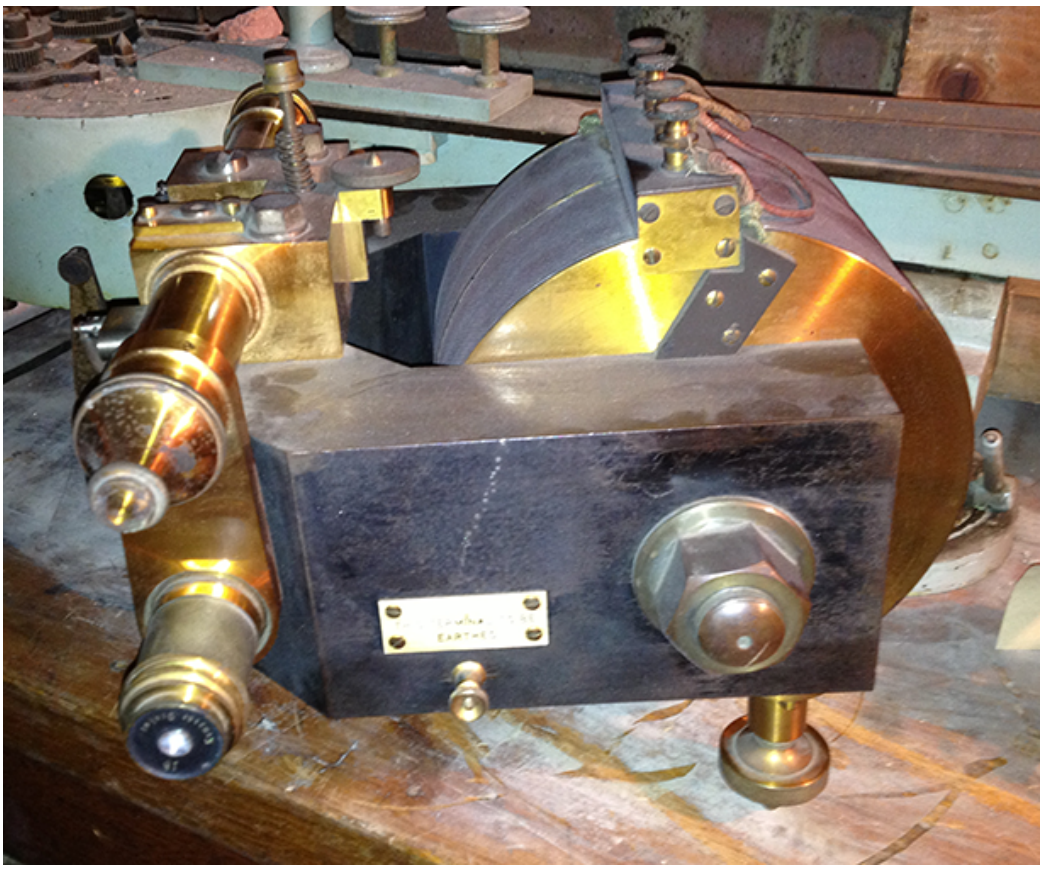

Figure 1.1: Matthews' moving-iron oscillograph. Photo courtesy of Alan Cattell, University of Cambridge. Special thanks to Roberto Inchingolo, University of Cambridge.

Adrian and Matthews [1] did more than just replicate Berger's [16] results. In the course of their experiments, they also discovered that a flashing stimulus (created by attaching a light to a gramophone motor) elicited an EEG response at the same frequency as the flashing stimulus [47]. This response is now known as the SSVEP.

[1] 1932 winner of the Nobel prize for his work on the function of neurons.

[2] The electrical engineer who first developed a differential amplifier for electrophysiological recordings [44, 127].

[3] It was much easier to record alpha activity from Adrian than to record it from Matthews, a very early example of inter-subject variability in EEG recordings [47].

Even in these early days of EEG recordings, the scientists exploring the use of this new tool recognized its potential. In their book on BCI, Wolpaw and Wolpaw [209] present one example in the form of a holiday card. On the card, Hans Jasper depicts his well wishes to Hans Berger as waves passing from his mind in the form of EEG signals and then transforming into words. It was already clear to Jasper that the ability to measure neural activity could be used for communication (see Wolpaw and Wolpaw [209] for image).

Jasper's vision of an EEG-based communication system has since been realized. In 1973, Jacques J. Vidal came up with the phrase "Brain-Computer Interface" and demonstrated the first BCI [195]. In 1988, the first BCI text-entry system (based on the P300) was developed by Farwell and Donchin [60] at the University of Illinois. More recently, Calhoun and McMillan [31] developed one of the the first SSVEP-based BCIs to facillitate hands-free control of computer systems at the Air Force's Armstrong Research Laboratory. Since then, research into the design of BCIs has intensified [74]. There are currently three main paradigms used to actuate a BCI: P300 [60], motor imagery [128], and SSVEP [31]. Over time, the performance of BCIs has steadily improved. A recent BCI interface by Chen [38] achieved a text-entry rate of 60 characters per minute, compared with the two characters per minute in the original paper of Farwell and Donchin [60].

1.2 SSVEP-based BCIs

As an introduction, SSVEP-based BCIs function in the following way. When a visual stimulus is flashed in the user's visual field, it causes an increase in EEG activity at harmonic frequencies of the stimulus [140]. These changes in activity are dependent on the user's spatial attention [135]. When a user attends to a flashing stimulus, the size of the SSVEPs elicited increase. If multiple stimuli are presented (each flashing at a unique frequency) then the user can make selections by focusing their attention on a specific flashing stimulus. This modulation of EEG activity based on spatial attention serves as the basis for most SSVEP-based BCIs [31, 36, 198, 2, 3, 146].

We have chosen to investigate SSVEP-based BCIs, because they can be used by a higher proportion of the population, have a higher information

transfer rate, and require less participant training than other (e.g., P300 or motor-imagery) BCIs. In a 2012 paper, Guger et al. investigated the proportion of the population who can use an SSVEP-based BCI [69]. They compared the results with two previous data sets for motor imagery-based BCIs [71] and P300-based BCIs [70]. The paper showed that 86.7% of participants could operate an SSVEP-based BCI with 90 to 100% accuracy, compared with only 6% of participants using a motor imagery-based BCI and 72.8% of participants using a P300-based BCI [69]. In addition, researchers have recently demonstrated several SSVEP-based BCIs for text-entry that outperform existing systems using P300 or motor-imagery. These papers showed that the rate of text-entry for SSVEP-based BCIs can exceed 20 characters per minute [3, 38], compared with 7-9 characters per minute with a P300 system [188], and 2-7 characters per minute with motor-imagery [23]. With regard to participant training, SSVEP-based BCIs do not require any participant training at all [36] as opposed to motor imagery and P300 systems, both of which require, at minimum, a few minutes of participant training.

1.3 Design of SSVEP-based BCIs

When designing SSVEP-based BCIs, one has to consider both the components and the application.

1.3.1 Components

All SSVEP-based BCIs consist of the same set of components: a stimulus, a user, EEG recording hardware, a classifier, and a user interface. The overall performance and user experience associated with any SSVEP-based BCI is dependent on each of these components and the interplay between them. For each component, let us consider their purpose, parameters that impact their behavior, and the existing challenges in their design.

Stimulus

The purpose of the stimulus is to evoke measurable changes in the neural activities of the user.

The physical properties of the stimulus have an effect on the amplitude and distribution of the SSVEP elicited from the user. For example, the frequency of the flash is know to affect the amplitude of the SSVEP. SSVEPs can be elicited and measured at the scalp for any frequency between 1 to 100Hz [77]. Lower frequency stimuli, however, tend to elicit larger amplitude SSVEPs than higher frequency stimuli [77]. In addition to frequency, contrast [32], color [163], intensity [163], and duty cycle [212] are known to influence the morphology of the SSVEP elicited from the user.

Current challenges in the design of an SSVEP stimulus include eliciting a large amplitude response from the user, safety [64], and comfort [111].

User

The user's role is to respond to changes in the user interface causing their own brain to generate a response to the desired stimulus. It is important to understand how SSVEPs are generated in the brain, differences in SSVEPs measured from different individuals, and how to improve the responses of the user.

Despite years of study it remains unclear how SSVEPs are generated in the brain. It is not known, for example, whether SSVEPs are generated through phase changes of ongoing oscillations in the brain [134] or through evoked amplitude changes in the brain [33]. Nor is it clear how the second harmonic component of the SSVEP is generated [156]. Understanding these (and similar) questions would enable improved stimulus design and perhaps help to explain performance differences observed between individuals.

Different populations may vary in their ability to use an SSVEP-based BCI. The majority of SSVEP-based BCIs are tested on young (predominantly college-aged) adults. There are relatively few studies of SSVEP-based BCIs involving older adults [5, 201, 199] and only a single study involving children [57]. These limited studies suggest that both older adults and children achieve lower performance than young adults when using SSVEP-based BCIs. Understanding these demographic differences would make it clear what populations of people could use an SSVEP-based BCI.

Motivation may play a significant role in the performance measured during laboratory studies. Experiments testing BCIs can be tedious and boring. Some research has shown that when participants are motivated, their perfor-

mance improves [103, 93], but there are relatively few systematic studies on this topic.

EEG Recording Hardware

The hardware used to record EEG from a user's scalp includes electrodes, an amplifier, and a digitization system.

EEG electrodes are the sensors used to measure the electrical activity generated by the brain from the scalp. Electrodes often vary in terms of size, materials [189], if they are either "wet" or "dry" [173], and how they interface with the amplifier and digitization system [131]. Traditional electrodes are metal disks (most commonly silver or tin), are "wet", and are attached to the scalp using mechanical force. These electrodes are called "wet" electrodes, because they also rely on electrolyte gel to improve electrical contact. These electrodes are slow to put on, can be uncomfortable or irritating to the user, and are difficult to wear for extended periods of time. Newer "dry" electrodes eliminate the need for electrolyte gel by using capacitive sensing [41], but still require mechanical force to be attached to the scalp, and are very sensitive to noise. One way to reduce the noise of electrodes is by including a preamplification and filtering stage very close to the electrode, however, this requires more complicated circuitry and can be expensive. The design of high performance, comfortable, and long-term wear electrodes remains a major challenge in the field.

The roles of the amplifier and digitization systems are to rescale the raw EEG signals measured from the scalp and convert these signals from an analog voltage to a digital signal for analysis by a digital computer. Raw EEG signals are measured in terms of a voltage and on the scale of microvolts. Most analog to digital converters (the digitization system) require signals between zero and five volts. Therefore, an amplifier must be used to increase the size of the EEG signal before it can be digitized. Modern digitization systems require less amplification, but reducing noise induced by the amplifier and digitization systems remains a challenge.

Classifier

A classifier is used to map changes in EEG activity into selections. The challenge in designing the classifier is to accurately predict the user's intent using as little data as possible.

A great deal of research goes into the design of classifiers for SSVEP-based BCIs. The traditional method for classifying SSVEPs involves the use of power spectral density analysis (PSDA). Since SSVEPs are generated in a very narrow frequency range, frequency based analysis allows isolation of the SSVEP from noise at other frequencies. The drawback of PSDA is that it generally involves analysis of a single EEG electrode; there is no built-in mechanism for combining EEG data from multiple channels. One solution to this problem was proposed by Friman [65] using a minimum energy combination (MEC) of channels. MEC improved performance over PSDA, but has since been supplanted by algorithms based on canonical correlation analysis (CCA) [112]. Since CCA has been used for nearly 10 years, a number of variants have been proposed, including multiway CCA [219], phase-constrained CCA [154], and multiset CCA [218]. Our laboratory has also worked on an updated CCA classifier that uses sequential classification to improve overall performance [87]. While each of these algorithms (including ours) provides a small increase in performance the original CCA algorithm presented by Lin [112] remains the gold standard.

User interface

The user interface (UI) defines how the user interacts with the BCI and its design depends on the application (see Section 1.3.2).

The physical design of the user interface has an impact on the performance of the BCI. Considering SSVEP-based BCIs for text-entry, there are very often more characters than stimuli, requiring the user to make multiple selections to input a single character. For example, the system of Cecotti [36] used a decision tree to make text selections. This meant that to type a letter (of 27 possible), three selections were required. The Bremen BCI [198] reduced the number of selections required to type a character by arranging letters in a grid format. The grid was organized so that letters that were more likely to be selected were closer to the center (such as the letters 'e' and 's')

reducing the average number of selection per character. Further reducing the number of selections per character is one way in which the performance of SSVEP-based BCIs could be improved.

Some applications may require special considerations in the design of the UI. Many people with LIS lose their ability to move their eyes left or right, while vertical gaze is often preserved [119]. Thus, a vertically oriented BCI may work better for these individuals, but most SSVEP-based BCIs for text-entry require both vertical and horizontal eye movement [36, 198, 3, 38]. There is a need within the field to think very carefully about the appropriate tasks for SSVEP-based BCIs [4] and in the case of individuals with disabilities to consider the limitations of those populations before designing the BCI.

1.3.2 Applications

The application of the SSVEP-based BCI has an effect on the design of SSVEP-based BCIs. The appropriate applications for SSVEP-based BCIs outside of the laboratory remains an open question within the field.

Currently there is not a single application for SSVEP-based BCIs outside of the research laboratory. P300 and motor imagery-based BCIs have been used to enable communication between those with LIS and the outside world [174, 176]. The only previous report of an SSVEP-based BCI to enable communication in those with LIS, however, reported limited success. In online tests of the system's performance, only one of the four individuals with LIS managed to communicate using the SSVEP-based BCI [106]). Other researchers have described potential applications for SSVEP-based BCIs in those without disabilities [4], but these systems are still constrained to research laboratories. In the laboratory, SSVEP-based BCIs are investigated for text-entry [198, 36], robotic navigation [2], gaming [98], and cursor control [39].

1.4 Organization of Dissertation

The contributions to the design of SSVEP-based BCIs in this dissertation are described in the following order: In Chapter 2, we describe a new method for investigating how SSVEPs are generated in the brain; In Chapter 3,

we describe experiments on the performance—in terms of accuracy, latency, bitrate, and engagement—of children using an SSVEP-based BCI. Control data, collected from adults, is also reported for the purpose of comparing performance between children and adults; In Chapter 4, a gel-less epidermal electronic system electrode is described. This electrode enables EEG activity to be recored from the non-hair bearing scalp. Compared with traditional "wet" electrodes, it does not require an electrolyte gel or mechanical force to hold it on the scalp. In Chapter 5, a potential application—user input for augmented and virtual reality systems—for SSVEP-based BCIs in those without disabilities is considered. Experiments comparing the accuracy and latency of inputs obtained from two SSVEP-based BCIs are compared with two traditional input mechanisms. In Chapter 6, an adaptive user interface for SSVEP-based BCI text-entry is described. This interface nearly doubles the performance of two existing SSVEP-based BCI text-entry systems implemented for the purpose of comparison. Finally, in Chapter 7, we summarize these contributions and considers potential directions for future work.

The dissertation includes material that has already been published (Chapter 6, [3]; Chapter 4, [146]; Chapter 2, [147]) or has been reviewed (Chapter 5) and requires revision.

CHAPTER 2

THE ELICITATION OF STEADY-STATE VISUAL EVOKED POTENTIALS DURING SLEEP[1]

2.1 Abstract

This chapter describes a new method—based on visual stimulation during sleep—for investigating how SSVEPs are generated in the brain. Specifically, we tested the hypothesis that it is possible to elicit SSVEPs through closed eyelids during NREM sleep. To test this hypothesis, SSVEP amplitudes were measured in eight subjects across two conditions of stimulation (stimulation on and stimulation off) and three brain states (waking, light sleep, and deep sleep). Results showed a significant interaction between stimulation and brain state. In particular, EEG activity at the frequency of stimulation was higher during both light sleep and deep sleep in the stimulation on condition than in the stimulation off condition. The fact that it is possible to elicit SSVEPs during sleep may provide a new way to study how SSVEPs are generated in the brain, one that might help resolve open questions such as identifying the SSVEP activation sequence or deciding if SSVEPs derive from evoked or oscillatory neural processes.

2.2 Introduction

For more than 50 years, steady-state visual evoked potentials (SSVEPs) have provided a tool for the study of visual information processing, the clinical as-

[1]This work has been previously published as [147] and is co-authored by S. Umunna and T. Bretl; Copyright ©2017, Psychophysiology, Wiley Periodicals, Inc. This is the peer reviewed version of the following article: [147], which has been published in final form at https://doi.org/10.1111%2Fpsyp.12807. This article may be used for non-commercial purposes in accordance with Wiley Terms and Conditions for Self-Archiving.

sessment of visual function, and the development of brain-computer interfaces (BCIs) [145, 194]. Typically measured using electroencephalography (EEG), SSVEPs were discovered by Adrian and Matthews (1934), just five years after Hans Berger's [16] initial description of the alpha rhythm. In the course of confirming Bergers discovery, Adrian and Matthews demonstrated that a repetitively flickering visual stimulus elicits EEG activity at the same frequency as the stimulus [1], a phenomenon now known as the SSVEP. Thirty years later David Regan studied SSVEPs more extensively, introduced them as a method for studying visual information processing [164], and clearly described several advantages of SSVEPs over transient visual evoked potentials (VEPs) [165]. Compared with VEPs, SSVEPs are: (1) easier to quantify [118, 165], (2) provide high signal-to-noise ratio (SNR) signals in less time [165], and (3) less prone to several common sources of noise [165] and artifacts [68, 158].

Despite the widespread use of SSVEPs, it is still not completely understood how they are generated in the brain. For example, consider that neither the activation sequence nor the neural processes that lead to the generation of SSVEPs is known. SSVEPs reflect the combined electrical activity from multiple neural sources within the brain [53, 61, 156]. It is believed that these individual sources are activated sequentially. The order in which these neural sources are activated, or the SSVEP activation sequence, remains an open question in the literature [53, 165]. To try to determine this activation sequence, Di Russo and colleagues [53] used a combination of source localization and phase analysis techniques. Based on these methods, they proposed that the activation sequence from earliest to latest was: V1, V5/MT, V3A, and then V4/V8. Di Russo et al., [53] specifically caution, however, that the overlapping nature of the SSVEP response precludes the exact determination of the neural activation sequence using phase analysis, beyond the usual problems associated with source localization [118].

Another open question, which Norcia et al. [145] labels the "nature of the underlying neural mechanism," is whether SSVEPs are generated through evoked [179] or oscillatory [123] neural processes. Some researchers hypothesize that SSVEPs are the result of time-locked activity in the cortex that is evoked by the stimulus [179] while others hypothesize that they are the result of a "phase-resetting" of an ongoing neural oscillation [134, 148]. Some evidence for the oscillatory hypothesis comes from the existence of resonance

frequencies, frequencies at which the response amplitude of SSVEPs is naturally larger [77]. However, these resonance frequencies can also be explained by the temporal superposition of waves as predicted by the evoked activity hypothesis [33]. Capilla et al. [33] provide evidence for the evoked hypothesis by showing that SSVEPs are well modeled by the superposition of time jittered VEPs presented at the same average frequency as SSVEPs. However, the rapid presentation of these VEPs may engage fundamentally different neural processes than those presented at much lower rates [145]. It is also possible that SSVEPs arise as the result of a combination of these two types of activity [45].

The motivation for this chapter is to provide a new method for investigating how SSVEPs are generated in the brain, one that might help resolve open questions such as the two we just described. If these questions could be resolved, researchers may be able to improve the interpretation of visual information processing experiments using SSVEPs [53], more precisely define their utility in the clinical assessment of visual function [53], and increase the performance of SSVEP-based BCIs [194]. The new method we propose is based on the elicitation of SSVEPs during sleep. We believe that eliciting SSVEPs during sleep would provide new insight into how these signals are generated in the brain, because: First, research over the course of 60 yearsoften using EEGhas established that information processing still occurs in the brain during sleep [79], despite a reduction in overt responsiveness to external stimuli. For instance, the auditory N1 and P2 event-related potentials (ERPs) can be elicited during both waking and sleep. These ERPs, however, are altered as a function of the participants brain state [46]. For example, the amplitude of the auditory N1 is reduced to baseline levels during NREM sleep but is apparent during REM sleep. The amplitude of the P2 on the other hand increases during NREM sleep and is visible during REM sleep [46].

Second, altered information processing during sleep offers the possibility of comparative studies to dissect SSVEP activity in new ways. Recent evidence suggests that the differences between ERPs elicited during waking and ERPs elicited during sleep are due to a reduction in cortical connectivity. Using a combination of transcranial magnetic stimulation (TMS) and EEG Massimini et al., [126] demonstrated that TMS stimulation during sleep caused a reduction in the response of areas that were cortically connected to the stim-

ulation site. Furthermore, the amplitude of this reduction was correlated with the depth of sleep.

Given that information processing still occurs during sleep, but cortical connectivity is reduced, it may be possible to infer the SSVEP activation sequence without resorting to the phase analysis techniques of Di Russo et al. [53]. As sleep deepens, neural sources that occur later in the activation sequence become cortically disconnected from earlier sources. This reduction in cortical connectivity may lead to a decrease in response amplitude from these later sources as compared to earlier sources. One would then predict that the SSVEP activation sequence could be determined by comparing the response amplitudes of different individual sources measured during sleep with the response amplitudes from those same sources measured during waking. With respect to the neural processes that lead to the generation of SSVEPs, it is reasonable to assume that the reduction in cortical connectivity will have an effect on the oscillatory activity occurring in the brain. If so, one would predict that the existence of SSVEP resonance frequencies would dissipate, or, at least, be attenuated, during sleep. Even though the mechanisms underlying visual steady-state responses and other sensory modalities may be fundamentally different, some evidence for this can be found in the auditory modality. In a study comparing steady-state auditory potentials elicited by modulated tones during waking and sleep, Cohen, Rickards, and Clark [43] found that the response at resonance frequencies was more attenuated during sleep than at other stimulation frequencies.

The question then, which is the one we answer in this chapter, is can SSVEPs be elicited during sleep? Effectively, this requires that it be possible to elicit an SSVEP through a participants closed eyelids, elicit and record an SSVEP during sleep without waking the participant, and measure the response using time-frequency analysis of the data.

It has been previously established that SSVEPs can be elicited through closed eyelids during waking. While the eyelids completely cover the eyes, they do not perfectly filter all light. In fact, along the visual spectrum, the eyelid acts as a red-pass filter. Up to 10% of red light (above 600nm) passes through the eyelid as well as 1-2% of light in the remaining visual spectrum (430nm - 600nm) [136, 167]. This property is what allows visual stimuli to be perceived through closed eyelids, a fact that is well demonstrated by Lim et al. [108] in their paper on the 'eyes closed' SSVEP-based BCI.

It is already known that VEPs can be elicited during sleep without waking the participant. For instance, a magnetoencephalography (MEG) study of visual evoked fields (VEFs)—VEFs are the MEG analog of the VEP—during sleep by Kakigi et al., [89] found that VEFs elicited during sleep are simpler than those elicited during waking. Their data, in support of Massimini et als. [126] hypothesis that sleep reduces cortical connectivity, showed that VEFs elicited during sleep exhibit a reduction in later stage components as compared with VEFs elicited during waking. Other studies have reported that it is possible to elicit VEPs in sleeping infants [10, 182]. The results from these studies suggest that, similarly to adults, brain state has an effect on the VEPs elicited from infants.

It remains unclear whether SSVEPs can be elicited during sleep—indeed, only a few studies have investigated repetitive visual stimulation during sleep. A study by Born et al. in [25] found that repetitive visual stimulations (which generate SSVEPs in EEG) cause cortical deactivation as measured using fMRI and PET, but did not report the presence of SSVEPs in the EEG. The only other previous reports of the elicitation of SSVEPs during sleep were conducted in the context of epilepsy research. Rodin, Daly, and Bickford [168] reported that repetitive stimulation during sleep elicited entrained EEG responses in the time domain [168], the experimenters did not specifically analyze the frequencies of the elicited responses, nor did they analyze SSVEPs across the sleep stages. In addition, they used a stimulation intensity of 250,000 foot-candles (2,500,000 lux), roughly 20 times brighter than the brightest sunlight [13]. A few studies have since followed up on the work of Rodin [105, 130, 170, 214], but they all investigated clinical populations with the goal of determining whether seizures can be induced during sleep. These researchers also continued to use very bright strobes as stimuli and analyzed the results in the time domain.

In this chapter, we examined whether SSVEPs could be elicited during sleep by investigating the EEG activity resulting from the presentation of a repetitively flickering stimulus (with a brightness of less than 1.5 lux) during waking and sleep. We hypothesized that the presentation of a visual stimulus would elicit an increase in EEG activity at the same frequency as the stimulus during both waking and NREM sleep. To test this hypothesis, we invited participants to sleep in our laboratory while we recorded their EEG. A head-mounted stimulator was then used to elicit SSVEPs during waking

and sleep. Results from eight participants confirmed the hypothesis that visual stimulation during sleep significantly increases EEG activity at the frequency of stimulation.

2.3 Method

2.3.1 Participants

Eight volunteers (five males, three females, 20-32 years old) participated in the study. All participants self-reported having no history of seizures, frequent or severe migraines, motor impairments, or sleep disorders. The experiments were approved by the University of Illinois Institutional Review Board. Each participant was informed about the procedure and signed an informed consent before the experiment.

2.3.2 Recording Parameters

Twenty-one channels of physiological data were recorded from each participant using solid tin electrodes at impedances of less than 10 kΩ. Sixteen channels of EEG data (Supplemental Figure 2.9) were recorded from the following 10-10 international sites [180]: right mastoid, FPz, F3, F4, FCz, C3, C4, CPz, PO7, PO3, POz, PO4, PO8, O1, Oz, and O2. Two channels of electrooculogram (EOG) were recorded to monitor for eye movements; one EOG electrode was placed approximately one centimeter lateral to and one centimeter below the outer canthus of the left eye the other EOG electrode was placed approximately one centimeter lateral to and one centimeter above the right eye [162]. All EEG and EOG electrodes were referenced to the left mastoid. Two channels of electromyogram (EMG) were recorded to monitor for muscle activity. These channels were placed equidistant from the midline of the chin approximately three centimeters apart and were bipolar referenced with one electrode placed on the mentalis muscle and the other electrode placed on the submentalis muscle. One bipolar channel of electrocardiogram (ECG) was recorded to measure heart rate and placed on the chest. A single ground electrode was situated on the dorsum of the nose. A James Long EEG amplifier (model TCP-128BA) was used to amplify the

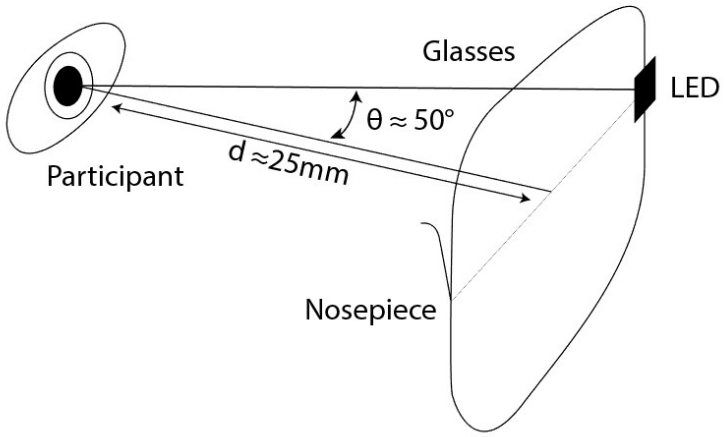

Figure 2.1: Diagram showing the setup of the visual stimulation system.

EEG and EOG signals (10,000x). All EEG and EOG data were analog filtered from 0.3 Hz to 30 Hz. The EMG and ECG channels were recorded using the same amplifier, but at a lower gain (2,000x) using different analog filter settings (1-300 Hz). The data was then digitized at 1000Hz using a National Instruments data acquisition unit (Model: NI PCI-6225).

2.3.3 Stimulation Hardware

The visual stimulation system (Figure 2.1) was created using a pair of glasses, two green light-emitting diodes (LEDs), and an Arduino Uno microcontroller (Arduino LLC, Somerville, MA). Each LED was placed at the lateral angle 50 to the center of the participants left and right eyes near the lateral canthus. A flicker frequency of approximately 7 Hz was chosen, because the fundamental frequency was less than the alpha range (8 Hz to 12 Hz). The method used to program the Arduino resulted in an exact frequency of 7.03 Hz. The duty cycle of the LEDs was 50%. The intensity of the LEDs was

measured using a photometer, emitting 1.5 lux at a distance of approximately 25 mm. The onset and offset of stimulation from the LED glasses were captured using a photodiode wired directly in the DAQ and sampled at 1000 Hz.

2.3.4 Experimental Procedure

On the evening of the experiment, the participant arrived at the laboratory one hour before his or her habitual bedtime (between 2300 and 0300 hours). All experiments were conducted in a sound-attenuated, light-controlled, and air-conditioned room. Following informed consent, the participant performed his or her nightly routine. When each participant was ready for sleep, they positioned themselves in a comfortable reclining chair for the duration of the study. The recording electrodes and LED stimulator glasses were then placed on the participant. Following setup, all experiments were monitored from an adjacent room. A baseline, consisting of two one-minute periods of SSVEP stimulation, was then recorded from each participant. During this baseline recording, the participants were asked to close their eyes, to relax, and to ignore the stimuli. After the baseline, participants were permitted to fall asleep. Participants were given between 20-40 minutes to fall asleep before SSVEP stimulation was started. The exact amount of time was different for each participant and determined by the experimenters. During each sleep stimulation period, the SSVEP stimuli flickered for five minutes. Each stimulation period was followed by an interstimulus interval of ten minutes. The length of this interstimulus interval was chosen ad-hoc by the experimenters. Each sleep recording consisted of two to eight stimulation periods. The number of stimulation periods was determined by allowing the participant to sleep for up to two hours or until he or she woke up, whichever came first. If a participant was awakened before the stimulation periods, or by the stimulation itself, they were given the option to try again or to end the experiment.

2.3.5 Data Analysis

All data were analyzed using MATLAB (The Mathworks Inc. Natick, MA).

Preprocessing

For each subject, two digital filters were first applied to each channel of the raw EEG data. (1) A 60 Hz notch filter with a 1 Hz bandwidth (-3db) was applied to the data for the purpose of removing power line noise and implemented using the iirnotch function in MATLAB. (2) A second-order infinite impulse response bandpass filter with a passband of 0.5-30 Hz was applied to reduce noise and implemented using the butter function in MATLAB. Both filters were applied both forward and backward to prevent any phase shifts in the data. After filtering, each channel of the EEG data was re-referenced to the average of the left and right mastoid. The preprocessed data for subject s04 averaged across channels O1, Oz, and O2 have been visualized in Figure 2.2 using the short-time Fourier transform (STFT).

Sleep Scoring

The sleep stage of each subject was scored using the sleepSMG toolbox (Stephanie Greer and Jared M. Saletin, Walker Laboratory UC Berkeley; http://sleepsmg.sourceforge.net/), a visualization tool for MATLAB. Nine channels of data were used for sleep scoring, two chin EMG channels, two EOG channels, and five EEG channels (C3, C4, O1, Oz, and O2). The continuous EEG data for each participant were first divided into 30-second epochs. Two raters then scored [17, 162] each EEG epoch independently as showing waking, light sleep (which we define as stage N1 or N2; [66, 132, 157]) or deep sleep (which we defined as stage N3). The two raters had an inter-rater reliability of 65%. Rater #2 agreed with Rater #1 for more than 80% of epochs labeled waking and 95% of the epochs labeled deep sleep. For light sleep, however, Rater #2 only agreed with Rater #1 48% of the time. The two raters also labeled epochs with artifacts for rejection from further analysis. Disagreements between these raters were resolved through consensus, and final labels were assigned to each epoch for further analysis.

Amplitude Spectral Density

To detect SSVEPs in the EEG data, we used amplitude spectral density (ASD). Since our sleep data was scored in 30-second epochs, we used the

same 30-second epochs for calculation of the ASD. An estimate of the power spectral density was computed for each channel of EEG data within each epoch (including both the baseline and sleep data) using the pwelch function in MATLAB. The pwelch function, with a signal length equal to the window length, is equivalent to calculating the single-sided ASD using the Fourier transform. Given that the two methods are equivalent, pwelch is a single function call and was used to reduce the risk of coding errors. A Hanning window was first applied to each 30-second epoch to reduce spectral leakage. Each signal was zero-padded to four times the length of the epoch to improve visualization. Since each epoch was 30 seconds long, there was no overlap between successive windows. The square root of the data was then taken to convert the results from power spectral density to ASD. Figure 2.3 shows an overlay of the ASD values, sleep score, and stimulation periods for subject s04.

Each estimate of the ASD was then binned into one of two stimulation conditions, stimulation off or stimulation on. Within each stimulation condition, the data was further subdivided into one of three brain states based on the results of the sleep scoring: waking, light sleep, or deep sleep. Note that the stimulation off waking condition and stimulation on waking condition included data from both the baseline session and data that was scored as waking during the sleep session. All estimates of the ASD within each bin were averaged across windows and channels O1, Oz, and O2 to create final estimates of the ASD for each subject in each condition [156]. Finally, the ASD value at the frequency of stimulation was extracted from each condition for further statistical analysis. This value, which we defined as the SSVEP amplitude, is similar to that of other researchers [9, 156]. The grand average ASDs for each condition are shown in Figure 2.4.

2.4 Results

All eight subjects who participated in our study completed the experiments. Technical issues during subject s03 resulted in the loss of half of the baseline data and half of the sleep data. Participant s08 reported difficulty falling asleep and was awoken by the stimulation, but did manage to sleep through one full stimulation period and one-half of a second stimulation period.

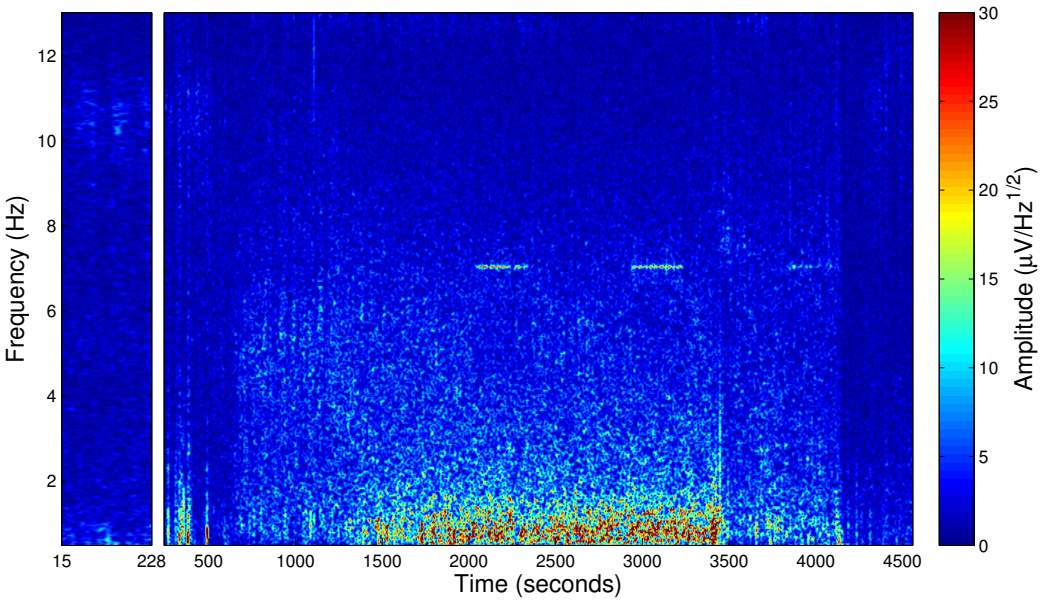

Figure 2.2: Short-time Fourier transform (STFT) showing sleep recording session for subject s04, averaged across channels O1, Oz, and O2. The image was created using the 'spectrogram' function in MATLAB with input parameters of a 30s-time window, a 29s-window overlap, and a Hanning taper to reduce spectral leakage. The three, five-minute, SSVEP stimulation periods can be seen at 7.03Hz.

Statistical analyses were conducted in SPSS Version 22 (IBM Corporation, Armonk, NY). The mean SSVEP amplitudes for each of the conditions and all eight subjects is reported in Table 2.1 and represented graphically in Figure 2.5. We performed an analysis comparing the difference in SSVEP amplitude using a two-way (brain state and stimulation) repeated measures ANOVA with three levels (waking, light sleep, and deep sleep). We first assessed that our data met the assumptions of the two-way ANOVA (no significant outliers, normally distributed data, and equal variances). Examination of the studentized residuals revealed no outliers for values less than -3 or greater than 3 standard deviations from the mean. To determine if the ASD values were normally distributed, a Shapiro-Wilk test was used. All conditions ($p > 0.05$) were normally distributed. Mauchlys test of sphericity was used to determine whether the ASD values from each of the conditions was of equal variance. The test revealed differences in variance across brain states ($\chi^2(2) = 8.01$, $p = 0.02$) and in the interaction between stimulation and brain state ($\chi^2(2) = 8.20$, $p = 0.02$). To account for these differences in variance, Greenhouse-Geisser correction was used. The corrected two-way

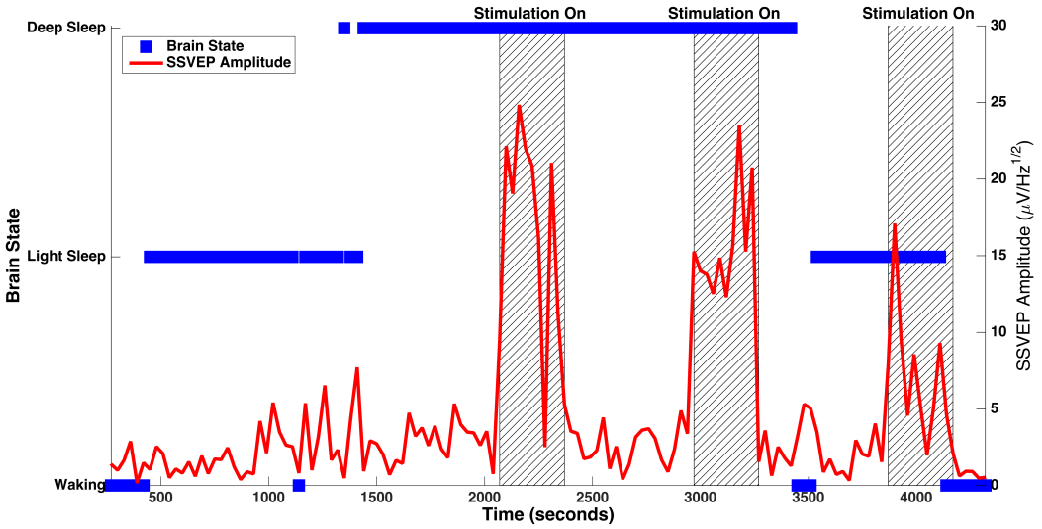

Figure 2.3: Plot that simultaneously overlays the scoring of sleep stage (floating bars), whether stimulation was on or off (shaded areas denote stimulation), and SSVEP amplitude (solid line) for subject s04 during the sleep recording session. The increase in SSVEP amplitude can be seen to correspond exactly with the onset of stimulation.

repeated measures ANOVA on SSVEP amplitude revealed an interaction between stimulation and brain state (F [1.15, 8.02] = 16.51, $p = 0.00$, $\eta_p^2 = 0.70$, uncorrected degrees of freedom were - 2,14).

Simple main effect tests with Bonferroni-Holm correction revealed additional differences within the data. Simple main effect test for brain state showed that SSVEP amplitudes were higher for stimulation on (M = 7.72, SD = 2.73) compared to stimulation off (M = 1.99, SD = 0.33) during light sleep (F [1, 7] = 30.21, $p = 0.01$, $\eta_p^2 = 0.81$) as well as stimulation on (M = 11.04, SD = 4.86) compared to stimulation off (M = 2.33, SD = 0.47) during deep sleep (F [1, 7] = 25.41, $p = 0.01$, $\eta_p^2 = 0.78$). Simple main effect tests of stimulation showed that there was a difference (F [2, 14] = 26.77, $p < 0.01$, $\eta_p^2 = 0.79$) between waking, light sleep, and deep sleep during stimulation off. Further pairwise comparisons showed that SSVEP amplitudes elicited during light sleep (mean difference = 0.64, $p = 0.01$) and deep sleep (mean difference = 0.98, $p = 0.01$) were higher than those during waking and SSVEP amplitudes elicited during deep sleep (mean difference = 0.34, $p = 0.01$) were higher than those recorded during light sleep. During stimulation on, there was also a difference (F [1.14, 7.99] = 22.55, $p = 0.01$, $\eta_p^2 = 0.76$, uncorrected degrees of freedom were - 2,14) between waking, light sleep, and

Table 2.1: Mean SSVEP amplitude ($\mu V/Hz^{1/2}$) computed for each subject binned by stimulation condition (stimulation off and stimulation on) and by brain state (waking, light sleep, deep sleep).

	Stimulation Off			Stimulation On		
Subject	Waking	Light Sleep	Deep Sleep	Waking	Light Sleep	Deep Sleep
s01	1.23	2.40	3.17	2.70	6.36	7.06
s02	1.97	2.27	2.73	2.72	6.41	14.62
s03	1.85	1.99	2.08	3.65	8.25	8.89
s04	1.56	2.26	2.56	1.57	7.65	16.80
s05	0.66	1.49	1.74	4.08	9.79	10.02
s06	1.38	1.56	1.99	6.70	12.73	17.90
s07	1.09	1.95	2.08	1.30	3.40	4.27
s08	1.01	1.96	2.25	2.01	7.15	8.74
Mean	1.34	1.99	2.33	3.09	7.72	11.04
Mdn	1.31	1.98	2.17	2.71	7.40	9.46
SD	0.44	0.33	0.46	1.74	2.73	4.87

deep sleep. Pairwise comparisons revealed that SSVEP amplitudes elicited during light sleep (mean difference = 4.63, $p < 0.01$) and deep sleep (mean difference = 7.94, p = 0.01) were higher than those during waking. There were two marginal effects that did not meet the threshold of significance when corrected for multiple comparisons. During waking, SSVEP amplitude in the stimulation on (M = 3.09, SD = 1.74) condition was marginally higher (mean difference 1.75, uncorrected $p = 0.03$, corrected $p = 0.06$, $\eta_p^2 = 0.52$) than it was during the stimulation off (M = 1.34, SD = 0.44) condition. Finally, in the stimulation on condition, SSVEP amplitude was marginally higher (mean difference = 3.32, uncorrected $p = 0.04$) during deep sleep than it was during light sleep. In accordance with the ranking procedure of Bonferroni-Holm, no correction factor was applied to this last comparison, but it does not meet the threshold of significance.

There were differences in the number of time windows averaged together to obtain measurements of SSVEP amplitude from different subjects and conditions (Table 2.2). To determine if these differences had any effect on the results, we conducted two additional analyses (1) a correlation analysis comparing the number of time windows with SSVEP amplitude and (2) an analysis of the bootstrap confidence intervals of the individual subject

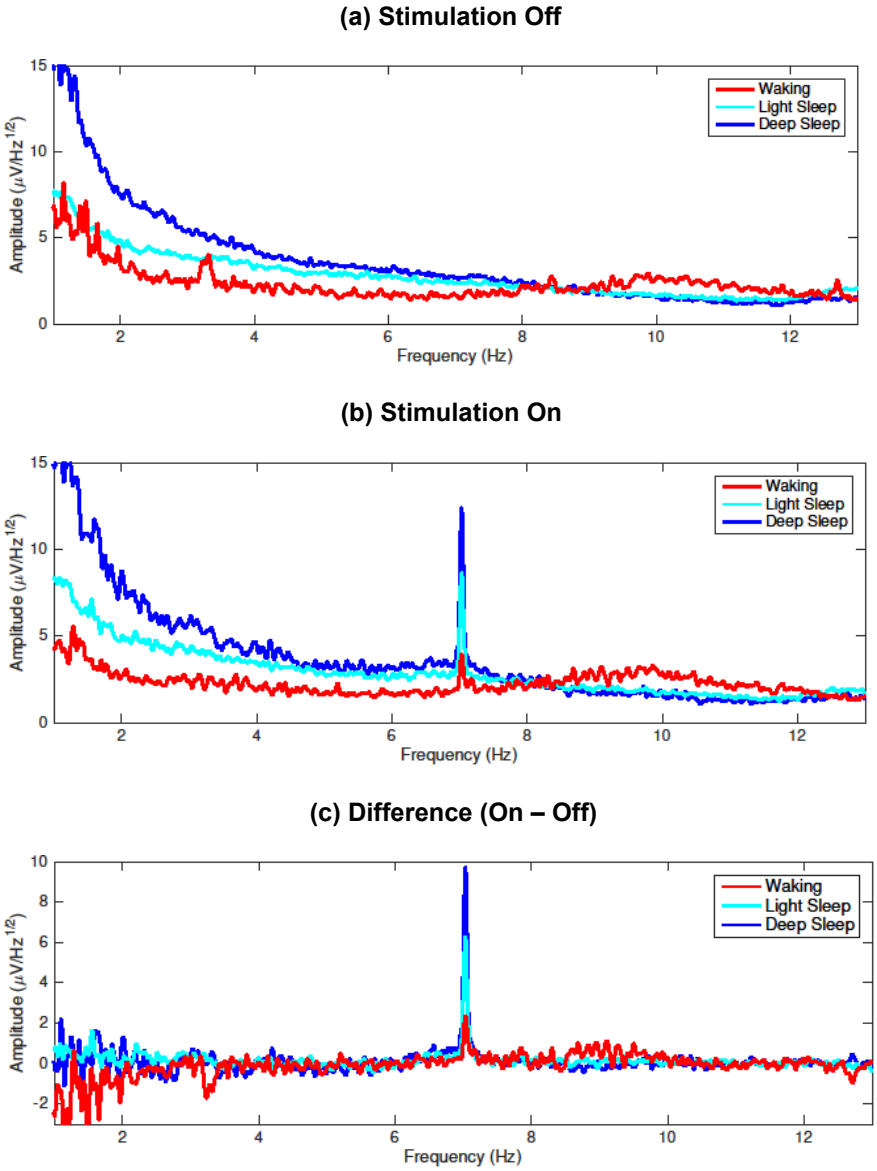

Figure 2.4: ASD values for frequencies between 1-13Hz, averaged across all subjects, for each condition. (a) Brain state (waking, light sleep, deep sleep) for the stimulation off condition. (b) Brain state (waking, light sleep, deep sleep) for the stimulation on condition. (c) Brain state (waking, light sleep, deep sleep) for the difference between the stimulation on condition and the stimulation off condition. The effect of stimulation is apparent at 7.03Hz.

Table 2.2: Number of time windows for each subject binned into each condition of stimulation (stimulation off and stimulation on) and brain state (waking, light sleep, deep sleep).

	Stimulation Off			Stimulation On		
Subject	Waking	Light Sleep	Deep Sleep	Waking	Light Sleep	Deep Sleep
s01	21	72	70	4	41	22
s02	5	86	59	5	30	11
s03	18	15	12	13	9	1
s04	6	42	46	4	8	18
s05	3	67	21	4	13	14
s06	44	97	21	33	19	7
s07	84	87	46	8	32	19
s08	238	43	4	17	10	4
Mean	52.38	63.63	34.88	11.00	20.25	12.00
Mdn	19.50	69.50	33.50	6.50	16.00	12.50
SD	79.75	28.03	23.68	10.11	12.53	7.56

data. When not corrected for multiple comparisons, there was a moderate correlation (r = -0.30, p = 0.04) between the number of time windows and the mean SSVEP amplitude (Supplemental Figures 2.10 and 2.11). If the data was analyzed by stimulation condition, however, there was no significant correlation. The results for stimulation off (r = -0.14 and p = 0.50) and stimulation on (r = -0.01 and p = 0.96) are shown in Figure 2.6. Bootstrap confidence intervals were used to test simple main effects within each subject following the procedures of Oru et al. [152]. For each subject and comparison, the individual trials of the two conditions of interest were resampled with replacement. These two sets of resampled data were then averaged and subtracted from one another to create a new estimate of SSVEP amplitude. As an example, consider subject s01 and a comparison of the light sleep stimulation off condition with the light sleep stimulation on condition. We first resampled the 72 light sleep stimulation off data trials (Table 2.2) and the 41 light sleep stimulation on data trials (Table 2.2) with replacement. Each of these resampled datasets was averaged, and the two resampled averages were subtracted from one another. This resulted in a measurement of the difference in SSVEP amplitude between the two conditions. This process was then repeated 1000 times. After 1000 iterations, the lowest 2.5% of values and the

highest 2.5% of values were trimmed to create a 95% confidence interval. If the resulting confidence interval did not include zero, it was inferred that there was a significant difference between the means at the $p < 0.05$ level. The confidence intervals for light sleep stimulation off vs. light sleep stimulation on and deep sleep stimulation off vs. deep sleep stimulation on are shown in Figure 2.7. For both conditions, every single subject showed a significant increase in SSVEP amplitude during stimulation. For s03 (stimulation on deep sleep), calculation of a bootstrap confidence interval was not possible, SSVEP amplitude was estimated from a single trial. Bootstrap confidence intervals for differences in the other simple main effects are reported in the supplemental materials (Supplemental Figures 2.12- 2.18).

Given the length of our stimulation periods (5 minutes), we examined the data for correlations between the length of time following stimulation onset and SSVEP amplitude. Using the data from the sleep session, the stimulation periods for each participant were extracted from the filtered EEG data. Then, each stimulation period was analyzed using the STFT. The input parameters for this STFT were a 30-second nonoverlapping window, Hanning taper, and no additional zero-padding. The STFT returned ten values, two for each minute of stimulation. These ten values represent the SSVEP amplitude at a different length of time following stimulation onset. For example, the first value contained data from 0-30 seconds after stimulation onset. Following this, the data was averaged across all subjects and simulation periods (Supplemental Figure 2.14). There appeared to be a moderate negative correlation (r = -.48) between SSVEP amplitude and time after stimulation onset, but it was not significant ($p = 0.16$).

2.5 Discussion

Our results confirmed the hypothesis that SSVEPs can be elicited during sleep. Recall that, in this chapter, we define SSVEP amplitude as the amplitude of EEG activity at the frequency of a target stimulus averaged across channels O1, Oz, and O2 (see Section 2.3.5). Statistical analyses showed an increase in SSVEP amplitude during the stimulation on condition as compared to the stimulation off condition for both light sleep and deep sleep (Figure 2.5). This result is important because it directly enables the inves-

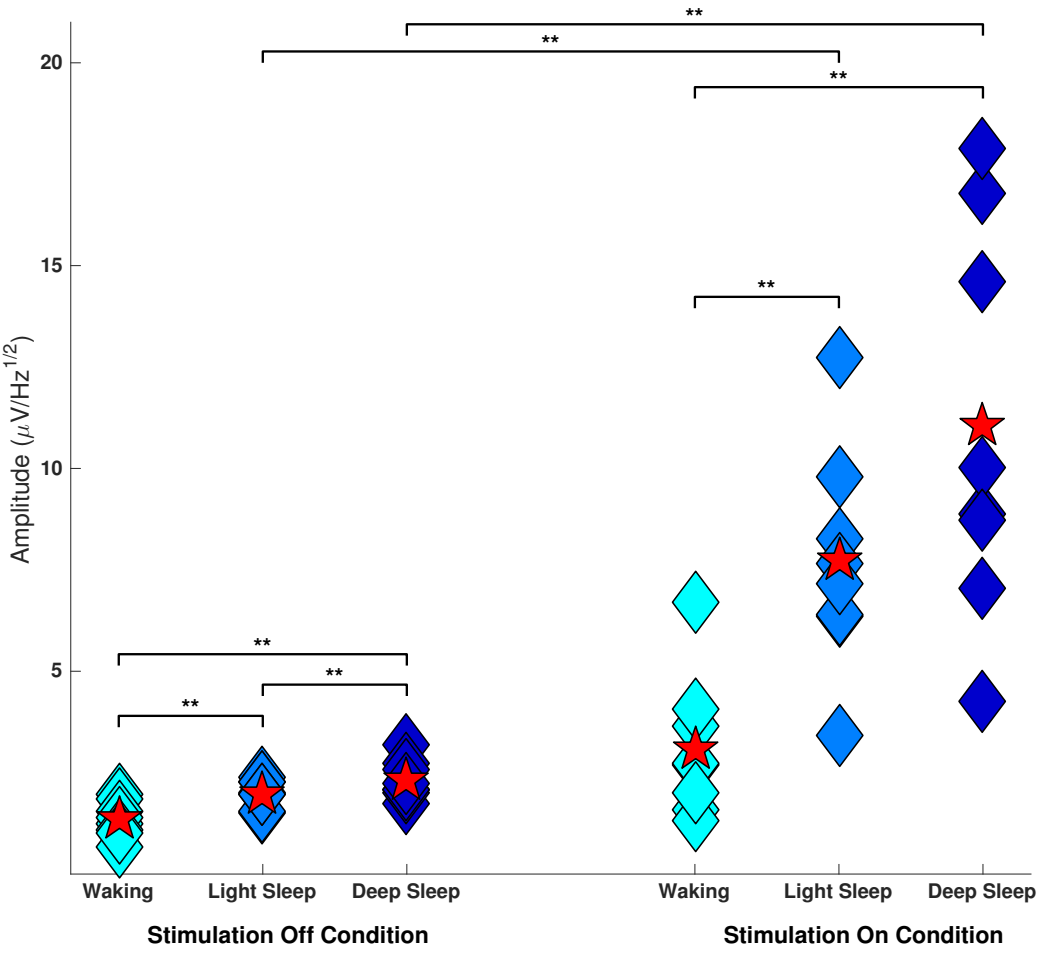

Figure 2.5: Scatterplot of SSVEP amplitudes for all subjects, brain states (waking, light sleep, deep sleep), and stimulation conditions (stimulation off, stimulation on). For each condition, mean amplitude across all subjects has been denoted with a star. Statistically significant ($p < 0.01$) simple main effects indicated with "**".

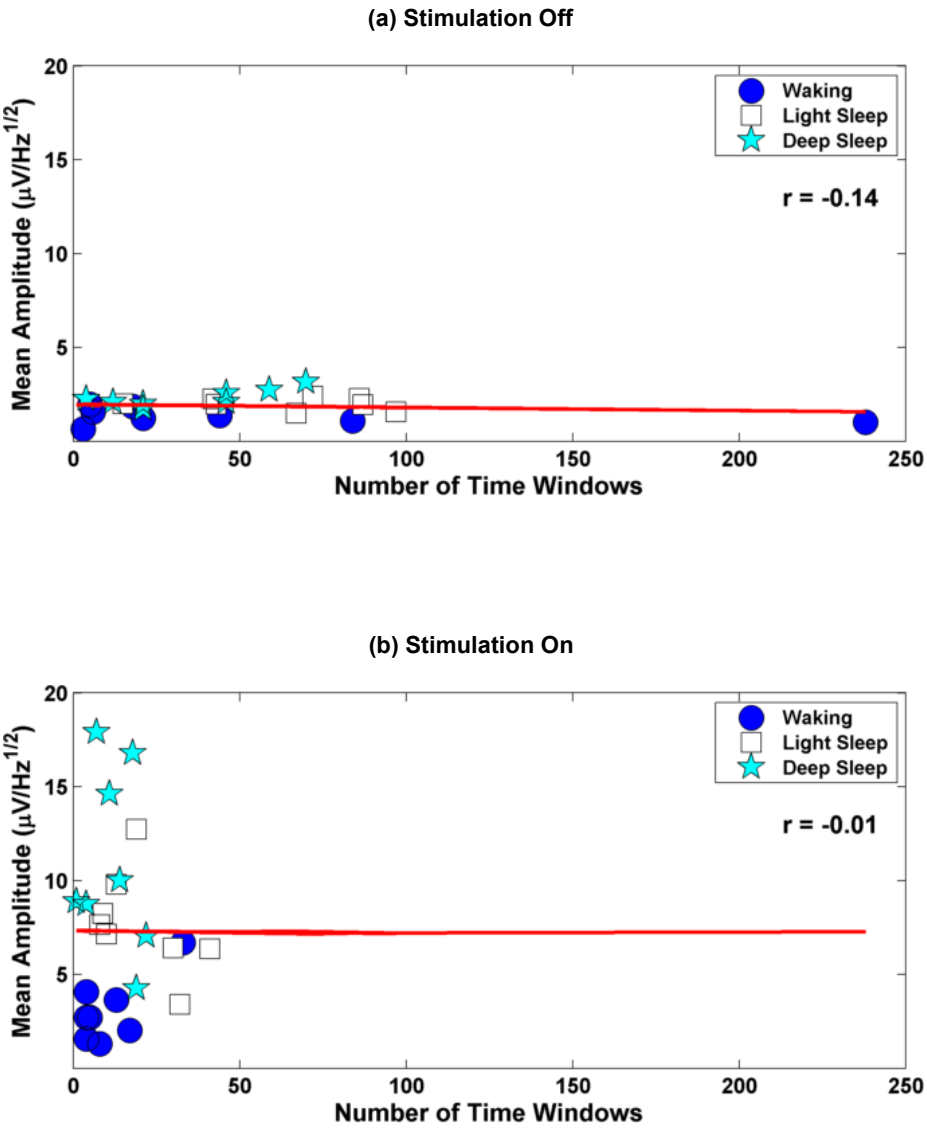

Figure 2.6: Scatterplot showing the number of time windows averaged together in a condition compared with the mean SSVEP amplitude for (a) Stimulation off (all brain states) and (b) Stimulation on (all brain states). A linear trend line has been added to each plot, and the correlation value is written in the upper right-hand corner.

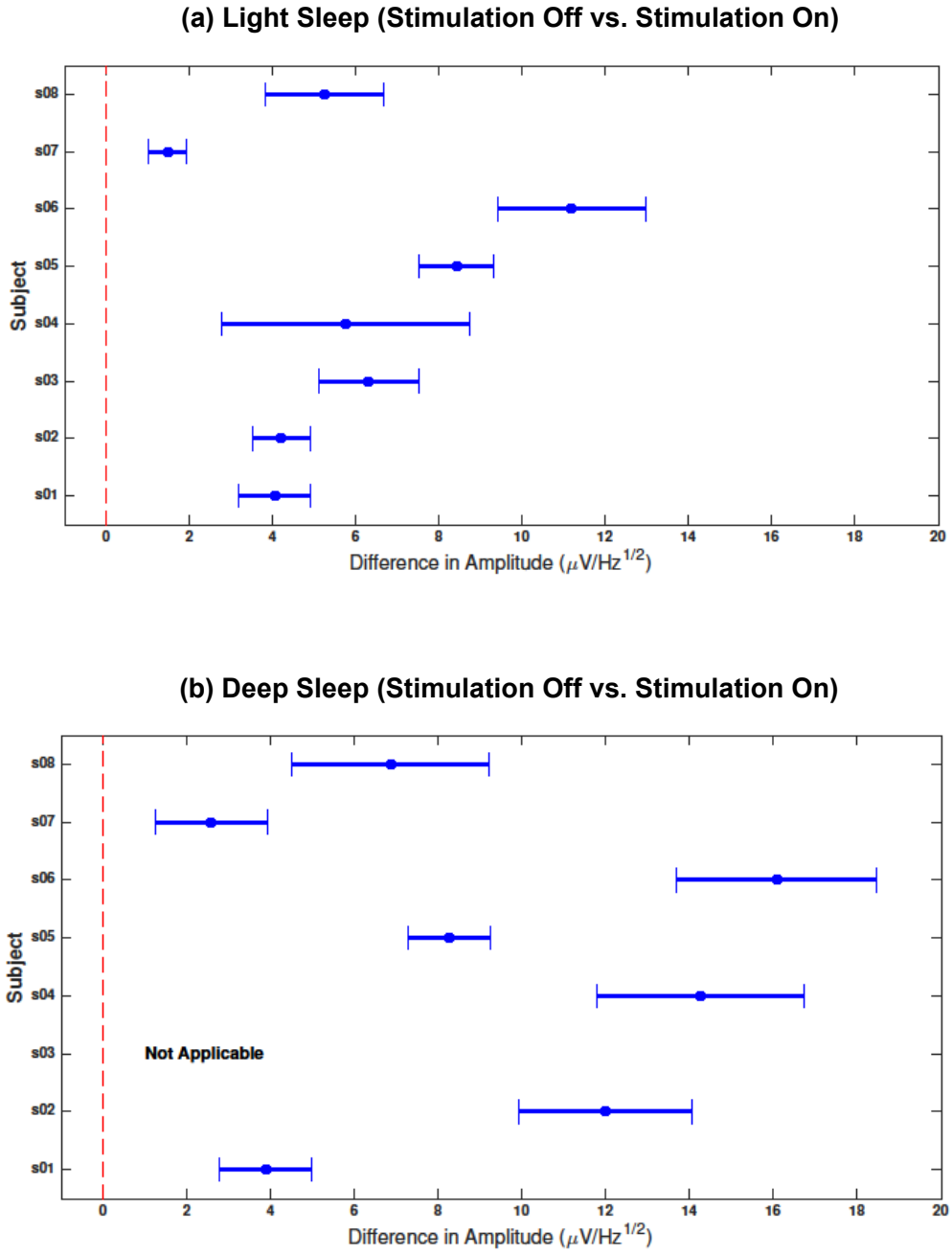

Figure 2.7: Bootstrap confidence intervals for the analysis of simple main effects within subjects. This figure shows the data for two conditions (a) stimulation off (light sleep) vs. stimulation on (light sleep) and (b) stimulation off (deep sleep) vs. stimulation on (deep sleep). Other comparisons are included in the supplemental materials document. For conditions with a single trial, calculation of the confidence interval was not possible (subject s03, stimulation on condition).

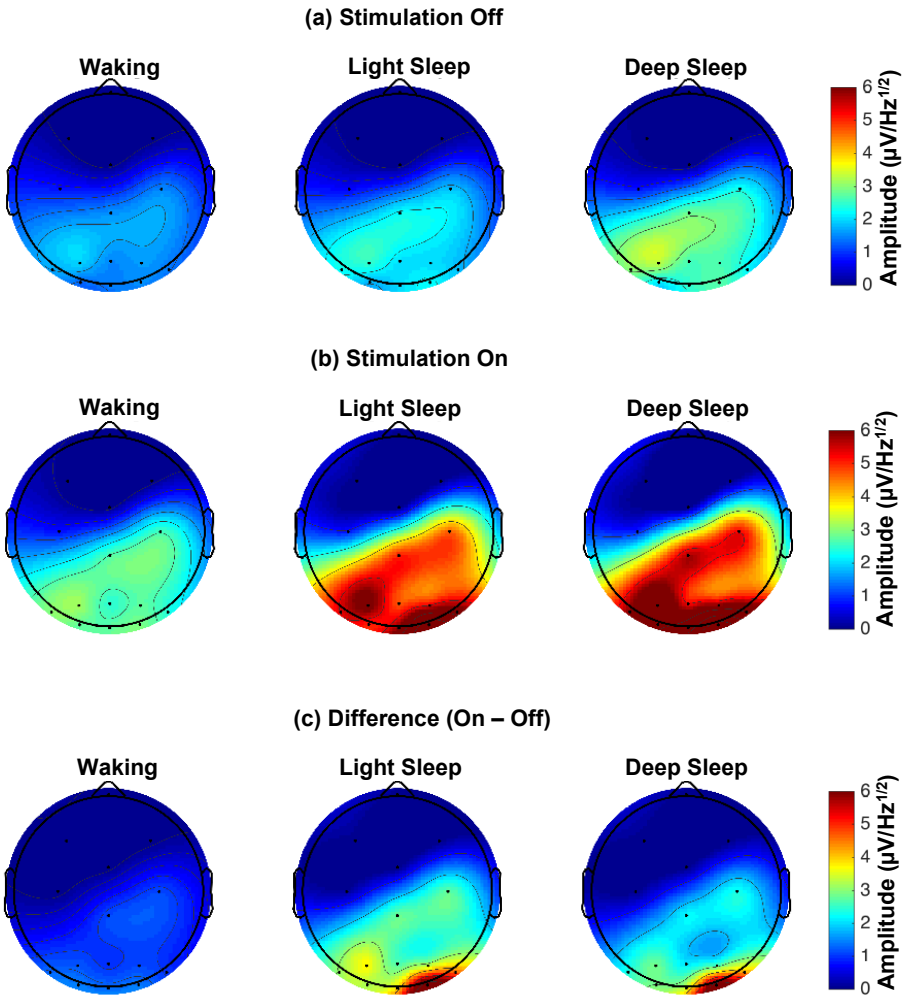

Figure 2.8: Topographic plot of the ASD values, averaged across all subjects, at the frequency of stimulation for the EEG channels. (a) Brain state (waking, light sleep, deep sleep) for the stimulation off condition. (b) Brain state (waking, light sleep, deep sleep) for the stimulation on condition. (c) Brain state (waking, light sleep, deep sleep) for the difference between the stimulation on condition and the stimulation off condition.

tigation of several open questions relating to how SSVEPs are generated in the brain. Specifically, sleep may provide a means to investigate the SSVEP activation sequence and the neural processes that lead to the generation of SSVEPs.

The data also show that the SSVEP amplitude is larger for the stimulation on condition during light sleep and deep sleep than it is during waking (Figure 2.5). Evidence from our study and others suggest that the effect of brain state on steady-state and transient evoked potentials is dependent on the type of stimulation. For example, previous studies have found that sleep reduces the amplitude of steady-state responses using auditory stimuli [43, 113]. Massimini et al. [126], however, showed that early EEG responses to TMS during sleep were larger in amplitude than they were during waking. Kakigi et al. [89] reported that the middle latency components of VEFs were larger during sleep and Shepherd, Saunders, & McCulloch [182] reported that the N1 and P2 amplitudes of VEPs elicited from infants increased during sleep. While our results are intriguing, they may have been affected by dark/light adaptation [187]. Even though the absolute light levels were the same during the baseline (used for most of the waking data) and the sleep experiments (used for all of the light sleep and deep sleep data), no time was given after the lights were turned off and before the baseline recording for the participants eyes to adjust. To test the effect of light adaptation on our results, we conducted a pilot study (Supplemental Analysis II) with two participants. SSVEP amplitude, through closed eyelids, was more than twice as large after 30 minutes of light adaptation than it was at baseline (Supplemental Figure 2.22). Another potential confound is that the majority of the waking data were from the baseline stimulations, which were only one-minute in length. The stimulation periods during the sleep sessions were five times longer. It is possible that the eyes adapted to the stimulations over the course of this time, although an analysis of SSVEP amplitude as a function of time after stimulation onset (Supplemental Figure 2.19) showed no significant correlation. Given our current results, the differences between the existing literature on steady-state and transient evoked potentials during sleep, and the limitations of our current study, further investigation of the changes in SSVEP amplitude that occur across brain states is warranted.

In the stimulation on condition, SSVEP amplitudes were marginally higher during deep sleep than they were during light sleep (Figure 2.5). The data

for these two conditions was collected more than 20 minutes after the lights had been turned off (which was unlikely to have been affected by dark/light adaptation; [187]) and provides further evidence that SSVEP amplitude increases from waking to light sleep to deep sleep. In addition, this is one of the first studies to report a difference in the amplitude of steady-state responses in light sleep vs. deep sleep. Neither Linden et al., [113] nor Cohen et al., [43] reported differences in the amplitude of steady-state responses between light sleep and deep sleep. To improve future studies, we suggest that the stimulation procedure is changed to reduce the variance of SSVEP amplitudes recorded in the stimulation on condition during deep sleep (Table 2.1). This high variance may have been caused, in part, by the limited number of epochs recorded during deep sleep. The experiments did not selectively stimulate participants during specific stages of sleep. The stimulations were a fixed time apart, which was much easier to program and implement, skewing the number of samples within each condition for each subject (Table 2.2). While no significant correlation was found between the number of time windows and the SSVEP amplitude for either the stimulation off or the stimulation on (Figure 2.6) conditions, implementation of an online sleep classification [56] system would allow better control of stimulation during specific stages of sleep. In addition, a more thorough comparison of SSVEP amplitude across brain states should include all of the stages of NREM sleep (N1, N2, and N3) as well as REM sleep (since this data was excluded from the present study).

SSVEP amplitude during waking (Figure 2.5) was only marginally higher in the stimulation on condition than it was in the stimulation off condition, we expected the difference between these two conditions to be larger. We attribute this result to five factors. First, the participants in our experiments were instructed to ignore (i.e. not attend to) the baseline stimuli. Unattended flickering stimuli elicit a much lower amplitude SSVEP than attended stimuli [139]. Second, the length of baseline stimulation (2 minutes total) was shorter than the stimulations used during sleep (5 minutes per stimulation period). The choice of two one-minute stimulation periods was made due to the worry that participants would fall asleep during the baseline. Although an analysis revealed no significant correlation between time following stimulation onset and SSVEP amplitude (Supplemental Figure 2.19), there appears to be a negative correlation between these two variables. Third, the effect size was smaller than expected, if a smaller effect size had been pre-

dicted, and more data had been collected, this result may have been different. Fourth, we always recorded the baseline before the participant went to sleep, potentially causing ordering effects. In the future, the order of the baseline and experimental sessions should be randomized. Finally, since these experiments were conducted using sleeping participants in a dark room, dark/light adaptation may have impacted the results [187] (Supplemental Figure 2.22).

For the stimulation off condition, there was an increase in SSVEP amplitude as brain state changed from waking to light sleep to deep sleep (Figure 2.5). These differences reached significance despite appearing to be much smaller in amplitude than the differences between the brain states in the stimulation on condition. We attribute this to two factors. First, SSVEP amplitude (Table 2.1) varied less during the stimulation off condition than during the stimulation on condition. Second, baseline EEG activity is known to change as a function of brain state. For example, theta activity (4-7 Hz) increases during sleep [49]. The frequency of stimulation used in this study (7.03 Hz) was very close to the theta range. Figure 4 shows that ASD values for all frequencies between 4 Hz and 8 Hz are larger during light sleep and deep sleep (for both the stimulation off and the stimulation on conditions) than during waking.

The topography of ASD values at the frequency of stimulation are shown in Figure 2.8. During waking, the topography of the stimulation on condition appears to be similar to those previously reported by Herrmann [77]. As brain state changes from waking to light sleep to deep sleep, the ASD values measured during the stimulation on condition appear to grow larger, similar to the analysis of SSVEP amplitude. The distribution of these ASD values, however, appears to remain the same with the largest ASD values recorded from near electrode Oz. Further analysis of changes in topography is limited by the number of electrodes used during the experiments, the distribution of these electrodes, and the fact that we did not control for the subjects position [166]. Future work investigating changes in the neural sources of SSVEP across brain state should use more electrodes since this is known to improve EEG source localization [99].

Finally, we acknowledge that many factors are known to affect SSVEP amplitude [220]. These factors include:

- Spatial location of the stimulus - All of the changes in the SSVEP re-

ported here were the result of LED stimulation near the lateral canthus of the eye (Figure 2.1). This location was chosen based on the previous work of Lim [108]. As lateral stimuli have been previously shown to lateralize SSVEP topography [184], the choice of a lateral stimulus location may have altered the experimental results.

- Brightness/contrast of the stimulus - we used a dim (approximately 1.5 lux) stimulus to demonstrate that SSVEPs could be elicited during sleep at brightness levels several orders of magnitudes less than those reported in the work of Rodin [168]. Previous research has shown that the amplitude of SSVEPs is related to the suprathreshold contrast of the stimuli [32]. Additionally, while the eyelid is known to act as a red-pass filter [136], it is unlikely that the filter characteristics are the same across individuals.

- Color of the stimulus - A green stimulus was chosen, ad-hoc, for use in these experiments. Studies show that stimulus color affects SSVEP amplitude in waking participants [163]. Duszyk et al. [55] recently revisited the impact of color on SSVEP amplitude and found that blue stimuli elicit a smaller response than other colors. Future experiments investigating color would have to account for the filtering characteristics of an individuals eyelids [136], but may provide additional insight into how SSVEPs elicited during sleep differ from those elicited during waking.

- Frequency of the stimulus - These experiments used a 7.03 Hz stimulus to avoid overlap with alpha activity (8-13 Hz) that spontaneously occurs during waking. Different flicker frequencies are known to elicit different SSVEP amplitudes with resonance peaks occurring at 10, 20, 40, and 80 Hz [77]. These resonance peaks are evidence for the oscillatory hypothesis of SSVEP generation [77, 123]. Since SSVEPs can be elicited during sleep, and the oscillatory dynamics of the brain change during sleep [49], a logical question to ask is whether these SSVEP resonance frequencies change or disappear during sleep. Changing any of these factors may lead to a different set of results and represent possible directions of future work.

2.6 Conclusion

The experiments presented here show that SSVEPs can be elicited during sleep using a dim (approximately 1.5 lux) stimulus, through closed eyelids, without waking the participant. We have also provided evidence that there may be amplitude differences in SSVEPs elicited during sleep compared with those elicited during waking. As discussed in the introduction, there are at least two specific hypotheses that can be tested based on this result: (1) Given that SSVEPs can be elicited during sleep and that cortical connectivity decreases with sleep [126], one could hypothesize that neural responses later in the SSVEP activation sequence will be attenuated more during sleep than earlier ones. (2) Given that SSVEP amplitude is dependent on frequency and that the oscillatory dynamics of the brain change during sleep [49], one could hypothesize that SSVEP resonance frequencies would change or disappear during sleep. While future work might concentrate on confirming these hypotheses, they represent just two examples of the types of hypotheses that can be tested since SSVEPs can be elicited during sleep.

2.7 Acknowledgement

This work was supported by NSF Grants No. 0955088 and 0903622. The authors would like to thank Bonnie Chen, Randy Lefkowitz, Siyuan Wu, and the ECE445 team for their efforts in the development of the stimulation hardware. Thanks to Joost Rommers, Kara Federmeier, Alex Iordan, Jessica Mullins, and Claudia Lutz for their helpful feedback and incredible insight. The authors would also like to thank the Christie Clinic Sleep Center for their insights on polysomnography and sleep scoring.

2.8 Supplemental Information

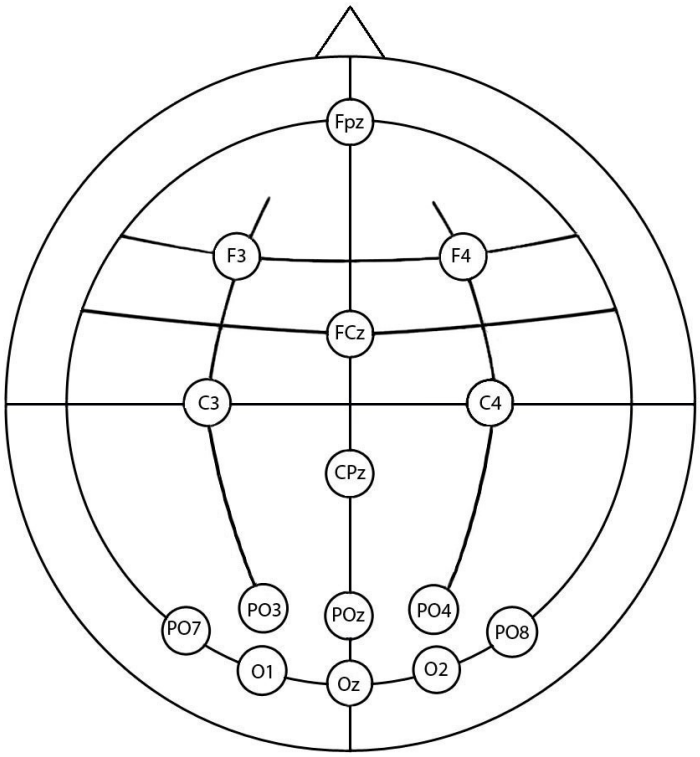

Figure 2.9: Locations of electrodes used to record EEG during experiments. In addition to the EEG electrodes shown in the diagram, there was an additional electrode on the right mastoid. All EEG signals were referenced to the left mastoid, and ground was placed on the nose.

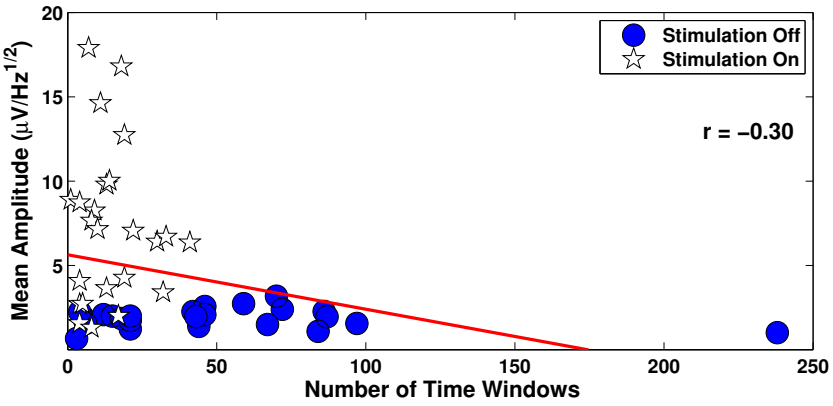

Figure 2.10: Scatterplot showing mean amplitude vs. number of time windows for all conditions (r = -0.30, p = 0.036).

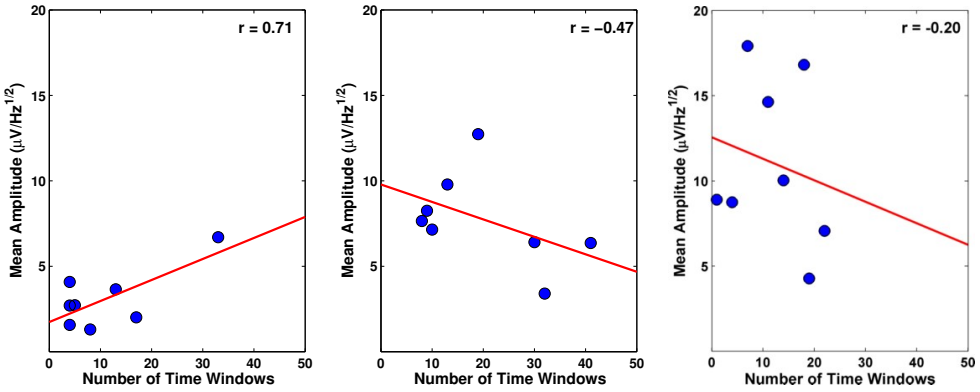

Figure 2.11: Scatterplots showing mean amplitude vs. number of time windows for the stimulation on condition (a) waking (r = 0.71, p = 0.047), (b) light sleep (r = -0.47, p = 0.242), and (c) deep sleep (r = -0.20, p = 0.642). These p-values are not corrected for multiple comparisons.

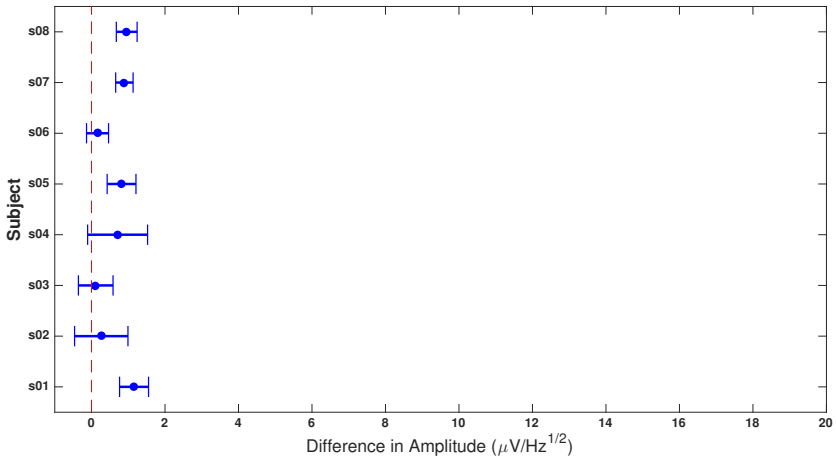

Figure 2.12: Bootstrap confidence intervals (95%) for comparison of stimulation off - waking vs. light sleep.

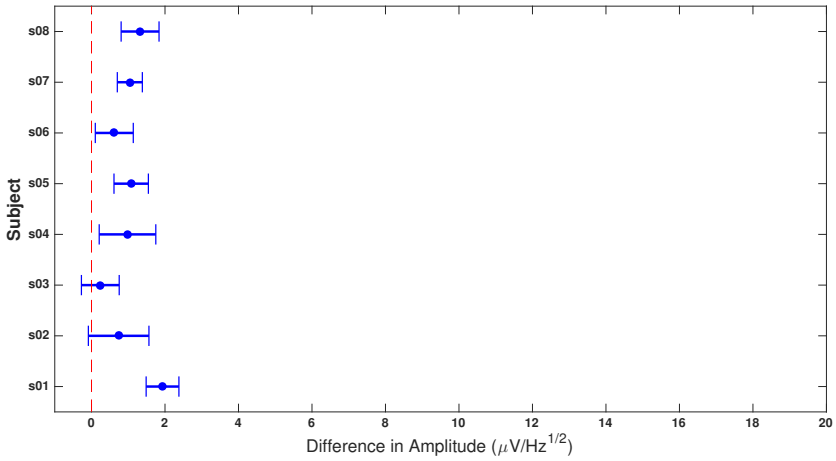

Figure 2.13: Bootstrap confidence intervals (95%) for comparison of stimulation off - waking vs. deep sleep.

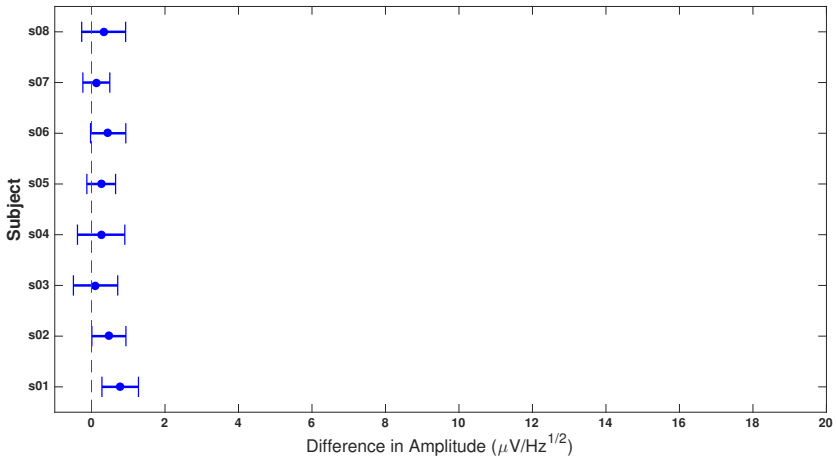

Figure 2.14: Bootstrap confidence intervals (95%) for comparison of stimulation off - light sleep vs. deep sleep.

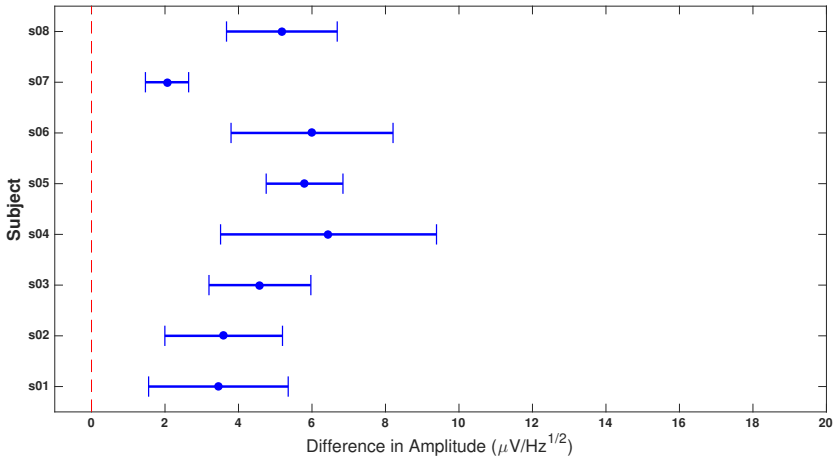

Figure 2.15: Bootstrap confidence intervals (95%) for comparison of stimulation on - waking vs. light sleep.

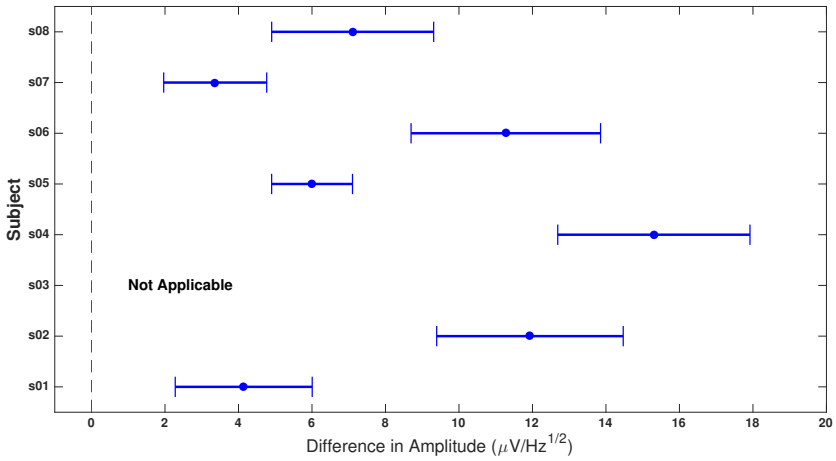

Figure 2.16: Bootstrap confidence intervals (95%) for comparison of stimulation on -waking vs. deep sleep.

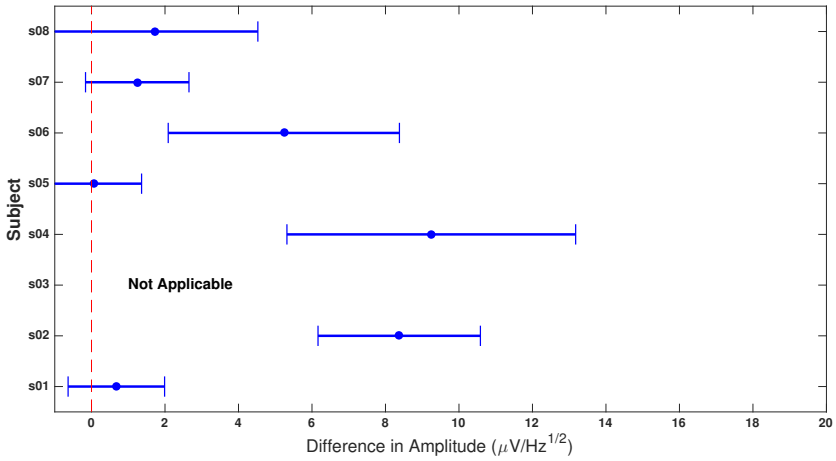

Figure 2.17: Bootstrap confidence intervals (95%) for comparison of stimulation on - light sleep vs. deep sleep.

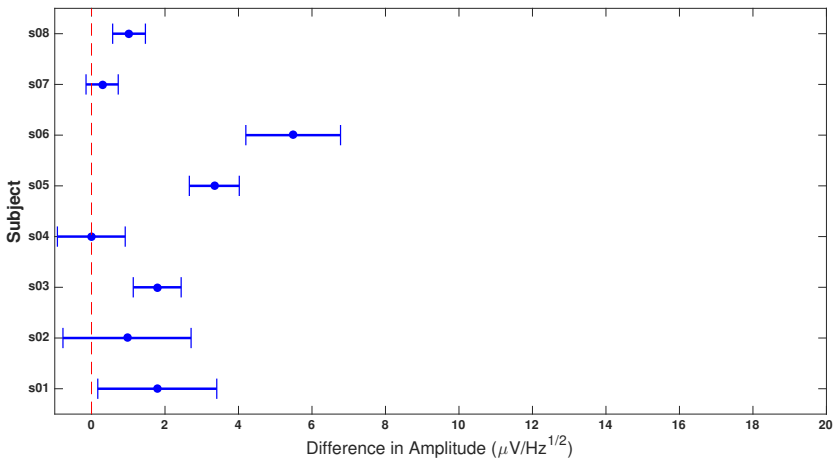

Figure 2.18: Bootstrap confidence intervals (95%) for comparison of waking - stimulation off vs. stimulation on.

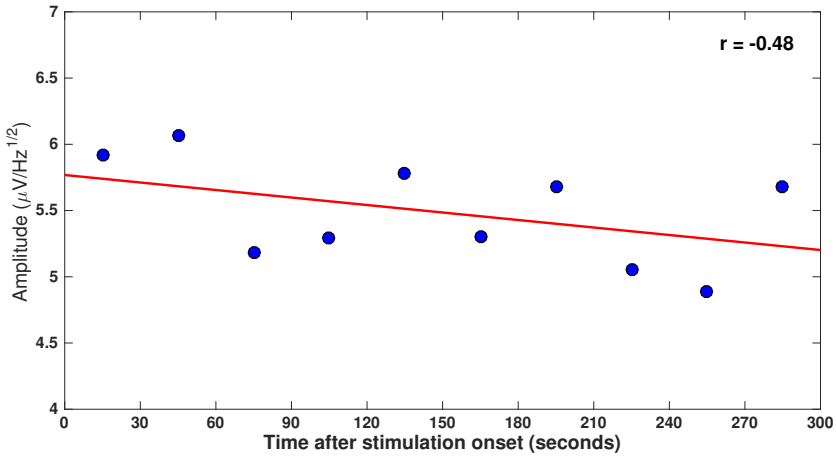

Figure 2.19: Mean SSVEP amplitude, averaged across all subjects and stimulation periods, elicited during sleep session as a function of time following stimulation onset.

2.8.1 Supplemental Analysis I

Data analysis showing the correlation between individual alpha frequency (IAF) and the SSVEP amplitude from each subject. This value was calculated by first averaging channels O1, Oz, and O2, and then computing the amplitude spectral (four second Hanning window, three-second overlap, and zero-padded to 16 times the length of the window). IAF was defined as the frequency with the maximum amplitude (Figure 2.20) between 8-14Hz [35]. IAF was calculated for each subject for both stimulation on (Table 2.3a) and stimulation off (Table 2.3b).

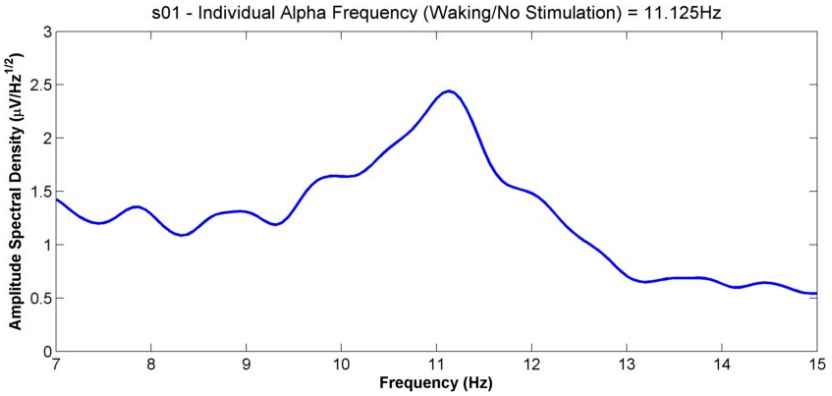

Figure 2.20: The ASD value for the individual alpha frequency for s01 during waking and the stimulation off condition.

IAFs for stimulation off were correlated with SSVEP amplitude measured during stimulation on condition. Before comparing these two data sets, the stimulation on data was baselined by subtracting the SSVEP amplitude of the stimulation off condition. This was done separately for each brain state. Scatterplots for each brain state (waking, light sleep, and deep sleep) can be seen in Figure 2.21. The correlations for each condition are the following:

Table 2.3: Simulation Study

(a) Individual alpha frequency by subject (stimulation off)

	S01	S02	S03	S04	S05	S06	S07	S08
IAF	11.13	9.75	9.18	10.44	9.93	10.13	10.25	11.81

(b) Individual alpha frequency by subject (stimulation on)

	S01	S02	S03	S04	S05	S06	S07	S08
IAF	11.81	9.75	9.18	10.31	9.94	10.18	10.38	11.81

waking (r = -0.22, p = 0.602), light sleep (r = -0.22, p = 0.602), and deep sleep (r = -0.25, p = 0.555). A consistent, but not significant, weak negative correlation can be seen in all three brain states.

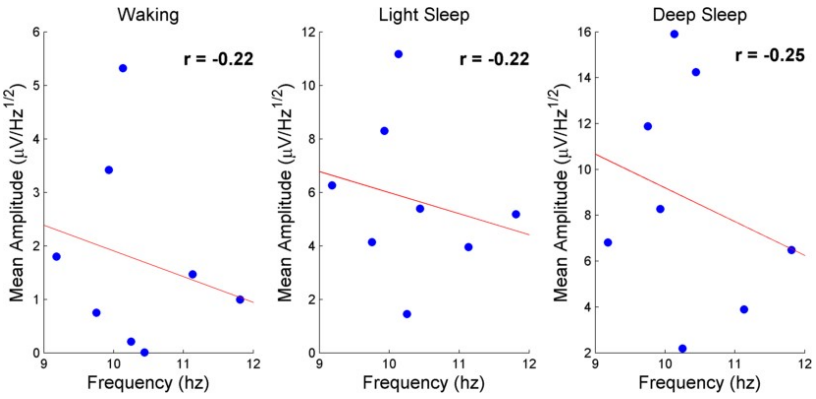

Figure 2.21: Scatterplots of the IAF for each subject during the stimulation off condition.

2.8.2 Supplemental Analysis II

Dark Adaptation - Version 1

This analysis looked at the effect of light adaptation on SSVEP amplitude. Two participants from our laboratory were asked to wear the same visual stimulator as used during the sleep experiment while their EEG was recorded. Following the methodology of [187] we conducted a pilot experiment with two conditions: (1) Baseline and (2) Light Adaptation. After setup, all lighting in the room was turned off. A five-minute baseline recording was then obtained (7.03Hz stimulation). During this baseline recording, each participant was asked to close their eyes and ignore the stimuli. Following baseline, the participant was asked to sit quietly in the dark room without falling asleep. The experimenters offered to talk with the participants during this period to help them. After a 30-minute light adaptation period, another five-minute stimulation period was conducted. Our analysis used EEG data from channels O1, Oz, and O2. The data from these channels and the two stimulation periods (baseline and light adaptation) were extracted for further analysis. SSVEP amplitude was calculated using pwelch in the same way as the sleep experiments (see Methods - Amplitude Spectral Density for details) using 30-second non-overlapping windows. This resulted in 10 SSVEP amplitude estimates for each subject and each condition. Finally, the results were converted to a percent change from the average of all of the baseline stimulation periods. The results of these experiments are shown below:

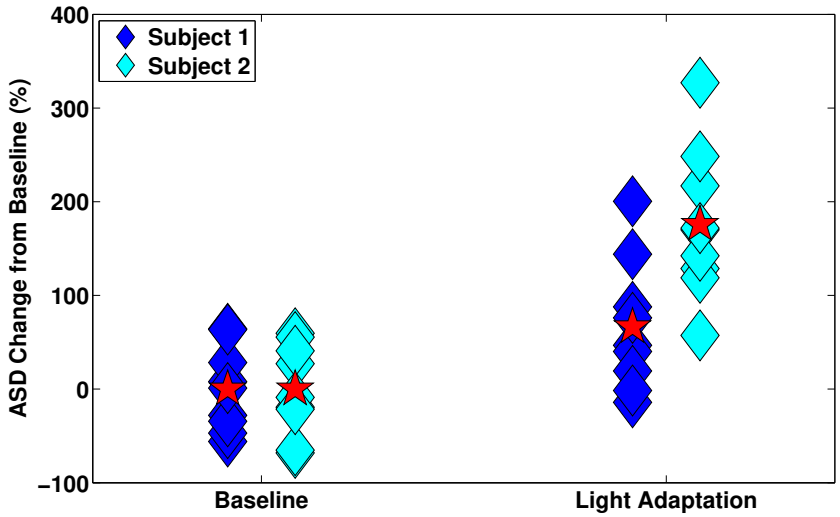

Figure 2.22: Scatterplots of the IAF for each subject during the stimulation off condition.

Dark Adaptation - Pilot Study

Introduction

This supplemental experiment tests the hypothesis that the amplitude of the fundamental frequency component of SSVEPs is larger during NREM sleep than it is during waking.

Previous research has investigated the effect of sleep on the fundamental frequency component of SSVEPs. Norton, Umunna, and Bretl [147] show that the fundamental frequency component of an SSVEP elicited by a 7Hz stimulus is larger during NREM sleep than it is during waking. Sharon and Nir [181] reported similar results for 3/5Hz stimuli, but that the amplitude of the fundamental frequency component of SSVEPs elicited by 8/10Hz stimuli are smaller during NREM sleep than during waking. Neither of these two studies, however, accounted for the fact that the amplitude of SSVEPs increase following dark adaptation [187]. In addition, Sharon and Nir [181] did not ask participants to either attend or ignore the stimuli during the baseline stimulation period. Attention is well known [135] to affect the amplitude of SSVEPs.

To test whether previously observed differences in the amplitude of the fundamental frequency component of SSVEPs elicited during sleep could be attributed to dark adaptation or attention, we compared data collected by Norton, Umunna, and Bretl [147] with data from two new experiments. Both experiments test how dark adaptation effects the amplitude of SSVEPs using the exact same stimulator as Norton, Umunna, and Bretl [147]. To test the effect of attention following dark adaptation, in one experiment participants were asked to pay attention to the stimuli and in the other experiment, participants were asked to ignore the stimuli. Our hypothesis was that the SSVEPs elicited during sleep would be larger than those elicited after dark adaptation. We hypothesized that this would be true when participants were asked to pay attention to a stimulus and when they were asked to ignore a stimulus.

Participants

There were eight participants in the no attention study and seven participants in the attention study.

Procedure

EEG recordings were made using the exact experimental setup described in Section 2.3.2 with the exception that no EMG, ECG, or EOG data was recorded. Participants were seated in the same room, using the same chair, and SSVEPs were elicited using the same stimulator described in Sections 2.3.3 and 2.3.4. After EEG setup, participants were given one of two sets of instructions. They were asked to either close their eyes, look straight forward, and ignore the stimulus or to close their eyes, looks straight forward, and attend to the stimulus. After receiving instructions, the lights in the room were turned off so that there was complete darkness and a baseline recording session was started. This baseline recording session consisted of two one-minute stimulation periods with two one-minute no stimulation periods in between and after. Following the baseline stimulation periods, participants were instructed that they could open their eyes and relax, but not fall asleep. To help the participants stay awake, they were also permitted to talk to the experimenter, listen to music, or listen to National Public Radio. This decision was followed by a dark adaptation period of 30 minutes, in which the participant remained in a completely dark room. Approximately 3 minutes before the end of the 30 minute dark adaptation period, any entertainment was stopped and the participant was again asked to close their eyes and either attend or ignore the upcoming stimulus (depending on what group they were in). A second stimulation period was then conducted and continuously stimulated the participant for five minutes. After the second stimulation period, the participant was asked to relax quietly for approximately two minutes before EEG recording was halted and the experiment ended. Participants were then thanked for their time.

Data Analysis

Data analysis was conducted using the same procedure detailed in Section 2.3.5. ASD estimates were calculated for each participant and condition. For both of the dark adaptation experiments (no attention and attention), the final ASD values were calculated in two steps. First the ASD values for the baseline (stimulation off) condition were subtracted from the baseline (stimulation on) and dark adaptation (stimulation on) conditions. The baseline (stimulation on) condition was then subtracted from the dark adaptation (stimulation on) condition. The sleep data used were from Chapter 2. As the effect of sleep on SSVEP amplitude was largest for deep sleep, we

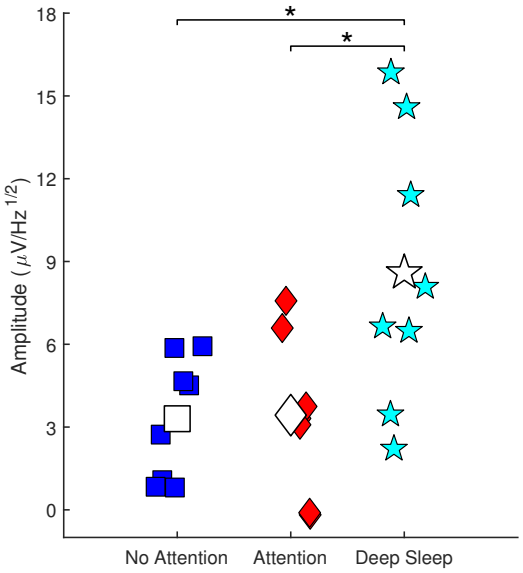

Figure 2.23: Fundamental Frequency

compared the dark adaptation data with data collected during deep sleep. The ASD values used for comparison with the dark adaptation data were obtained by subtracting the deep sleep (stimulation off) data from the deep sleep (stimulation on) data.

Results

A one-way ANOVA on SSVEP amplitude revealed an effect of the experiments on SSVEP amplitude (F [2,20] = 5.51, $p = 0.01$). Pairwise comparisons revealed that SSVEP amplitudes elicited during deep sleep were larger those elicited after dark adaptation when the participant was instructed to ignore the stimulus (mean difference = 5.29, $p = 0.02$) and that SSVEP amplitudes elicited during deep sleep were larger those elicited after dark adaptation when the participant was instructed to attend to the stimulus (mean difference = 5.16, p = 0.03).

Discussion

These data support the hypothesis that SSVEPs elicited during deep sleep are larger than those elicited following dark adaptation. This result is true when participants are asked to ignore the visual stimulus as well as when participants are asked to ignore the visual stimulus.

CHAPTER 3

THE PERFORMANCE OF 9-11 YEAR OLD CHILDREN USING AN SSVEP-BASED BCI FOR TARGET SELECTION[1]

3.1 Abstract

In this chapter, we report the performance of 9-11 year old children using a steady-state visual evoked potential (SSVEP)-based brain-computer interface (BCI) and provides control data collected from healthy adults for comparison. The only previous investigation of children in a similar age range using SSVEP-based BCIs reported low performance (∼50% accuracy), but here children made online selections much more accurately (∼80%). Experiments were conducted in two phases, a training phase and an experimental phase. An offline analysis of the data collected during the training phase was used to set two parameters for a classifier and to screen participants who did not achieve a minimum accuracy of 85%. Eleven of the 14 children and all 11 of the adults who completed the training phase met the minimum accuracy requirement. During the experimental phase, children selected targets with a similar accuracy (79% for children versus 78% for adults), latency (2.1 seconds for children versus 1.9 seconds for adults), and bitrate (0.50 bits/second for children and 0.56 bits/second for adults) as adults. Children also selected a similar number of targets as during a bonus round where participants were allowed to select as many targets as they wanted. This study provides data that shows that children can use an SSVEP-based BCI with higher performance than previously believed and provides a baseline for studies investigating differences in performance between children and adults using SSVEP-based BCIs.

[1]This work includes significant scientific contributions from J. Mullins and T. Bretl.

3.2 Introduction

Non-invasive brain-computer interfaces (BCIs) enable users to control external devices (such as computer systems [197, 3], prosthetic arms [81, 215], and robotic vehicles [54]) using brain activity. The primary application of BCIs is to replace [209] function in those with severe motor disabilities that are the result of injury [22] or disease [96, 174]. They also, however, may be useful for rehabilitation (such as after a stroke [183]) or to supplement [109] and/or improve[18] the natural capabilities of healthy individuals.

Most current BCI systems rely on brain activity measured using electroencephalography (EEG). EEG is a non-invasive and relatively inexpensive tool for measuring the brain's naturally generated electrical activity. There are several brain signals that can be measured using EEG and then used as inputs for BCIs. These include signals related to imagined movement [96], the detection of infrequent targets [60], or spatially distinct sounds [80]. Here, we consider EEG-based BCIs that use brain signals elicited by repetitive visual stimulations, more commonly known as steady-state visual evoked potentials (SSVEPs).

SSVEP-based BCIs rely on the fact that repetitive visual stimulation elicits brain activity at the same speed (measured in frequency or flashes per second) as the stimulus [194]. In addition, the amplitude of the brain activity elicited by the stimulus is dependent on the user's attention [135]. This means that if there are multiple stimuli flashing at different rates, the stimulus that the user attends to (the *target*) will elicit a larger amplitude response than the stimuli that the user ignores. In practice, the user's target is unknown and must be inferred through analysis of the EEG signals. This analysis, known as classification, outputs a guess of the user's target, called the *predicted target*. This process of the user attending to targets and the classification system predicting targets enables a user to select a specific stimulus from the available set of stimuli and is the basis of all SSVEP-based BCIs.

There are three common ways to measure the performance of an SSVEP-based BCI user. *Accuracy* is the proportion of times the predicted target matches the intended target [57]. *Latency* is mean time from target onset to classification [199, 3]. *Bitrate* is the number of bits per second that are transmitted, and is often preferred over other measures because it accounts for both accuracy and latency. Common ways of quantifying bitrate are the

information transfer rate (ITR) [211] and the Nykopp bitrate (NBR) [149]. We use NBR to quantify bitrate in this chapter, since it addresses several well-known limitations of ITR [95].

Given that the goal of most SSVEP-based BCIs is to replace function in those with severe motor disabilities and that these disabilities affect many different groups of people (with different ages, genders, etc.), it is important to understand how SSVEP-based BCI performance varies among these different groups. As an example, consider that SSVEP-based BCIs are often tested with young adults, but the average age of patients who have locked-in syndrome (LIS) is approximately 50 (this estimate is based on the average age of 151 LIS patients reported by Bruno et al. [28]). Then consider that Lesenfants et al. [106] found that only one out of six LIS patients (average age 49 $\pm$ 19.7 years) could use their SSVEP-based BCI systems with better than chance accuracy, but 80% of young adults could use their system. If the goal is to understand what causes these differences, logically it would be helpful to know how many middle-aged and older adults can use SSVEP-based BCIs and how their performance with these systems compares with young adults.

Prior studies of these *demographic* differences in the performance of SSVEP-based BCIs have reported mixed results. Allison [5] assessed the performance of more than 100 people between the ages of 18 and 79 at a large computer expo (CeBIT 2008). While younger people tended to perform at higher bit rates, there were no significant differences between performance and age or performance and gender. A follow-up paper by Volosyak [201] also found no differences between people of different ages. Two more recent papers, however, have reported differences between young adults and older adults in the context of SSVEP-based BCIs. Hsu [82] compared SSVEP-amplitudes (for use in a BCI) in young adults, older adults, and ALS patients. They found that young adults produced larger SSVEPs with a higher signal to noise ratio at an occipital electrode site compared to older adults and ALS patients. In addition, Volosyak [199] recently investigated differences in performance between young adults (between the ages of 19 and 27) and older adults (between the ages of 54 and 76) while using an SSVEP-based BCI for text-entry. The results of this study showed that younger adults achieved a higher average bitrate than older adults.

While the aforementioned studies have considered adults of different ages,

only one previous study has investigated the performance of children compared with adults when using SSVEP-based BCIs. In this study, Ehlers [57] asked children of different ages to control an SSVEP-based BCI for text-entry. What Ehlers found was that children were less likely to complete the task and input characters with much lower accuracy than adults do. Ehlers concluded that children were not yet able to generate a reliable SSVEP due to developmental differences with adults. While the data presented in this study are an important contribution to the literature on SSVEP-based BCI, several confounding factors may cast doubt on the conclusion. For example, the children were tested in a noisy school environment, one that may have distracted them from the task. In addition, it is not clear whether the children struggled with the SSVEP-based BCI for text-entry or whether they would struggle with SSVEP-based BCIs in general [92]. Furthermore, Ehlers only reported accuracy, but not the latency or the bitrate of the adults or the children. The results from Ehlers study are even more confusing when previous cognitive neuroscience research is considered. In a 2006 study, Birca [20] reported that there were no differences in SSVEP magnitude between children and adults. In a later follow-up, however, Birca [21] reported that 8-11 children had larger SSVEP responses over the occipital region than adults.

The small number and conflicting results of these prior studies leave open the question of whether or not children can use SSVEP-based BCIs with good performance. This limits the applicability of SSVEP-based BCIs to the replacement of lost function in those with severe motors disabilities—including LIS [29]—that affect children. To help resolve this question, we describe a new study in this chapter that measured the performance of 9-11 year old children using an SSVEP-based BCI. We also measured the performance of adults for the purpose of comparison. Our study consisted of two phases, a short training phase and a longer experimental phase. Data collected during the training phase were used to choose parameters for our classifier and to screen out participants with exceptionally low performance (11 of 14 children and 11 of 11 adults met minimum performance requirements). Data collected during the experimental phase were used to measure accuracy, latency, and bitrate. In this study, both children and adults were given the opportunity to continue using the SSVEP-based BCI for as long as they chose (up to 10 minutes)—the number of trials completed by each participant was used as an additional comparison between the two groups.

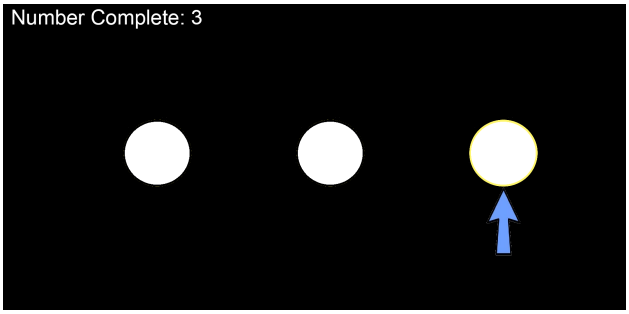

(a) Targets for the short training phase

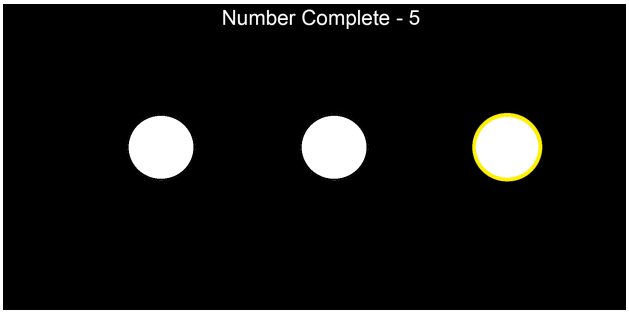

(b) Targets for the longer experimental phase

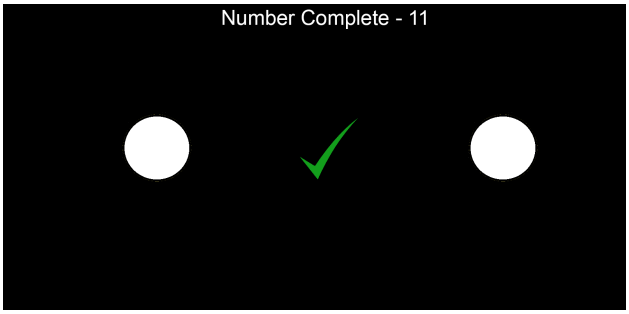

(c) Feedback after selection during the longer experimental phase

Figure 3.1: Graphical representations of the experimental interface. (a) Shows how targets were identified with an arrow during the short training phase. (b) Shows how the target was highlighted during the longer experimental phase. (c) Shows the feedback given to the user after the classifier guessed the predicted target. Note that the size of the targets and text have been enlarged to improve readability.

3.3 Method

3.3.1 Participants

Twenty-six able-bodied volunteers (sixteen 9-11 years olds, Mean = 9.73 and eleven adults aged between 19-68, Mean = 38.00) participated in our study. Participants were recruited through email bulletins and word of mouth. Two adults participants had previous experience with a BCI (S12 and S20). All subjects had normal or corrected-to-normal vision and no prior history of neurological illness. Each participant was compensated with a small gift (less than $5.00US) for their time. This study was approved by the Institutional Review Board at the University of Illinois at Urbana-Champaign.

3.3.2 EEG Recording

EEG signals were recored from six tin electrodes. The electrodes were placed on the surface of the scalp located at 10-5 international sites: PO3, POZ, PO4, O1, OZ, and O2 [151]. The channels were grounded at the right ear and referenced to the top of the head (location CZ). The signals were recorded at impedances of less than 10kΩ. All EEG signals were band-pass filtered from 1Hz to 30Hz, amplified using a James Long bioamplifier, and digitized at 128Hz (National Instruments Model PCI-6225). BCI2000 [171] was used to visualize and record the preprocessed EEG signals.

3.3.3 Experimental Procedures

All experiments were conducted in a cool and sound attenuated room with dim ambient lighting. The participants were seated in a comfortable office chair between two speakers facing an LED computer monitor (24-inch BenQ XL2420T). After completing the consent process, each subject was asked to complete a brief survey with basic background questions, based on the questionnaire used by Allison [5]. After the survey was completed, the participants completed a short training phase and a longer experimental phase. After the experiments, participants also completed an additional test that will be discussed as a part of different study. In all experiments participants

were asked to focus their visual attention on a target blinking presented on the monitor. For both the short training phase and the longer experimental phase the targets were three white ovals flashing between white and black at 6.2Hz, 8Hz, and 10Hz.

3.3.4 Training Phase

Each participant completed a short training phase to calibrate the BCI system and to screen them for use with the BCI.

Data from the training phase was used to set free parameters of the classifier (Section 3.3.6). The participants were given verbal instructions and allowed to start the application when they were ready by pressing a key on the keyboard. Once the short training phase started, an arrow specified the target during each trial (Figure 3.1a) and this target was highlighted with a yellow outline. Participants were instructed to overtly focus their attention on the target for the entire trial. Each trial lasted five seconds, with a short pause between trials. The order of the specified targets was randomized with each of the three frequencies specified as the target five times for a total of 15 trials. The short training phase took no more than five minutes. Following training, the participants were given time to relax while the experimenter calibrated the BCI system with the training data.

During the analysis of the training data, if the participant never achieved an 85% accuracy, they were deemed to be unable to use the SSVEP-based BCI and any data collected during the longer experimental phase was excluded from further analysis.

3.3.5 Experimental Phase

During the longer experimental phase, users were asked to select a sequence of targets using our SSVEP-based BCI. When the experiment was started, a splash screen was displayed while the experimenter described the task. After the researcher provided instructions on how to use the application, the participant was allowed to press a key on the keyboard to begin the experiment.

Similar to the short training phase, the interface used in the longer exper-

imental phase displayed three stimuli. The target that the participant was supposed to select was the same as in the short training phase, except there was no arrow pointing to it (Figure 3.1b).

Participants were instructed to select targets by overtly shifting their visual attention. If the classifier guessed a target, a check mark was shown at the the location of the predicted target (Figure 3.1c) and a tone provided audio feedback that a selection had been made. Participants were given up to 5 seconds to select a target during each trial. If no target was selected within 5 seconds, the trial ended and the next trial began. The application paused for one second between trials. Real-time feedback on the number of trials completed was provided at the top of the interface.

The longer experimental consisted of four rounds and a bonus round at the end. Each round contained 15 trials. The order of the targets during each round was randomized. Each of the three stimulation frequencies was specified as the target five times during each round. At the end of each round, a message was displayed indicating the round number and the system paused for six seconds. During the bonus round, participants were allowed to select targets for as long as they wanted, up to 10 minutes. The frequency of the targets were selected at random, the experimenters did not guarantee an equal number of targets from each frequency. At the end of the longer experimental phase a short message was displayed to the user, letting them know the session was completed.

3.3.6 Signal Processing

A classifier, based on canonical correlation analysis (CCA), was used to determine the predicted target. Our algorithm for the classification of SSVEP targets using CCA was similar to the one described by Lin [112] with three notable differences.

1. We considered only two harmonic frequencies.
2. A threshold (τ) was used to enable asynchronous control.
3. Two free parameters, τ and the amount of data considered by the classifier (window-length [t]) were set using training data.

For additional details on the classifier used in this study, see Section 3.6.

Determining Window-length and Threshold

As discussed in Section 3.3.6, the purpose of the short training phase (Section 3.3.4) was to set the t and τ. After each participant completed the short training phase, individual five-second trials were extracted from the training data. After trial extraction, there were five trials for each of the three target frequencies. Using this data, a search was performed to find the parameters that maximized the participant's Nykopp bitrate (NBR) [149]. The NBR was computed for $t = [0.25, 0.5, ..., 5]$ and for $\tau = [0, 0.01, ..., 1]$. The values of t and τ that maximized NBR were subsequently used for classifying targets during the longer experimental phase.

There were two differences in the way that the parameters were calculated for different subjects. First, for children, the minimum value of t was set to be 1.250 seconds. For the adults, the minimum value of t was set to be 0.5 seconds. Second, for five of the children—denoted with asterisks in Table 3.4—the parameters were calculated considering three harmonic frequencies instead of two. The potential impact of these difference will be considered in the results (Sections 3.4) and discussion (Sections 3.5).

3.4 Results

Of the 26 people who participated in our study, 22 were able to complete the entire experiment. One child was excluded due to a technical issue (software crash). The remaining three subjects (three children) were excluded due to low performance. Two of the children who were excluded appeared distracted during the short training phase. They did not pay attention to the screen nor did they appear to attempt the task. Data from participants who did not achieve a minimum accuracy of 85% within five seconds of stimulation during the short training phase (Section 3.3.4) were excluded from the analysis of the longer experimental phase.

In our study, there were four primary measurements of performance.

1. **Accuracy** - Accuracy was calculated as a count of the number of times that the predicted target was equal to the target divided by the total number of trials.
2. **Latency** - The average amount of time (measured in seconds) that

elapsed between the onset of the stimuli and the classification of the predicted target.

3. **Nykopp Bitrate (NBR)** - Calculated using the definition of Nykopp [149, 95, 172], a quantity that describes the amount of information transmitted over a noisy channel per unit of time and reported in terms of bits/second. Our calculation of NBR is based on the formulas found in Kronegg, Voloshynovskyy, and Pun [95].
4. **Trials in bonus round** - A count of the number of trials that each participant completed in the bonus round.

3.4.1 Training Phase

We report our analysis of the training data in two ways. First, we qualitatively describe the τ and t values used during the experiments. Second, we describe an analysis of the data that was performed after all of the data was collected. In both cases, 11 of the 14 children and all 11 adults who completed the short training phase exceeded our threshold for being able to use an SSVEP-based BCI.

Parameters from Experiments

The results obtained during the training phase are described in Tables 3.4-3.5. The data for the participants included in the study are described in Table 3.1 (children) and Table 3.3 (adults). Note that there were two differences in the way that τ and t were calculated for the participants who were children. (1) For five of the children—denoted with asterisks in Table 3.4—the calculation of τ and t included three harmonic frequencies, instead of two (two harmonics were always used during the longer experimental phase). (2) The minimum value of t for children was set to be 1.250 seconds while the minimum value of t for adults was 0.500 seconds. Post-hoc Mann-Whitney U tests with no correction for multiple comparisons found that the t values used for classification in the participants who were children (Mean = 1.545 seconds, Mdn = 1.375 seconds, SD = 0.45 seconds) were longer ($p = 0.02$) than those used for the participants who were adults (Mean = 1.227 seconds, Mdn = 1.000 seconds, SD = 0.85 seconds). Although, one adult (participant

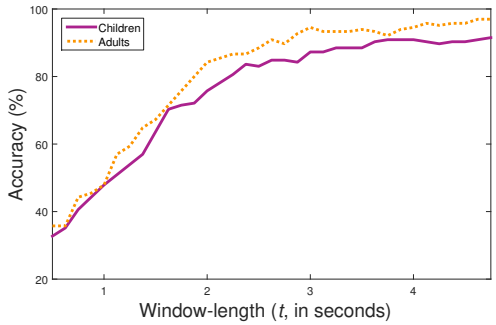

(a) Training phase accuracy (children versus adults)

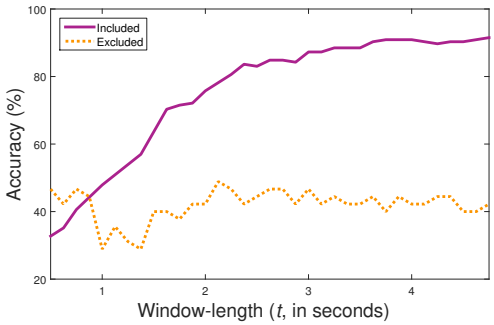

(b) Training phase accuracy (included children versus excluded children)

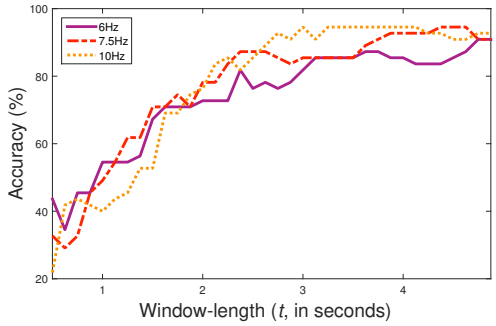

(c) Training phase accuracy for each stimulation frequency (children)

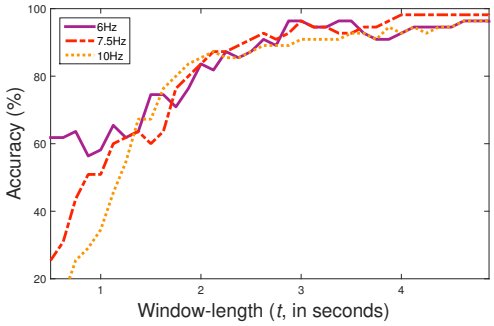

(d) Training phase accuracy for each stimulation frequency (adults)

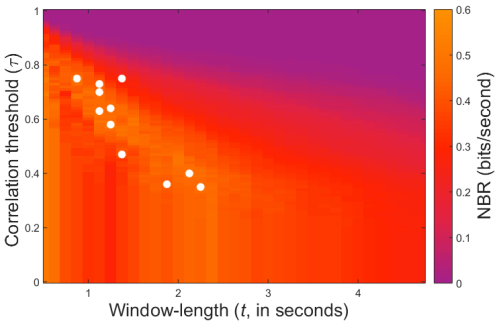

(e) Bitrate as a function of t and τ (children)

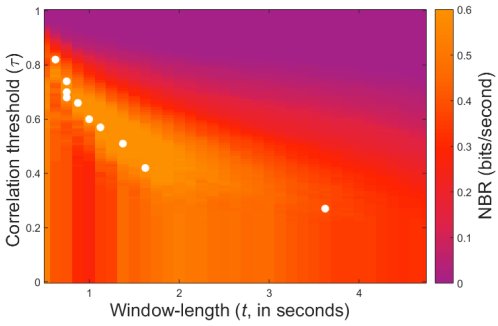

(f) Bitrate as a function of t and τ (adults)

Figure 3.2: Performance of participants from data collected during the training phase. Accuracy of (a) included children versus included adults, (b) included children versus excluded children, (c) included children for each stimulation frequency, and (d) included adults for each stimulation frequency as a function of t for $\tau = 0$. Images showing bitrate calculated for each t and τ for (e) included children and (f) included adults. The t and τ values used in the experimental phase are denoted using a white dot.

$S16$) had a t of 3.625 seconds, 1.375 seconds longer than any of the children who participated in the study. There was no difference in the τ values calculated for children (Mean = 0.56, Mdn = 0.58, SD = 0.15) compared with

adults (Mean = 0.60, Mdn = 0.60, SD = 0.15).

Post-Experiment Analysis

Since there were differences in the classifiers (Section 3.3.6) used to calculate the t and τ values for children versus those calculated for adults, we performed an additional analysis of the training data after the experiments were completed. This analysis used the exact same classifier for all participants. This post-experiment analysis (using the Mann-Whitney U test with no correction for multiple comparisons) of the training data (Tables 3.1- 3.3) for the included participants did not reveal any differences ($p < 0.05$) between children and adults in terms of accuracy, latency, or NBR. During the training phase, the children would have selected targets with a similar accuracy (Mean = 92%, Mdn = 93%, SD = 6%) as adults (Mean = 96%, Mdn = 93%, SD = 3%), latency (Mean = 1.93 seconds, Mdn = 1.83 seconds, SD = 0.40 seconds) as adults (Mean = 1.75 seconds, Mdn = 1.74 seconds, SD = 0.74 seconds), and NBR (Mean = 0.72 bits/seconds, Mdn = 0.78 bits/second, SD = 0.20 bits/second) as adults (Mean = 0.90 bits/second, Mdn = 0.91 bits/second, SD = 0.26 bits/second). Similarly to the analysis of the parameters used during the experiments, the t calculated for children (Mean = 1.43 seconds, Mdn = 1.25 seconds, SD = 0.45 seconds) were slightly longer ($p = 0.04$) than for adults (Mean = 1.23 seconds, Mdn = 1.00 seconds, SD = 0.85 seconds). There were not, however, any differences in the values of τ for children (Mean = 0.58, Mdn = 0.63, SD = 0.16) and adults (Mean = 0.60, Mdn = 0.60, SD = 0.15). Figure 3.2a represents the similarity between the children and the adults graphically. When the accuracy of classification for a τ of 0 is plotted against t, we can see that children and adults improve in accuracy as a function of t. Figure 3.2b shows accuracy curves for the participants who were excluded from the study. Unlike the included children, the accuracy of excluded children (for $\tau = 0$) does not increase as much as a function of t. These same accuracy as a function of t curves are shown by frequency of stimulation for children (Figure3.2c) and adults (Figure3.2d). Figure 3.2e shows the τ and t values calculated for each child overlaid on a image of the average NBR for each possible value of τ and t. A similar image for the adults is shown in Figure 3.2f.

Table 3.1: Post-Experiment Analysis of Data from Training Phase (Included Children)

Subject	t	τ	Accuracy	Latency	NBR
S01	1.375	0.75	0.87	2.40	0.51
S02	1.125	0.70	0.87	1.38	0.79
S03	2.125	0.40	0.87	2.41	0.44
S04	1.375	0.47	1.00	1.57	1.01
S05	0.875	0.75	1.00	1.58	1.00
S06	2.250	0.35	0.87	2.60	0.46
S07	1.125	0.63	0.93	2.14	0.69
S08	1.250	0.58	0.93	1.70	0.78
S09	1.250	0.64	0.93	1.70	0.78
S10	1.875	0.36	0.87	1.92	0.62
S11	1.125	0.73	1.00	1.83	0.86
Mean	1.432	0.58	0.92	1.93	0.72
Mdn	1.250	0.63	0.93	1.74	0.91
SD	0.448	0.16	0.06	0.40	0.20

Table 3.2: Post-Experiment Analysis of Data from Training Phase (Excluded Children)

Subject	t	τ	Accuracy	Latency	Bitrate
S23	0.500	0.00	0.40	0.50	0.42
S24	0.500	0.00	0.40	0.50	0.98
S25	0.500	0.00	0.60	0.50	1.05
Mean	0.500	0.00	0.47	0.50	0.82
Mdn	0.500	0.00	0.40	0.50	0.98
SD	0.000	0.00	0.12	0.00	0.35

Lower the threshold to chance and find the window-length and threshold that give the highest bitrate.

Table 3.3: Post-Experiment Analysis of Data from Training Phase (Included Adults)

Subject	t	τ	Accuracy	Latency	Bitrate
S12	1.000	0.60	0.93	1.17	1.14
S13	1.375	0.51	0.93	1.76	0.75
S14	1.125	0.57	1.00	1.86	0.85
S15	0.750	0.70	1.00	1.80	0.88
S16	3.625	0.27	0.93	3.76	0.35
S17	1.625	0.42	0.93	2.13	0.62
S18	0.750	0.68	0.93	1.12	1.18
S19	0.750	0.74	0.93	1.43	0.93
S20	0.875	0.66	0.93	1.19	1.11
S21	0.625	0.82	1.00	1.33	1.20
S22	1.000	0.60	1.00	1.74	0.91
Mean	1.227	0.60	0.96	1.75	0.90
Mdn	1.000	0.60	0.93	1.74	0.91
SD	0.849	0.15	0.03	0.74	0.26

3.4.2 Experimental Phase

A post-hoc analysis of the data (using the Mann-Whitney U test) did not reveal any differences between the children and adults in terms of accuracy, latency, or NBR for the first four rounds of the experimental phase. Nor was there a difference between children and adults in the number of targets selected during the bonus round of the experimental phase. Both children (Mean = 79%, Mdn = 83%, SD = 14%) and adults (Mean = 78%, Mdn = 80%, SD = 11%) achieved similar levels of accuracy during the experimental phase and both groups had worse performance during the experimental phase than during the training phase. In terms of latency, the children (Mean = 2.106 seconds, Mdn = 2.073 seconds, SD = 0.48 seconds) were almost 0.2 seconds slower than the adults (Mean = 1.917 seconds, Mdn = 1.710 seconds, SD = 0.73 seconds). Children (Mean = 0.50 bits/second, Mdn = 0.49 bits/seconds, SD = 0.20 bits/second) also transmitted information at a slightly lower NBR than the adults (Mean = 0.56 bits/second, Mdn = 0.59 bits/second, SD = 0.25 bits/second). Finally, children selected slightly fewer targets in the bonus round (Mean = 27.27 targets, Mdn = 17.00 targets, SD = 28.92 targets) than the adults (Mean = 36.54 targets, Mdn 28.00 targets,

SD = 30.45 targets).

The data were also inspected for differences in accuracy and latency of selection of targets by frequency (Figure 3.4) and round (Figures 3.5). No differences were found.

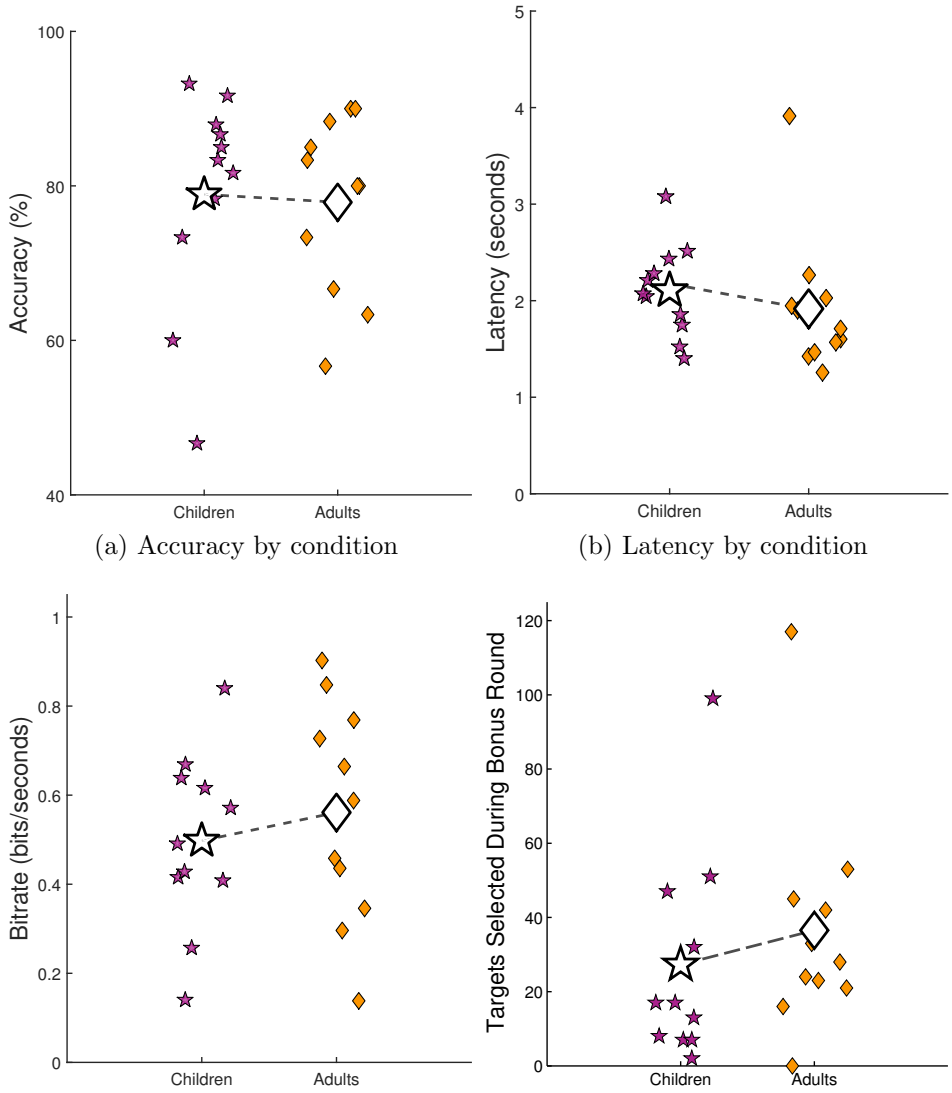

(a) Accuracy by condition

(b) Latency by condition

(c) Nykopp bitrate by condition

(d) Targets selected in bonus round by condition

Figure 3.3: Performance of participants during the experimental phase in terms of (a) accuracy, (b) latency, (c) NBR, and (d) number of targets selected during the bonus round.

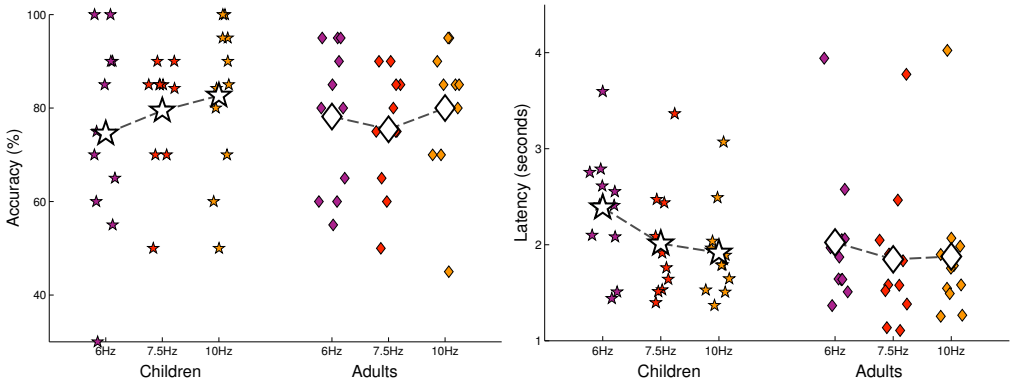

(a) Accuracy for each stimulation frequency (b) Latency for each stimulation frequency

Figure 3.4: Performance of included children versus included adults during the experimental phase by stimulation frequency in terms of (a) accuracy and (b) latency.

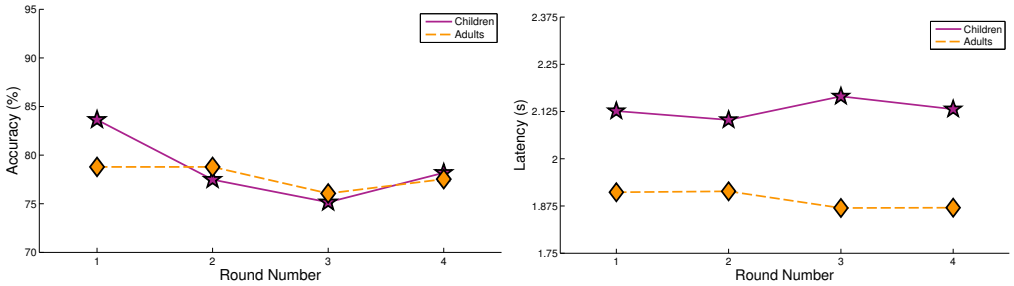

(a) Accuracy by round (b) Latency by round

Figure 3.5: Performance of included children versus included adults during the experimental phase by round in terms of (a) accuracy and (b) latency.

3.5 Discussion

This study demonstrated that 9-11 year old children are able to use an SSVEP-based BCI with much higher accuracy than previously reported. This is also the first work to report their performance in terms of latency, bitrate (NBR), and engagement. Furthermore, the results showed that the accuracies and NBRs of the children who completed the experimental phase were nearly identical to that of the adults who completed the experimental phase. The remainder of the discussion is organized by phase: first we discuss the training phase, we then discuss the experimental phase, and we conclude by considering future work.

3.5.1 Training Phase

A short training phase was used to calibrate the BCI system and to screen participants for inclusion in the experimental analysis. Data from the short training phase show that 11 of the 14 children (Table 3.1) and all 11 adults (Table 3.3) included in this study met the minimum threshold for inclusion in the experimental analysis. Three children did not meet the criteria for their data to be included in the experimental analysis (Table 3.2).

The experimenters noted that two of the excluded children were visibly distracted during the short training phase. In general, the experimenters noticed that the children appeared more physically engaged during the experimental phase than during the training phase. During the experimental phase children made physical adjustments such as sitting up straighter in their chairs or moved their heads to be aligned with the SSVEP-targets. They did not make these same adjustments during the training phase. Previous work evaluating engagement has shown physical movement is linked to levels of engagement [114]. It is possible the observed behavior in our study could be an indication of increased engagement during the experimental session.

An offline analysis of the data from the training phase revealed a trend in the data where adults selected targets with a shorter latency and higher bitrate than children (Figure 3.2a). It is possible that—if a difference exists—this reflects developmental differences between 9-11 year old children and adults. Ehlers [57] hypothesized that developmental differences could explain why children performed with a lower accuracy than adults. Another possible explanation is that children were not properly motivated to engage with the training task, resulting in lower performance.

3.5.2 Experimental Phase

In the experimental phase children and adults were asked to select a sequence of targets using an SSVEP-based BCI. An analysis of the experimental phase demonstrates that the accuracies and NBRs of the children who completed the experimental phase was nearly identical to that of the adults who completed the experimental phase. This inspiring result indicates that 9-11 year old children are able to use an SSVEP-based BCI with similar performance

to adults. In addition, this result provides evidence that SSVEP-based BCIs could be used to replace lost function in children with physical disabilities.

There were several differences between our experiments and the only previous study of SSVEP-based BCIs for children. First, the environment in which the children completed the experiments was different. In Ehlers et al. [57] children performed the experiments in a noisy school environment, while in our experiments they were in a quiet laboratory environment. Second, the tasks were different. The children in our study used the SSVEP-based BCI to complete a simple target selection task. In Ehlers et al [57], children completed a text-entry task. Text-entry is a very common platform for SSVEP-based BCI experiments [3, 197], but may not be appropriate for children [92]. Third, our experiments used slightly different stimulation frequencies. The frequency of stimulation is known to have an affect on the amplitude of the elicited SSVEP [197]. Fourth, we conducted a short training phase to set two classifier parameters before the longer experimental phase. It is possible that any of these methodological differences could explain why children in our study had higher performance than the similar age group of children in the study by Ehlers et al. [57].

Children selected targets slightly slower (but not significantly slower) than adults. This could be attributed to several factors during the longer experimental phase. One possibility is that children do not generate an SSVEP response as quickly as adults do. An alternative possibility is that the way the short training phase was conducted limited the speed with which children could select targets.

3.5.3 Future Work

Given the high performance of the children in this study, it would be interesting to know how younger children compare to the 9-11 year olds investigated here. Data collected during the experiments of Ehlers et al. [57] suggest a slight downward trend in accuracy with low-frequency stimuli as a function of age. Ehlers et al. [57] did not report any significant differences, however, between children of 6.73, 8.08, or 9.73 years-of-age. Our study provides a baseline data for 9-11 year old children that could be used as a basis of comparison with data collected from younger children.

In summary, our data make several contributions to the development of SSVEP-based BCIs for children. We report that of the fourteen 9-11 year children who participated in our study, 11 of them achieved an 85% accuracy or above during a short training phase. Furthermore, of the 11 children who completed the longer experimental phase, they achieved an average accuracy of 79% in 2.1 seconds. We obtained a much higher classification accuracy than the only other previous investigation of SSVEP-based BCIs for children. In addition, the results suggest that the performance of children may be relatively similar to adults using the same SSVEP-based BCI. Finally, this data is the first reported on children to include performance in terms of accuracy, latency, and bitrate.

3.6 Classification of the Predicted Target

These equations are based on the original description of canonical correlation for classification of SSVEP targets by Lin [112]. Assuming k stimuli at frequencies $f_1 ... f_k$, CCA considers two sets of variables X and Y_k and finds two weight matrices w_X and w_{Y_k} that maximize the correlation ρ_k between them.

$$\rho_k = \frac{w_x^T \Sigma_{XY_k} w_{y_k}^T}{\sqrt{w_x^T \Sigma_{XX} w_x w_{y_k}^T \Sigma_{Y_k Y_k} w_{y_k}}} \tag{3.1}$$

When CCA is used to detect an SSVEP, X represents a matrix of EEG data (m channels by n samples) and Y_k represents a matrix of sine and cosine reference waves (r reference waves by n samples) at harmonic h frequencies of stimulus k.

$$Y_k = \begin{bmatrix} sin(2\pi ft1) \\ cos(2\pi ft1) \\ \vdots \\ sin(2\pi fth) \\ cos(2\pi fth) \end{bmatrix} \tag{3.2}$$

ρ_k is initially a vector with a length equal to the smaller of m and r,

however, here we consider $\rho_k = max(\rho_k)$. If

$$max(\rho) > \tau \tag{3.3}$$

then the classifier's best guess (the predicted target) is

$$\hat{k} = argmax(\rho_k) \tag{3.4}$$

Each trial of the training phase was analyzed in the following way. The analysis of each trial started at time 0, the time of stimulus onset. The data from time 0 to time t was then considered, if the $max(\rho_k)$ does not exceed the threshold, then the window slid in steps of 0.125 seconds. After the window is moved, ρ_k is recomputed and compared to the threshold again. This process continues until ρ_k exceeds τ or until t extends beyond the end of the trial. In the case that ρ_k exceeded the threshold, $\hat{k}$ is then compared to the target $x^\star$. If ρ_k does not exceed τ before the end of the trial, then this was modeled in the calculation of NBR as an erasure.

3.7 Supplemental Information

Table 3.4: Data from Training Phase (Included Children)

Subject	t	τ	Accuracy	NBR
S01*	1.375	0.75	0.87	0.57
S02*	1.250	0.77	0.87	0.78
S03	2.500	0.43	0.87	0.47
S04	1.375	0.47	1.00	1.01
S05*	1.250	0.57	0.94	0.94
S06	2.250	0.35	0.87	0.46
S07*	1.375	0.58	0.93	0.71
S08	1.250	0.58	0.93	0.78
S09	1.250	0.64	0.93	0.78
S10	1.875	0.36	0.87	0.62
S11*	1.250	0.72	1.00	0.78
Mean	1.545	0.57	0.92	0.72
Mdn	1.375	0.58	0.93	0.78
SD	0.450	0.15	0.05	0.18

* - Denotes that 3 harmonics and erasure were used for calculation of window-length and threshold.

Table 3.5: Data from Training Phase (Included Adults)

Subject	t	τ	Accuracy	NBR
S12	1.000	0.60	0.93	1.14
S13	1.375	0.51	0.93	0.75
S14	1.125	0.57	1.00	0.85
S15	0.750	0.70	1.00	0.88
S16	3.625	0.27	0.93	0.35
S17	1.625	0.42	0.93	0.62
S18	0.750	0.68	0.93	1.12
S19	0.750	0.74	0.93	0.93
S20	0.875	0.66	0.93	1.11
S21	0.625	0.82	1.00	1.20
S22	1.000	0.60	1.00	0.91
Mean	1.227	0.60	0.96	0.90
Mdn	0.849	0.60	0.93	0.91
SD	1.000	0.15	0.04	0.25

CHAPTER 4

SOFT, CURVED ELECTRODE SYSTEMS CAPABLE OF INTEGRATION ON THE AURICLE AS A PERSISTENT BRAIN-COMPUTER INTERFACE[1]

4.1 Abstract

In this chapter, a new design for an electroencephalograph (EEG) electrode that does not require electrolyte gel or mechanical fasteners is described. Recent advances in electrodes for noninvasive recording of electroencephalograms expand opportunities collecting such data for diagnosis of neurological disorders and brain-computer interfaces. Existing technologies, however, cannot be used effectively in continuous, uninterrupted modes for more than a few days due to irritation and irreversible degradation in the electrical and mechanical properties of the skin interface. Here we introduce a soft, foldable collection of electrodes in open, fractal mesh geometries that can mount directly and chronically on the complex surface topology of the auricle and the mastoid, to provide high fidelity and long-term capture of electroencephalograms in ways that avoid any significant thermal, electrical, or mechanical loading of the skin. Experimental and computational studies establish the fundamental aspects of the bending and stretching mechanics that enable this type of intimate integration on the highly irregular and textured surfaces of the auricle. Cell level tests and thermal imaging studies establish the biocompatibility and wearability of such systems, with examples of high-quality measurements over periods of 2 weeks with devices that remain mounted throughout daily activities including vigorous exercise, swimming, sleeping,

[1]This work has been previously published as [146] and is co-authored by Dong Sup Lee, Jung Woo Lee, Woosik Lee, Ohjin Kwon, Phillip Won, Sung-Young Jung, Huanyu Cheng, Jae-Woong Jeong, Abdullah Akce, Stephen Umunna, Ilyoun Na, Yong Ho Kwon, Xiao-Qi Wang, ZhuangJian Liu, Ungyu Paik, Yonggang Huang, Timothy Bretl, Woon-Hong Yeo, and John A. Rogers

and bathing. Demonstrations include a text speller with a steady-state visual evoked potential-based brain-computer interface and elicitation of an event-related potential (P300 wave).

4.2 Introduction

For more than 80 years, electroencephalography (EEG) has provided an effective noninvasive means to study human brain activity [72, 16]. EEG is instrumental in a wide range of clinical and research applications, from diagnosing epilepsy [185] to improving our understanding of language comprehension [97] and the development of brain-computer interfaces (BCI) [11]. Conventional EEG recording systems, particularly the physical interface between the sensor (commonly known as an electrode) and the head, have limitations that constrain the more widespread use of EEG monitoring. Electrodes typically consist of rigid metal disks mechanically secured to the head with a mesh cap and chin strap, where electrolyte gels [173] enable efficient electrical coupling by reducing the impedance at the skin interface. This arrangement causes skin irritation (erythema) and leads to electrical degradation for periods of use that extend more than a few hours, typically caused by drying of the electrolyte gel [63]. Recent technologies replace the gel [73, 116] with needles [73, 116], contact probes [116, 169], capacitive disks [41, 150], conductive composites [101, 137], or nanowires [141]. Such dry electrodes have some promise, but they require multistep preparations, obtrusive wiring interfaces, and/or cumbersome mechanical fixtures. These shortcomings limit the potential for long-term use in diagnosis of neurological disabilities [30, 125] or in persistent BCI [30, 205]. For example, although microneedle electrodes can record EEG signals for a few hours [204], the interface does not offer the robustness, comfort, or ease of use needed for sustained operation. Capacitive electrodes that incorporate thin, reversible adhesives to the surface of the scalp avoid some of these drawbacks, but current designs involve bulky rigid electrode structures with thicknesses in the range of several millimeters [102]. Although long-term EEG recordings are possible, this device construction [102] is susceptible to mechanically induced delamination, such that it cannot remain mounted during bathing, and it must be physically protected during sleep. Improved versions offer shapes that allow insertion into the

ear canal [100] but in a way that obstructs hearing while retaining some of the other disadvantages of the scalp-mounted systems. All of these methods also use separate sets of electrodes and interconnect wires for reference and ground. Clearly, opportunities remain for EEG recording systems that enable uninterrupted use for weeks or longer, ideally with a form of integration that is imperceptible to the subject, without significant mass, thermal or mechanical loading of the skin, and an ability to operate even during the most demanding activities, such as vigorous exercising, swimming, or showering. Spatially compact designs with complete electrode systems that can locate on regions of the head that are known to afford the strongest EEG signals are also important. In this chapter, we explore the surfaces of the outer ear (the auricle) and adjacent regions (the mastoid) as mounting locations for a type of ultrathin, foldable neural electrode platform that is capable of longterm, high-fidelity EEG recording of signals commonly used in BCI. The combined area of the auricle and mastoid represents a uniquely attractive location due to its electrical isolation from other regions of the scalp and the established use of the auricle as an effective point for reference/ground measurement electrodes [48, 115]. Mounting an electrode directly on the complex topography of the auricle presents daunting engineering challenges in integration but ones that can be overcome through the use of materials and design strategies reported here. The result is a soft, skin conformal system that can remain well bonded to the skin of these regions for more than 2 weeks, with unmatched capabilities in continuous monitoring and without the variability and uncertainty that follows from approaches that require frequent removal and reapplication. Experimental and computational studies capture the underlying physics associated with the conformal integration onto auricle surfaces, where the levels of surface curvature lie significantly beyond anything examined in past work. An integrated collection of electrodes and interconnects yields EEG data that, when used with appropriate classification algorithms, provide a long-term BCI that is compatible with steady-state visually evoked potentials-based text spellers and event-related potential (P300 wave) recordings. Studies of the fidelity of EEG alpha rhythms collected over long time periods, together with cell level tests of toxicity and skin level evaluations of biocompatibility, demonstrate advantages of these approaches.

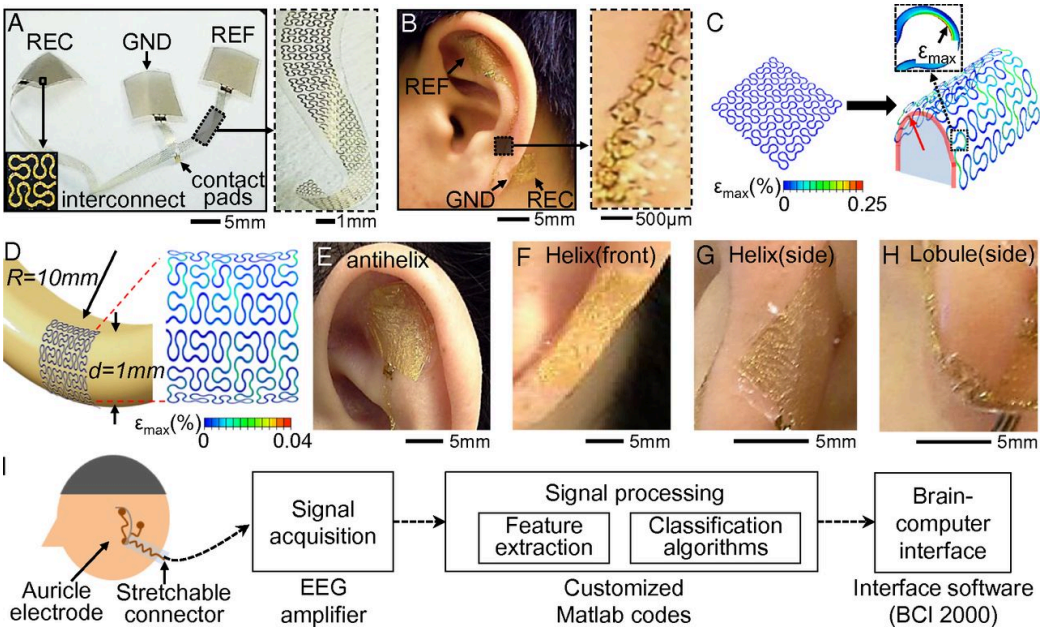

Figure 4.1: Fractal device architectures and mechanical properties of EEG measurement systems. (A) Epidermal electronics with fractal layouts, composed of three electrodes (REC, GND, and REF) and interconnect (Left), with magnified view of the latter (Right). (B) Device laminated on the auricle and mastoid (Left) and the magnified interconnect (Right). (C) FEM results of fractal structures upon mechanical bending (180°) with the radius of curvature of 0.5mm. (D) FEM results for simultaneous bending along two orthogonal axes (R, distance between tragus and outer edge of the ear; d, thickness of ear lobule). (E-H) Images of mounted devices on different regions of the ear, including the crura of antihelix, helix, and lobule. (I) Schematic illustration and a flowchart about the overall EEG recording process.

4.3 Materials and Method

4.3.1 Fabrication of Epidermal Electrodes

The device preparation used conventional microfabrication techniques. A silicon wafer served as a support for a sacrificial layer of polymethyl methacrylate (100 nm in thickness) and an overcoat of polyimide (1.2μm in thickness). Metal evaporation, photolithography, and etching defined fractal layouts. A water-soluble tape (3M) allowed retrieval of these structures after dissolution of the sacrificial layer, thereby enabling transfer onto a silicone elastomer (3μm in thickness), supported by a water dissolvable polymer sheet.

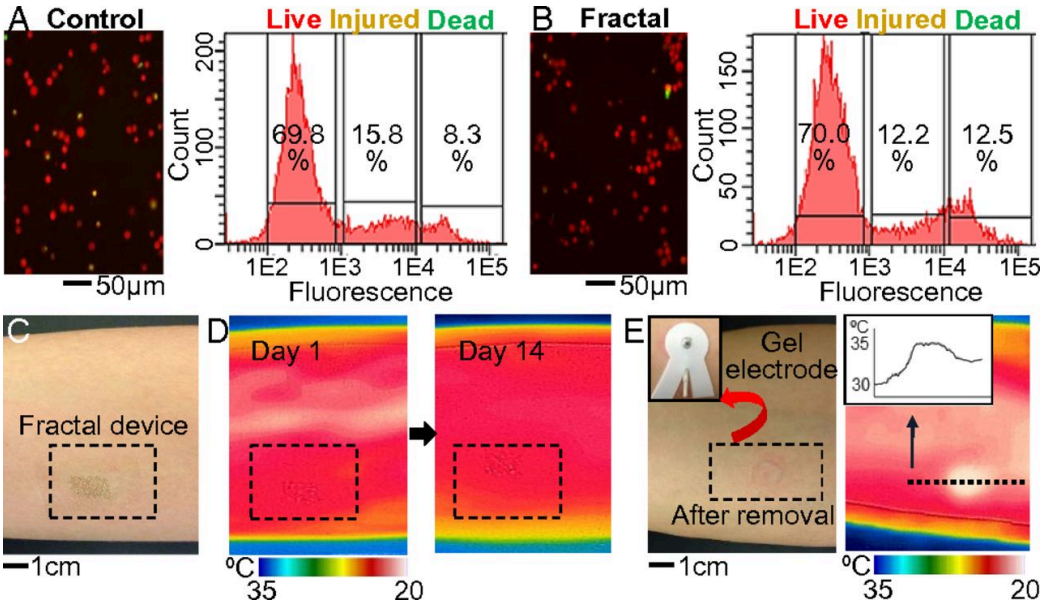

Figure 4.2: Assessments of biocompatibility by infrared thermography (IRT) and through cell-based studies. (A) Keratinocytes cultured on a control (Petri dish) with fluorescence microscopic image (Left) and quantitative measurement of cell viability (Right). (B) Keratinocytes cultured on a fractal device for comparison. (C) Image of a fractal device mounted on the forearm. (D) IRT images of the skin surface collected during 2 weeks reveal no adverse effects. (E) Image of a gel electrode removed after 1 day (Left) and IRT image showing erythema, elevated temperature on the skin (Right).

4.3.2 Fabrication of Tripolar Electrodes

The fabrication of tripolar electrodes involved formation of multiple layers of Au-PI (via)-Au using standard microfabrication techniques. An additional step of metal evaporation yielded a 500-nm-thick layer of Au for connection with the prepatterned Au through the PI layer. Patterning, retrieval, and transfer of fractal traces followed the same methods used for fabrication of epidermal electrodes, described above.

4.3.3 Fabrication of Capacitive Electrodes

The processing for capacitive devices included spin coating of a dielectric layer (3-μm-thick elastomer) on Au electrodes. This layer protected the electrodes and allowed only capacitive coupling to the skin, thereby ensuring electrically safe, robust recording of EEG. Such structures are also reusable

and compatible with cleaning using soap and water

4.3.4 Calculation of the Signal-to-Noise Ratio

This calculation used the Welch periodogram in MatLab (Mathworks) across the bandwidth of 5-30 Hz. Averaging the periodograms calculated for each trial yielded a single power spectrum. The power of the noise signal corresponds to the average value of those bins in the frequency domain outside of the range of the frequency of the signal ($\pm$0.3 Hz) or any of its harmonics. The power of the signal corresponds to the sum of the maximum power in the frequency range of the signal and its first two harmonics minus the average power of the bins at the frequency of stimulation. EEGLAB (function: topoplot) [51] plotted the SNR values as a topographical map.

4.3.5 Experiments on Human Subjects

The experiments for recording of EEG alpha rhythms and thermal imaging with TCR and capacitive electrodes involved three volunteers and were all performed at Virginia Commonwealth University [institutional review board (IRB) approved protocol: HM20001454]. The experiments for SSVEP and P300 recording were conducted at the University of Illinois at Urbana-Champaign (IRB approved protocol: 13453).

4.4 Results and Discussion

Figure 4.1A presents a completed device that includes mesh electrodes for recording (REC), ground (GND), and reference (REF), joined by a stretchable interconnect, all on a soft (modulus: 20 kPa), elastomeric film (thickness: 3 μm). The physical properties associated with this design allow lamination onto the contoured surfaces of the skin in and around the ear, to enable long-term measurements of EEG. The electrically active part of the system consists of filamentary serpentine traces (300-nm-thick and 30-μm-wide patterns of Au with 1.2-μm-thick layers of polyimide above and below), in a spatially varying, self-similar design formed with a Peano curve as the building block. This fractal layout represents an extension of recently reported ideas [76]

but where the configuration spans the entire system level to yield enhanced levels of mechanical compliance, tailored with orientational anisotropies that match the requirements for auricle integration. In particular, the interconnects use all vertical Peano curves to maximize stretchability along their longitudinal axes; the electrodes, by contrast, use a half-and-half design to balance stretchability in all directions (Figure 4.1A). The result is an overall device construct that has an effective modulus lower than that of the skin ($\sim$130 kPa) [91], to ensure conformal contact [85] and robust adhesion [216].

A critical feature of the mechanics appears in Figure 4.1B, which shows a device wrapped onto the triangular fossa, crura of antihelix, and lobule of the ear as well as the mastoid. The ability to adopt the complex surface textures of all areas of the auricle is unique to this class of ultrathin, extremely bendable electronics, largely unexplored in previous reports [91, 67, 75, 120, 155]. Mounting of the device begins with removal of hair using a razor (Gillette), if necessary, followed by mild rubbing of the auricle area using a sterile alcohol pad (Dukal Corporation) to clean the surface. Electrodes and interconnects are manually placed on the desired locations by using plastic tweezers (Ted Pella, Inc.). Soft bonding from van der Waals interactions holds the device on the skin. Gently spraying water onto the device dissolves the polymer backing layer [polyvinyl alcohol (PVA); Haining Sprutop Chemical Tech] and leaves the soft, ultrathin elastomer in contact with the skin. Careful device handling and complete dissolution of the polymer backing are important to successful mounting. The main consequence of improper mounting is high background noise in the EEG data.

The magnified image in Figure 4.1B illustrates how the stretchable interconnects maintain contact with the skin (antihelix) by conforming the uneven surfaces. These behaviors follow from exceptional levels of both bendability and stretchability, as revealed by finite element method (FEM) analysis. Figure 4.1C shows FEM results for bending and folding, where the bend angle is 180° and the radius of curvature is 0.5 mm. The maximum principal strain in the metal layers is only 0.25% (elastic limit of Au: 0.3%) [76]. Additional results in Figure 4.1D show mechanical bending simultaneously along two orthogonal axes with relevant radii of curvature (10 mm; comparable to the distance between the tragus and outer edge of the ear) and diameters (1 mm; comparable to the thickness of the ear lobule). The experimental observations (Figure 4.1E-H) are consistent with the predicted responses, as

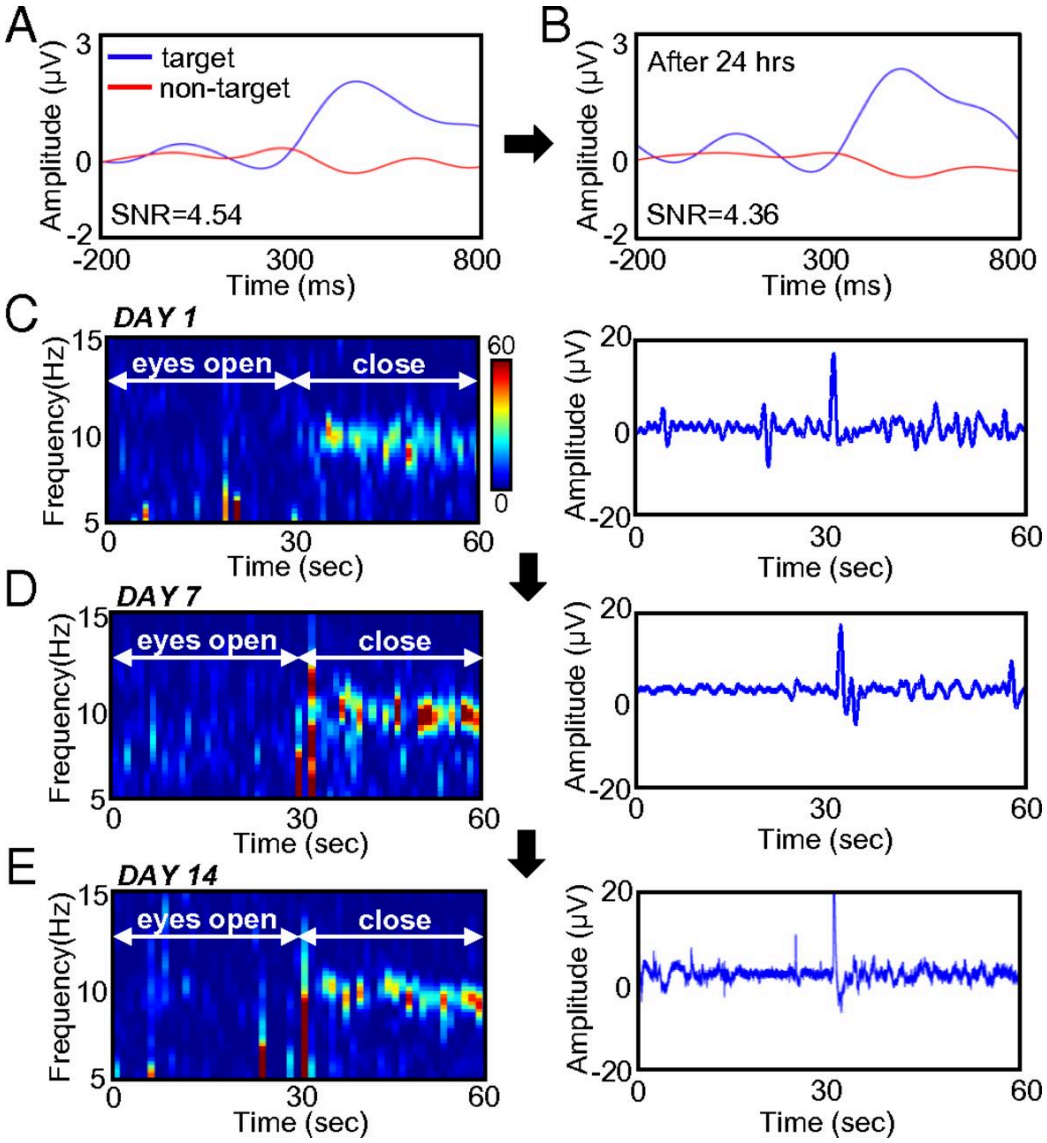

Figure 4.3: Long-term recording of EEG. (A and B) Set of P300 data collected with an LTE electrode, immediately after mounting (A) and after 24 hours (B). The SNR values are similar. (C-E) EEG alpha rhythms measured with a set of LTE electrodes for 14 days. (Left) Spectrograms showing the amplitudes as a function of the frequency for 1 minute Signals after 30 seconds are clearly detected when the eyes are closed. (Right) Plots presenting raw EEG signals. The data show no significant differences in signal amplitudes or patterns during 2 weeks of continuous wear.

illustrated by capabilities for mounting and wrapping on the ear. Further FEM analysis under uniaxial tensile loads indicates that the electrodes and interconnects can be stretched by up to ∼50%. These results suggest an ability to accommodate larger than average skin deformation (10-20%) [91, 85]

up to and including the maximum strains (∼50%) associated with motion of the knee joint.

This auricle-mounted system can be used in a sequential process for recording and interpreting EEG signals for BCI (Figure 4.1I). Standard EEG signals such as alpha rhythms can be readily captured. The three electrodes including the REC (mastoid), REF (upper antihelix), and GND electrode (earlobe) form a bipolar montage. This setup measures the differential amplitudes (REC and REF), and the GND prevents nonspecific, parasitic signals from the body. In addition to a soft, dry interface to the skin and an ability to conform to the auricle, a key point of interest is the related capabilities for long-term use

The epidermal electrode incorporates well-characterized, biocompatible materials [silicone [76], gold [202], and polyimide [12]]. Studies using keratinocyte cells demonstrate biocompatibility, as shown in Figure 4.2A-E. Fluorescence microscope images compare the status of cultured cells in three categories: live, injured, and dead by using a cell viability assay (Life Technologies) (Figure 4.2A and Figure 4.2B). The numbers of live cells grown on a device and on a control (cell culture Petri dish) are identical within statistical uncertainties. Directly relevant studies involve devices mounted onto subjects for comparative assessments using infrared thermography [52, 153]. Data indicate no adverse effects up to 2 weeks (Figure 4.2C and Figure 4.2D), where a thin overcoat of spray-on-bandage material (3M) ensures survivability during normal daily activities, such as exercising, showering, or swimming. Conventional gel electrodes, by contrast, show clear signs of erythema (elevated temperature in Figure 4.2E) after 1 day. Furthermore, the gels exhibit a ∼50% reduction in volume due to evaporative drying over 6 hours, consistent with the previous observations [206, 107, 110] of significant increases (2-4 times) in skin-electrode impedance due to the gel dehydration (within 6 hours). Evaluations used gel electrodes mounted on a skin replica (polydimethylsiloxane; Dow Corning), placed on a hot plate (Super-Nuova; Thermo Scientific) to mimic the human skin (temperature: ∼37°C). These and other drawbacks render such conventional gel electrodes unsuitable for continuous, long-term use.

The results in Figure 4.3 establish that the long-term epidermal (LTE) electrodes presented here offer fidelity in EEG measurement that compares favorably to that of conventional electrodes. The main advantage of the LTE

technology is in its long-term utility, as demonstrated in recordings using electrical connections established in reversible fashion at the peripheral pad terminations of the Peano fractal interconnects. The mechanically compliant, reversible interactions facilitated by van der Waals forces provide low electrical resistance for EEG recording. Before the electrical connection, gentle rubbing with a sterile alcohol pad cleans the surface of the pad and connector. A portable, compact microscope (AnMo Electronics) enables exact positioning of the connector. During the course of the experiments, involving multiple cycles of measurements, we observed no significant degradation of the connector. Rather, eventual failure of the system occurs due to peeling of the device electrodes from the skin, likely associated with accumulation of exfoliated cells from the stratum corneum.

A thin layer ($\sim$1 μm) of spray-on bandage, applied once or twice a day, facilitates strong bonding to the skin and provides environmental protection [85]. Bipolar EEG recordings collected at various time points during 2 days (recording of P300, as described in a subsequent section) and 2 weeks (recording of alpha rhythms) with normal living behaviors such as working, exercising, or showering illustrate the electronic viability. Qualitative monitoring by contact microscopy reveals no adverse effects such as rashes, redness, or allergic reactions. Figure 4.3A and Figure 4.3B show P300 data collected over 24 hours on the skin (mastoid and forehead). The signal-to-noise (SNR) ratio corresponds to the ratio of the signal power (from target) to the noise power (from nontarget). The SNR values for these two cases are nearly identical, and they are comparable to the signals obtained using freshly applied conventional electrodes with conductive gels.

Another example of long-term use involves recording of EEG alpha rhythms from the auricle and mastoid over a 2-week period. Alpha rhythms typically have frequencies between 8 and 12 Hz, centered at $\sim$10 Hz [11]. Recordings during wakeful relaxation with the eyes closed and open appear in Figure 4.3C-E. Frames on the left show EEG spectrograms for frequencies between 5 and 15 Hz; the graphs on the right present typical raw EEG signals. The sharp features that appear at $\sim$30 s correspond to signals that arise from blinking. The overall data reveal no significant differences from day 1 to day 14. The polymer overcoat (sprayon bandage) is breathable, thereby avoiding adverse side effects associated with sweating during activities involved in the longterm evaluations. The slightly increased levels of background noise, es-

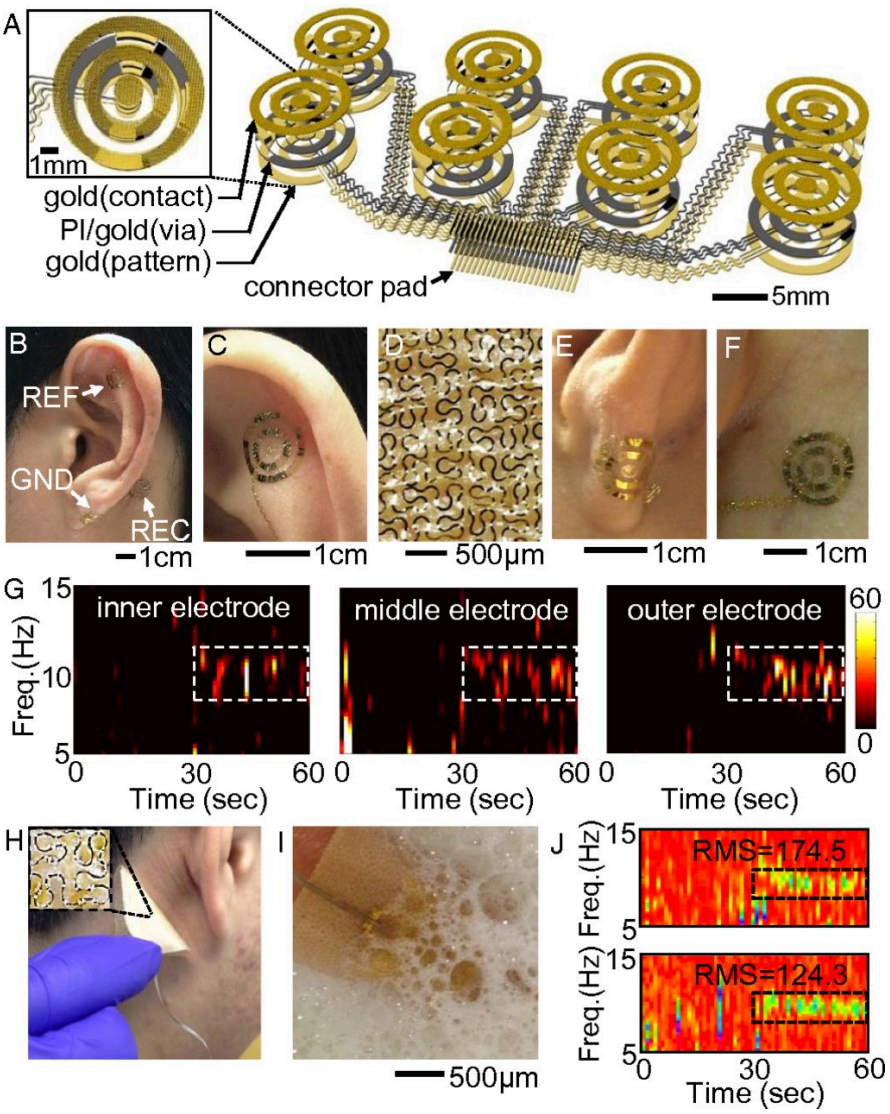

Figure 4.4: EEG electrodes with tripolar concentric ring (TCR) and capacitive designs. (A) Schematic illustration of TCR electrodes where a single set of three rings occupies the same area as a conventional metal electrode. (B-F) Images of TCR electrodes. (B) Integrated set of electrodes on the auricle and mastoid. (C) Enlarged view of the REF (upper antihelix). (D) Magnified view of fractal meshes. (E) GND on lobule. (F) REC on mastoid. (G) Spectrograms of EEG alpha rhythms recorded by the TCR electrodes including inner, middle, and outer rings. (H) Capacitive electrode mounted on the skin by a silky fabric. (I) Process of washing the electrode in soap water. (J) EEG alpha rhythms to compare signals before and after washing the electrode for ten cycles. The RMS values show the retained device functionality.

pecially on day 14, may arise from the buildup of naturally exfoliated dead cells on the skin surface [216].

Tripolar concentric ring (TCR) and capacitive electrodes offer enhanced spatial resolution and increased levels of robustness and electrical safety in operation (Figure 4.4). LTE designs afford an ability to exploit TCR layouts in ways that avoid the electrical blurring effects that occur with electrolyte gel-based systems [159]. Here a single set of three ring-shaped electrodes can occupy the same area as a single, conventional electrode (1 cm in diameter) (Figure 4.4A).

The 3D schematic illustration in Figure 4.4A shows an array of eight epidermal TCR-LTE electrodes with top fractal electrodes (Au), interlayer dielectric (PI) and metal (Au), and a base layer of interconnects and connector pads (Au) for interfaces to external data acquisition systems (Section 4.3). The magnified illustration in Figure 4.4A shows a TCR set where the top electrodes consist of fractal half-and-half patterns with a Peano design motif.

Figure 4.4B-F illustrates TCR-LTE electrodes mounted on the auricle and mastoid, supported by a 3-μm-thick elastomer. As with the basic structures of Figure 4.1, each case involves conformal contact against these curvilinear surfaces. A set of TCR-LTE electrodes can readily measure EEG alpha rhythms with REC (mastoid), REF (upper antihelix), and GND (lobule) (Figure 4.4). Figure 4.4C-F presents magnified images. Figure 4.4G presents spectrograms of EEG alpha rhythms from each ring electrode (inner, middle, and outer), which reveal an increased power ($\sim$10 Hz frequency) after the subject closed eyes (30-60 seconds).

Figure 4.4H-J summarizes capacitive designs using an elastomeric insulating layer (3 μm in thickness) over the electrodes (Section 4.3). This capacitive layout electrically isolates the metal components of the device from the skin [84] to avoid direct electrical loading and also to allow multiple cycles of cleaning with soap and water and disinfection with isopropyl alcohol antiseptic [76]. Here the capacitive electrode (fractal Peano half-and-half) bonds to a silky, washable, silicone material (Enaltus) (Figure 4.4H). For recording of EEG alpha rhythms, capacitive electrodes laminate onto the skin (mastoid and forehead for the REC and REF, respectively). Figure 4.4I demonstrates the ability to wash these electrodes in soap/water. For recording, the output passes to a preamplifier with ultrahigh input impedance ($>$ 5 109 Ω and $\sim$110 pF; BioRadio 150; CleveMed) to allow signal acquisition with low loss.

This system provides a common-mode rejection ratio of 90 dB. Recording used 60-Hz notch and low-pass (Butterworth) filters and a sampling rate of 960 Hz, with a gain of ∼50 dB. EEG alpha rhythms acquired before (top) and after (bottom) ten cycles of washing appear in Figure 4.4J. The spectrograms clearly show alpha rhythms after 30 seconds with the eyes closed, with negligible differences between these cases.

The recording of EEG data and the device capabilities for continuous long-term use can be illustrated through BCI experiments. Visually evoked potentials serve as the basis for BCIs based on steady-state visually evoked potentials (SSVEP) and the P300 event-related potential. Attentional processes [138] affect the signal amplitudes, thereby rendering information on a set of user-intended targets as the basis for a BCI. Figure 4.5 presents results from a BCI for a text speller. The experimental setup in Figure 4.5A includes the visual stimuli, a participant wearing the electrodes, an amplifier, an analog-to-digital converter, classifier, and software (BCI2000) [171]. Three male volunteers with normal or corrected-to-normal vision demonstrate the feasibility of an SSVEP-based BCI. The experiment involved testing and experimental sessions on different days. Initial evaluations with a set of 40 conventional electrodes (Figure 4.5B) yielded data to guide optimal positioning of electrodes. The numbers in Figure 4.5B correspond to the channels, with a reference electrode on the ear. An optical tracking system (Polaris Vicra; NDI) identified the precise locations. Following the digitization process, each participant attended to a series of SSVEP stimuli. EEG recordings occurred during the course of 60 trials, each with a single stimulus flickering at 6, 6.67, 7.5, 8.57, or 10 Hz for 20 seconds, with 5 seconds between trials and a null condition. The algorithms to determine optimal placement and to classify the online experiments were based on canonical correlation analysis (CCA) [112, 19]. This process is visualized using a topographic map of the SNR ratio (Figure 4.5B). Figure 4.5C presents an alternative representation of this data according to the channels (subject 2 at a stimulation frequency of 8.57 Hz).

Figure 4.5D illustrates the text speller interface, which includes a question posed to the user, defined as a mapping from the visual targets to a set of possible characters. The highlighted characters in Figure 4.5D illustrate such a mapping. Each visual target flickers at a unique frequency, allowing a CCA-based classifier to determine the users desired character. The simplified

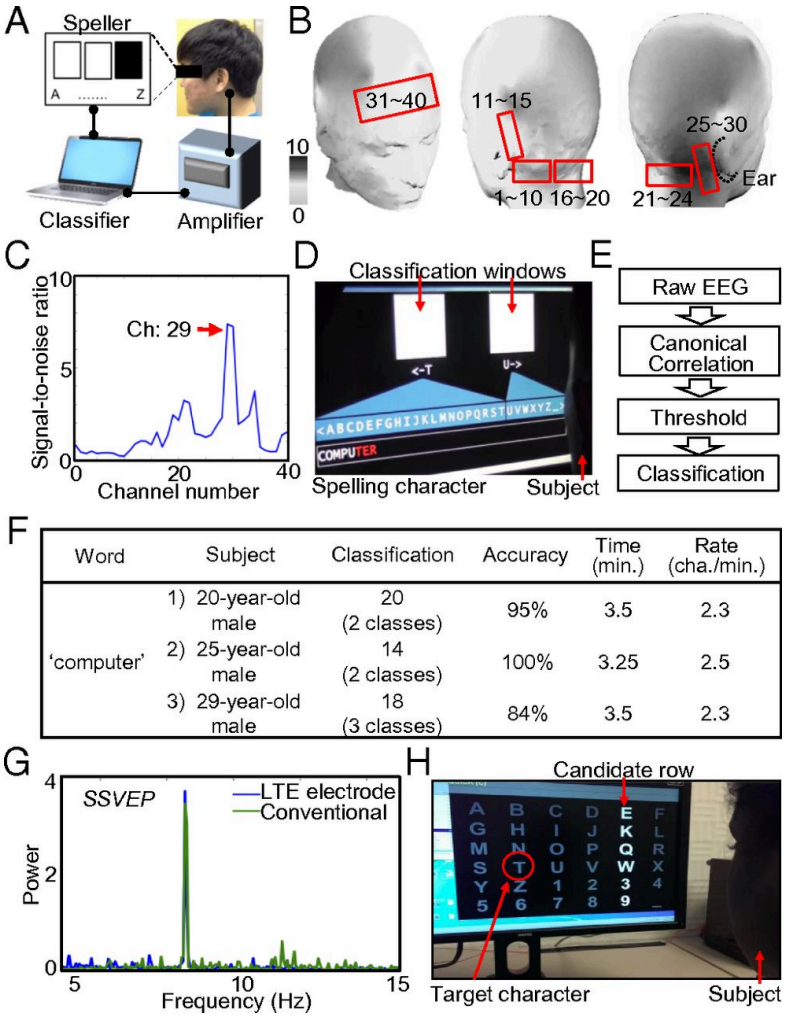

Word	Subject	Classification	Accuracy	Time (min.)	Rate (cha./min.)
'computer'	1) 20-year-old male	20 (2 classes)	95%	3.5	2.3
	2) 25-year-old male	14 (2 classes)	100%	3.25	2.5
	3) 29-year-old male	18 (3 classes)	84%	3.5	2.3

Figure 4.5: Recording of steady-state visually evoked potentials (SSVEP) and P300 and their use for brain-computer interfaces. (A) Experimental setup for SSVEP-based text speller, showing a visual stimulation, a volunteer wearing electrodes, and a signal amplifier and classifier. (B) Brain mapping with 40 electrodes to identify locations that yield the highest signals. (C) Plot of SSVEP signal quality according to the location. (D) Image of the text speller interface including visual stimulation, classification algorithm, and a volunteer watching the flickering windows. (E) Flowchart of the simplified classification process. (F) Summarized performance of three subjects in the spelling task. The averaged spelling rate for computer with word prediction is 2.37 characters/min, and the averaged accuracy is 93%. (G) Comparison of the signals for LTE and conventional gel electrodes. Both exhibit similar patterns and amplitudes. (H) Image of the P300-based text speller to record the event-related potentials to identify the desired letter.

classification steps appear in the flowchart of Figure 4.5E. When the user chooses a target, the interface updates a model of its belief and then selects a new query. Three subjects attempted to spell "computer" with the assistance of word prediction algorithms [3]. Figure 4.5F summarizes the performance for three subjects. The averaged spelling rate is 2.37 characters per min, which is only a factor of two to three times slower than a full cap system that uses 8-10 electrodes on the hairy scalp (4-7 characters per min) [36]. Figure 4.5G compares an SSVEP from an LTE electrode with that from a conventional electrode (subject 2, channel 23). The results exhibit similar patterns and amplitudes.

P300 event-related potentials (ERP) provide an additional example of a BCI (Figure 4.5H). This study began with acquisition of baseline data using conventional electrodes at four sites (each auricle, mastoid, and forehead) and compared with LTE electrodes to measure P300 ERP. A participant responded to a series of words including "brown", "fox", "epidermal", and "electrode". Our data primarily show components of the P300 at 0.3-4 Hz. The data were baseline corrected to the 200-ms period before the stimulus onset and then averaged to yield an ERP. The result of the recorded P300 ERP (Figure 4.3A and Figure 4.3B) clearly distinguishes responses to target and nontarget stimuli.

The collection of results presented here illustrates that extremely compliant electrodes allow integration with demanding regions of the head such as the auricle, for long-term EEG recording, without gels, via direct contact or capacitive coupling. The system level fractal design for both the electrodes and the interconnects is a critical feature that affords excellent levels of both bendability (>180°) and stretchability (>50%). Thermal imaging and EEG studies provide evidence for noninvasive, biocompatible interfaces to the skin, with electrical properties that support invariant recording quality over periods that extend to 2 weeks. Areas for future work include further modeling and experimental study of tripolar electrodes and development of wireless communication and power supply systems that can co-integrate with these auricle mounted electrodes.

CHAPTER 5

"OK BRAIN": A COMPARISON OF SPEECH, TOUCH, AND SSVEP-BASED BCI INPUTS FOR HEAD-MOUNTED DISPLAYS[1]

5.1 Abstract

In this chapter, the application of steady-state visual evoked potential (SSVEP)-based brain-computer interfaces (BCIs) for augmented and virtual reality head-mounted displays (HMDs) is explored. Specifically, steady-state visual evoked potential (SSVEP)-based brain-computer interfaces (BCIs) were evaluated as an input mechanism for HMDs. This evaluation compared the performance of three input mechanisms (speech recognition, touch gestures, and SSVEP) on a commercially available HMD with SSVEP-based BCI on a desktop monitor. The results of this comparison study showed that users of an SSVEP-based BCI on a desktop monitor can complete a binary decision task with greater than 98% accuracy in an average of 1.21 seconds, resulting in an average bitrate of 0.76 bits/second. A post-hoc non-inferiority analysis showed that the bitrate of the SSVEP-based BCI on a desktop was as high or higher than speech recognition or touch gestures. While SSVEP-based BCI on an HMD was significantly slower than SSVEP-based BCI on a desktop and touch gestures, it still achieved 96% accuracy after 2.2 seconds. These results show that SSVEP-based BCIs may provide a viable input mechanism for HMDs and, in particular, suggest that there may be conditions under which SSVEP-based BCIs are comparable in performance to existing HMD input mechanisms.

[1]This work includes significant scientific contributions from J. Mullins, E. Johnson, O. Choudhary, T. Bretl, and C. Shin.

5.2 Introduction

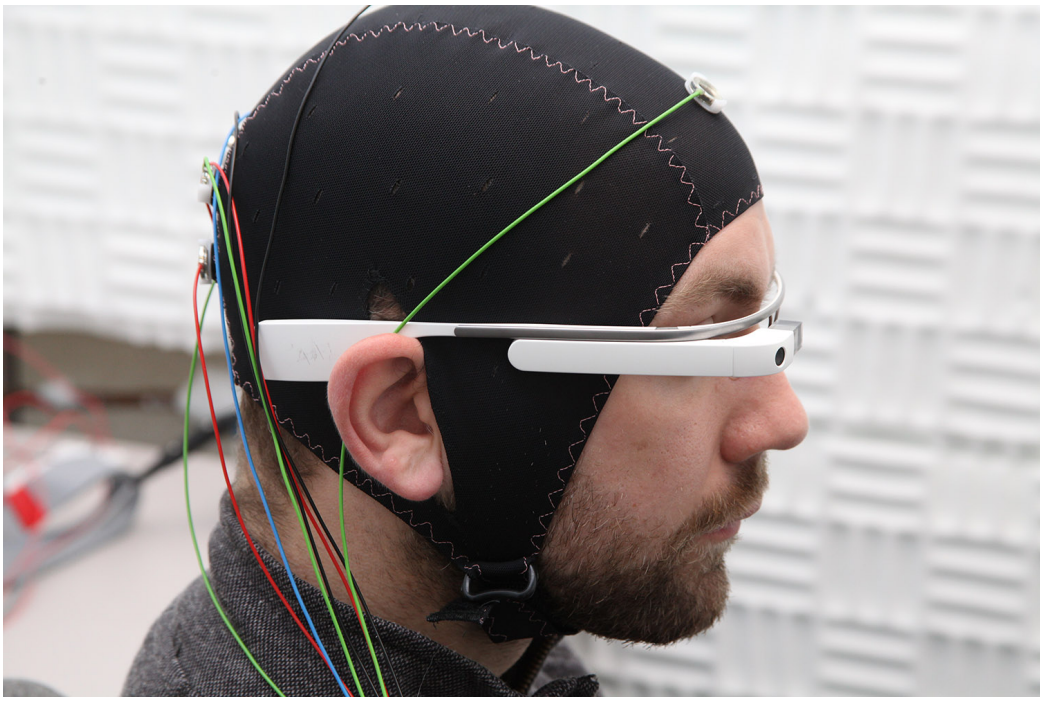

Figure 5.1: User wearing head-mounted display and EEG electrode cap.

Augmented reality head-mounted displays (HMDs) provide a method for enhancing our interactions with our environment by superimposing virtual objects over real ones. Common interactions include object selection or manipulation, navigation, and application control [26]. For example, researchers have demonstrated the use of augmented reality HMDs for annotating academic posters [190], providing real-time navigation during exercise routines [143], and for controlling a speech loudness application [129].

A variety of input mechanisms are used to interact with HMDs. Some input mechanisms like speech recognition, touch gestures, and head movements are already part of commercial devices. Other input mechanisms like hand-to-face gestures [178], 3D hand-held controllers [78], and gaze tracking [191] are the topic of active research.

Non-invasive brain-computer interfaces (BCIs) based on electroencephalography (EEG) are another potential input mechanism for use in HMDs. While different EEG signals can be used to obtain inputs for a BCI, here we consider the use of steady-state visual evoked potentials (SSVEPs). SSVEP-based BCIs rely on the brain's natural response to a repetitively flickering stimu-

lus. When a user allocates their attention to a flickering stimulus, it causes an increase in EEG activity at the same frequency as that stimulus [135] as well harmonic frequencies of that stimulus [140]. Since this change in EEG activity is related to the user's spatial attention, the user is able to select a single target from a set of potential targets simply by moving their attentional focus. This allows SSVEP-based BCI designers to treat an SSVEP stimulus as a button that a user activates via their attention. SSVEP-based BCIs have previously been shown to provide fast and reliable inputs [197] with little to no training [8].

There have been relatively few studies of SSVEP-based BCIs for virtual or augmented reality applications. Legény et al. [104] examined how SSVEP stimuli could be integrated into a virtual environment, concealing them in the wings of simulated butterflies. Faller et al. [59] developed an application framework for controlling a 3D avatar using SSVEP-based BCIs. They then demonstrated this framework by having participants navigate an avatar through an apartment in both virtual [59] and augmented reality [58] scenarios.

While these works have shown that it is possible to use an SSVEP-based BCI for HMDs, there are no studies comparing the performance of SSVEP-based BCIs to existing HMD input mechanisms. The lack of research could be due to the perception that BCI input performance is much worse than that of currently existing input mechanisms [161, 117] (also discussed by Allison [4]). Recent research by Koo and Choi [94] support this perception in the context of HMDs by reporting SSVEP-based BCI input accuracies of between 38% and 94% using 12 seconds of stimulation with a virtual reality device [94]. Using a traditional SSVEP stimulator, however, Volosyak [197] demonstrated that users could input commands with a six-class SSVEP-based BCI with 100% accuracy in as little as 1.3 seconds.

In this chapter, we evaluated the performance—in terms of bitrate—of SSVEP-based BCI in comparison to existing HMD input mechanisms. Based on the perception that the performance of BCI-based inputs is inherently slow, we hypothesized that inputs obtained from an SSVEP-based BCI would have a significantly lower bitrate than existing input mechanisms on an HMD. To test this hypothesis, we asked subjects to use four different input mechanisms to complete a binary decision task. Three input mechanisms were implemented on a commercially available augmented reality HMD, the Google

Glass, including: touch gestures, speech recognition, and SSVEP-based BCI. The fourth input mechanism, SSVEP-based BCI on the desktop, was included as the "gold-standard" of current BCI research. Contrary to our expectations, there was no significant difference between the SSVEP-based BCI on the desktop, speech recognition, and touch gestures. Furthermore, only touch gestures and the SSVEP-based BCI on the desktop provided a significantly higher bitrate than SSVEP-based BCI on the HMD.

Based on our results, we also performed post-hoc analyses of non-inferiority to test whether the performance of SSVEP-based BCI on the desktop was as good or better than speech recognition and touch gestures. Results from these tests showed that SSVEP-based BCI on the desktop was non-inferior to both the speech recognition and touch gesture conditions. While the post-hoc nature of these tests precludes strong conclusions, they do provide evidence that SSVEP-based BCIs are a viable option for HMDs, one that warrants further study.

5.3 Method

5.3.1 Participants

We performed experiments with 12 able-bodied volunteers. All participants had normal or corrected-to-normal vision and no history of neurological illness. The experiments were approved by the University of Illinois Institutional Review Board.

5.3.2 EEG Recording

EEG signals were extracted from six tin electrodes located at 10-5 international sites: PO3, PO4, POZ, O1, OZ, O2.[151] Electrode impedances did not exceed 10kΩ. All electrodes were referenced to location CZ with a ground electrode placed on the right ear lobe. The EEG signals were amplified using a James Long bioamplifier, band-pass filtered from 1Hz to 30Hz, and digitized at 1000 Hz using a National Instruments data acquisition unit (Model PCI-6225). All signals were recorded and visualized using BCI2000 [171].

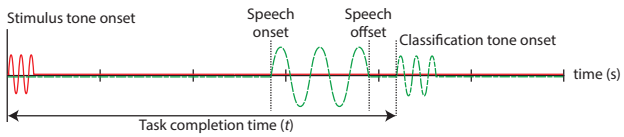

(a) speech recognition

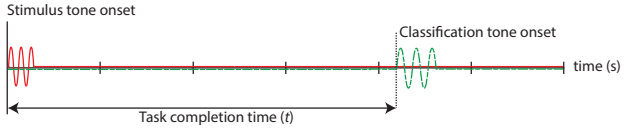

(b) touch gestures

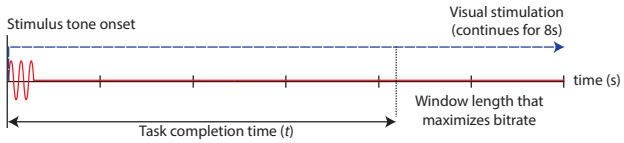

(c) SSVEP (desktop)

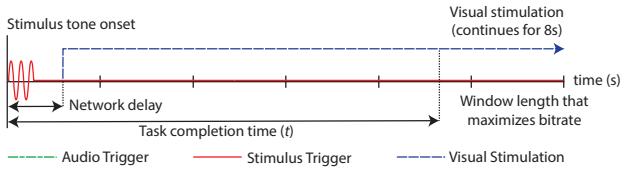

(d) SSVEP (HMD)

Figure 5.2: Performance comparisons were dependent on the task completion time (t), as described in the 5.3.4 subsection of the Chapter 5.3. The diagrams show how task completion time was calculated for (a) speech recognition, (b) touch gestures, (c) SSVEP (desktop), and (d) SSVEP (HMD).

5.3.3 Experimental Procedures

All experimental sessions were conducted in a cool and sound attenuated room with dim ambient lighting. Each subject completed one experimental session consisting of four conditions presented in a randomized order using a Latin square design. Each condition was designed to test the participant's performance with a single input mechanism. The four input mechanisms were: speech recognition, touch gestures, SSVEP with stimuli on a desktop PC, and SSVEP with stimuli on the HMD. Prior to starting each condition, participants were given the opportunity to practice with the input mechanism. During the experiments, the participant was seated in a comfortable desk chair in front of two speakers and a computer monitor. The two speakers were placed 24 inches in front of the participant with one speaker 18 inches to the participant's right and the other 18 inches to the participant's left.

Custom experimental software, developed in MATLAB (The MathWorks, Natick, MA) using PsychToolBox [27], was used to produce a sequence of auditory stimuli. Each auditory stimulus was a 330 Hz tone lasting for 100ms presented by either the left or the right speaker. Stimulus onset times for all four conditions were recorded by wiring the audio signals from MATLAB directly into the data acquisition unit. Timing diagrams for each of the four conditions are visualized in Figure 5.2.

Speech Recognition Condition

Speech commands were input into the Google Glass (software version XE22) using a custom Android application (Android API 19; Android Studio 1.1.0 for Mac). The participant was presented with a randomized sequence of auditory tones from either the left or the right speaker. The participant was asked to say "Left" if the tone was on the left and "Right" if the tone was on the right. Following a speech command, the Google Glass was programmed to play an audio chirp at the time of classification. This audio chirp was recorded by a microphone mounted on the Google Glass. The microphone was wired directly into the data acquisition unit and sampled at 6000 Hz. After the classification chirp, feedback on the predicted selection was provided to the user and the expected/predicted responses were logged. The application was then reset in preparation for the next trial. Data from 36 speech recognition trials was collected.

Touch Gestures Condition

Touch gestures were input into the Google Glass (software version XE22) using a custom Android application (Android API 19; Android Studio 1.1.0 for Mac). Starting with their hands on the desk in front of them, an auditory tone prompted the user to input a touch gesture onto the Google Glass' built-in touchpad. Each participant was asked to swipe forward on the touchpad for a stimulus on the right or backward on the touchpad for a stimulus on the left. We chose this mapping, because these exact same gestures are used to navigate right and left in the main menu of the Google Glass. Following the classification of a touch gesture, the Google Glass was programmed to play an audio chirp. These audio chirps were recorded by a microphone

mounted on the Google Glass wired directly into the data acquisition unit and sampled at 6000 Hz. After classification, feedback on the predicted selection was provided to the participant and the expected/predicted responses were logged. Data from 36 touch gestures trials was collected.

SSVEP (Desktop) Condition

During the SSVEP with stimuli on a desktop PC condition, which we label "SSVEP (desktop)", participants were asked to respond to a sequence of SSVEP stimuli presented on an LCD monitor (24-inch BenQ XL2420T). Each participant was seated 24 inches from the monitor and asked to place their head in a chin rest to maintain a constant distance between the user and the SSVEP stimuli. The SSVEP stimuli were presented using a custom application written using PsychToolBox [27]. Each SSVEP stimulus was programmed to flicker at one of four possible frequencies: 6Hz, 7.5Hz, 8.57Hz, or 10Hz. Since it is well known that the amplitude of the SSVEP varies by individual and frequency [5], 72 trials of data were collected, 12 trials for each combination of the four frequencies. This allowed the experimenters to evaluate different SSVEP frequency combinations for each user. During each trial, an audio tone prompted participants to attend to one of two SSVEP stimuli for eight seconds. Each stimulus was located on opposite sides of the monitor and subtended a visual angle of approximately 9° (computed following recommendations of the American Clinical Neurophysiology Society [186]). The frequency of the two SSVEP stimuli and the location of the auditory tone were randomized. After 36 trials, the participant was permitted an approximately one minute break. The order of the stimuli were logged for future analysis.

SSVEP (HMD) Condition

During the SSVEP with stimuli on the HMD, which we label "SSVEP (HMD)", participants were asked to respond to a sequence of SSVEP stimuli presented on the Google Glass (software version XE22). These stimuli were presented using a custom Android application (Android API 19; Android Studio 1.1.0 for Mac). In our application, we found the fastest reliable refresh rate of the Google Glass to be 33Hz. This necessitated the use of different stimula-

tion frequencies than in the SSVEP (desktop) condition. Therefore, the four stimulation frequencies used were: 4.725Hz, 5.475Hz, 6.575Hz, and 8.25Hz. As in the SSVEP (desktop) condition, 72 trials were collected, 12 trials for each combination of the four frequencies. The auditory tone prompted the user to attend to the left or right stimulus—each of which subtended a visual angle of approximately 5°—for eight seconds while their EEG responses were recorded. A network connection between the auditory stimulus presentation software and the Google Glass was used to control the onset of the SSVEP stimuli. The frequency of each of the two SSVEP stimuli and the location of the auditory tones were randomized. After 36 trials the participant was permitted an approximately one minute break. The order of the stimuli were logged for future analysis.

5.3.4 Data Analysis

First, individual trials for each condition were segmented. The stimulus onset time for each trial was determined using the envelope of the audio tone. The start of the tone was defined as the first time when the envelope crossed a threshold of three times the mean envelope level.

Speech Recognition and Touch Gestures Conditions

The audio chirp denoting the time of classification and recorded with the microphone was used to determine the trial end time. This data was band-pass filtered from 1200-2600Hz (speech recognition) and 1200-2200Hz (touch gestures) to isolate the chirp. The envelope was then calculated and the trial end time was determined as the first time to cross a threshold of three times the mean envelope. For each of the 36 trials, a task completion time (t) was calculated as the trial end time minus the stimulus onset time, and an average task completion time (T) was computed as the expected value of t across all of the trials. Task completion accuracy (P) was computed for each condition as the number of trials where the predicted stimulus matched the desired stimulus. Finally, since task completion time and task completion accuracy are dependent measures, we chose to compare the four input mechanisms using information transfer rate (ITR), a measure that simultaneously accounts for both of these variables that is commonly used to measure the

performance of BCIs [210]. ITR was computed as:

$$ITR = \frac{\log_2 N + \log_2 P + (1-P) * \log_2 \frac{1-P}{N-1}}{T} \tag{5.1}$$

Where N represents the number of classes (in our case two).

SSVEP (Desktop) and SSVEP (HMD) Conditions

The auditory prompts for all of the conditions were generated using the same PsychToolBox script on a PC and the trial onset times were determined using the same method as the one used for the speech recognition and touch gestures conditions.

During the experiments, we chose to turn SSVEP stimulation off between the trials. This meant, during the SSVEP (HMD) condition, that an activation signal had to be sent to the Google Glass. This activation signal was sent over a wireless network and subject to network delay (Figure 5.2d). We quantified this delay by measuring the time from when we sent the activation signal to the time that the Google Glass sent back a message notifying PsychToolBox that it had received this activation signal. This delay was not insignificant. As a result, we chose to reject all SSVEP (HMD) trials with a network delay that exceeded 0.25s.

For the SSVEP (desktop) and SSVEP (HMD) conditions, the 72 trials were subdivided into six subsets of 12 trials. Each subset only contained trials from one pair of stimulation frequencies (four possible frequencies, choose two). For each subset, a classification analysis was performed. For this analysis, we used the classifier described by Lin et al. [112], based on canonical correlation analysis (CCA). CCA is a multivariate statistical analysis technique that finds a linear combination of independent (X) and dependent (Y) variables using two corresponding weight matrices w_x and w_y that maximize:

$$\rho_f = \frac{w_x^T \Sigma_{XY} w_y^T}{\sqrt{w_x^T \Sigma_{XX} w_x w_y^T \Sigma_{YY} w_y}} \tag{5.2}$$

Using the EEG data as X, Y was composed of sine and cosine waves at the frequency of stimulation (our specific formulation included three harmonics). More details of this method can be found in Lin [112]. For each trial, two

correlation values (ρ_{f1} and ρ_{f2}) were computed, one for each of the two stimulation frequencies. The stimulation frequency with the highest CCA value was predicted to be the desired stimulus. An accuracy was computed for each subset as the number of trials where the predicted stimulus matched the desired stimulus. This accuracy is dependent on a free parameter called window-length. Window-length represents the amount of EEG data (measured in seconds) considered by the classifier. For example, a 0.5s window length would include EEG data from trial onset to 0.5s following trial onset. A 1s window-length would include data from the trial onset to 1s following the trial onset. For each subject, each condition, and each subset, we tested a range of possible window-lengths from 0.5-5 seconds in 0.01 second steps. To optimize the BCI to the individual participants, we selected a combination of three frequency pairs (from the six available) for further analysis. The ITR of each combination (six subsets, choose three) of frequency pairs was first analyzed. We chose the combination of frequencies that resulted in the highest ITR. Finally, from this optimal set of frequencies, the window-length (and associated accuracy) that gave the highest possible ITR was selected for comparison with the other input mechanisms Figure 5.3c.

5.4 Results

All participants were able to complete all four conditions. Before analysis, we rejected 5% of SSVEP (HMD) condition trials, due to excessive network delay (as discussed in Section 5.3.4).

5.4.1 Superiority Testing

The task completion times and accuracies for all four conditions are shown in Table 5.1. These data are also represented graphically in Figure 5.3. For seven subjects, the SSVEP (desktop) condition was the fastest. For four subjects, the speech recognition condition was the fastest and for one subject the touch gestures condition was the fastest. In general, the task completion times for the SSVEP (HMD) condition were higher than the other methods, but one subject was as fast as 1.23 seconds.

Figure 5.3c shows the distribution of bitrate data from each of the four

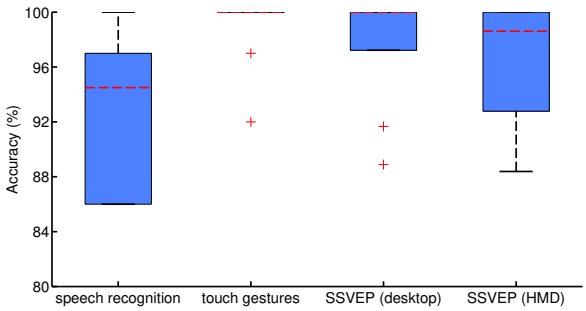

(a) Accuracy by condition

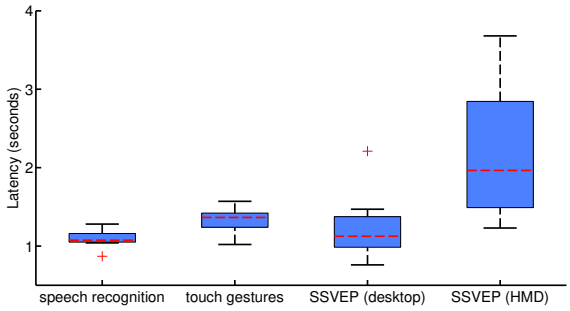

(b) Latency by condition

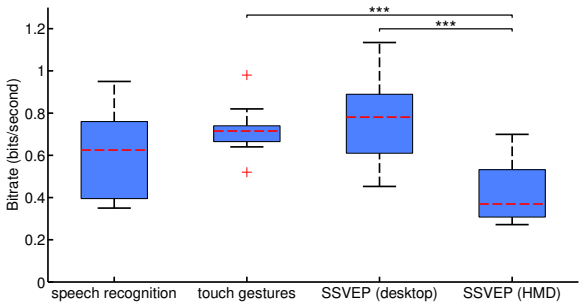

(c) Bitrate by condition

Figure 5.3: Box plot comparisons of (a) accuracy, (b) latency, and (c) bitrate for each input mechanism. Within each boxplot, all four conditions are included (speech recognition, touch gestures, SSVEP (desktop), SSVEP (HMD). The dashed red lines indicate the median value for each condition. The edges of the boxes represent the 25^{th} and 75^{th} percentiles, the whiskers of the plot represent variability outside of this range and outliers are denoted with crosses. The "***" indicates significance $p < 0.001$.

conditions. The SSVEP (desktop) condition had the highest mean ITR of 0.76 bits/second. Statistical analysis was conducted in SPSS. Using a repeated measures ANOVA with Greenhouse-Geisser correction, a significant difference ($F(3, 33) = 12.519, p = 0.001$) was found between the input mech-

anisms. Using pairwise comparisons with Bonferroni correction, both the SSVEP (desktop) condition ($p < 0.001$) and the touch gestures condition ($p < 0.001$) were found to provide a significantly higher bitrate than the SSVEP (HMD) condition.

For SSVEP-based BCIs, there is a trade-off between task completion speed and accuracy. Figure 5.5a shows this trade-off averaged across subjects for the SSVEP (desktop) and the SSVEP (HMD) conditions. Figure 5.5b shows a similar trade-off for ITR as a function of window-length. The SSVEP (desktop) condition uniformly provided a higher bitrate, regardless of window-length.

	speech recognition			touch gestures			SSVEP (desktop)			SSVEP (HMD)		
	t	P	ITR	t	P	ITR	t	P	ITR	t	P	ITR
S01	1.08	97	0.75	1.37	100	0.73	0.76	97	1.07	1.43	100	0.70
S02	0.87	86	0.48	1.14	92	0.52	1.35	100	0.74	2.31	100	0.43
S03	1.04	86	0.40	1.26	97	0.64	2.21	100	0.45	3.68	100	0.27
S04	1.12	86	0.37	1.36	100	0.74	0.96	100	1.04	1.48	97	0.55
S05	1.05	100	0.95	1.02	100	0.98	1.1	100	0.91	1.74	94	0.38
S06	1.19	97	0.68	1.36	100	0.74	1.15	100	0.87	3.12	100	0.32
S07	1.07	100	0.93	1.44	100	0.69	0.99	92	0.59	1.50	88	0.32
S08	1.28	89	0.39	1.57	100	0.64	1.05	97	0.78	2.19	92	0.27
S09	1.13	97	0.71	1.22	100	0.82	0.98	89	0.51	3.40	100	0.29
S10	1.20	86	0.35	1.44	100	0.69	1.15	100	0.87	1.67	100	0.60
S11	1.05	97	0.77	1.40	100	0.71	1.47	100	0.68	2.57	94	0.27
S12	1.05	92	0.57	1.39	100	0.72	1.40	97	0.58	1.23	89	0.40
Mean	1.09	93	0.61	1.33	99	0.72	1.21	98	0.76	2.2	96	0.40

Table 5.1: Task completion time (seconds), task completion accuracy (%), and ITR (bits/second) averaged across trials, for each subject and condition.

5.4.2 Non-Inferiority Testing

Our results did not support the hypothesis that inputs obtained using either speech recognition or touch gestures provided a significantly higher bitrate than those obtained using SSVEP (desktop). It is not appropriate, however, to conclude that a failure to reject the null hypothesis is the same as saying that the SSVEP (desktop) condition has performance that is as good or better

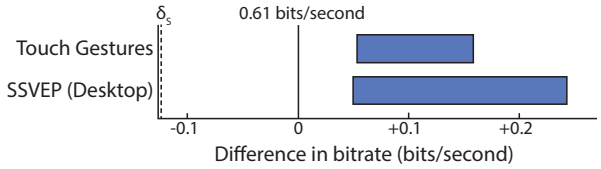

(a) Speech recognition non-inferiority

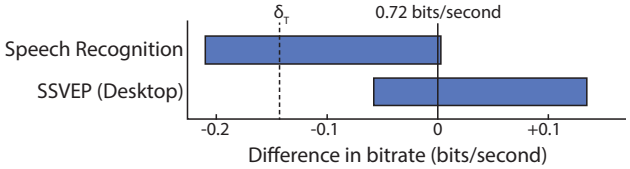

(b) Touch gestures non-inferiority

Figure 5.4: Non-inferiority comparisons for (a) speech recognition and (b) touch gestures.

than that of the speech recognition or touch gesture input mechanisms. The proper way to test this hypothesis is through the use of non-inferiority testing.

The purpose of non-inferiority testing—commonly used in clinical drug trials—is to provide statistical evidence that two treatments are close enough in performance "that one cannot be considered superior or inferior to the other" [203]. How researchers define "close enough" is dependent on the context. Regardless of the study, however, this value is commonly known as the margin of non-inferiority and is mathematically denoted by δ. Here, we chose $\delta = 20\%$. This choice is based on a conservative estimate of the just-noticeable-difference (JND)—the minimum difference required to be noticed by a user—of time perception.[177]

We conducted a post-hoc two one-sided test (TOST) in MATLAB [203], the results of this test are represented in Figures 5.4a and 5.4b. For this analysis, we assumed $\alpha = 0.05$ and did not correct for multiple comparisons. The TOST test revealed that for the speech recognition condition ($\delta_S = 0.12$ bits/second), one could conclude that the ITR of the touch gestures and SSVEP (desktop) conditions was as high or higher than speech recognition. The test also showed that for the touch gestures condition ($\delta_T = 0.15$ bits/second) that one could conclude that the ITR of the SSVEP (desktop) condition is as high or higher than touch gestures.

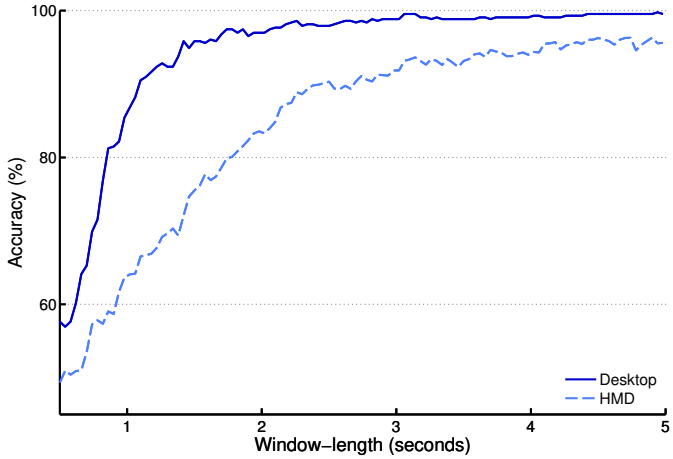

(a) Average classification accuracy as a function of window-length

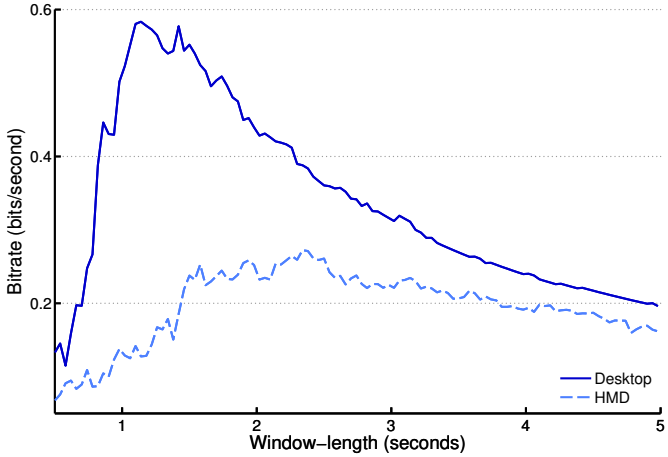

(b) Average bitrate as a function of window-length

Figure 5.5: (a) Accuracy and (b) bitrate versus window-length for the SSVEP (desktop) and the SSVEP (HMD) conditions averaged across all participants.

5.5 Discussion

The SSVEP (desktop) condition had the highest mean bitrate (Table 5.1) of all of the tested input mechanisms. This result was different than what was originally hypothesized. Neither the speech recognition condition nor the touch gestures condition resulted in a significantly higher bitrate than the SSVEP (desktop) condition. Furthermore, a supplemental non-inferiority analysis suggests that the bitrate of the SSVEP (desktop) condition is as high or higher than any of the other input mechanisms tested here, although

this hypothesis needs to be stated *a priori* and re-tested in order to verify it in future work.

The results also demonstrate that participants were able to use an existing HMD for SSVEP-based inputs with an average latency of 2.2s and an average accuracy of 96%. While this was slower than the other input mechanisms, this study is one of the first to use SSVEP on an HMD [90] and is the first that we are aware of to use SSVEP on the Google Glass. The differences in performance between the SSVEP (desktop) and SSVEP (HMD) conditions can be attributed to network delay and other factors known to effect the amplitude of SSVEPs, including: stimulation hardware [213], stimulation frequencies [77], stimulus size [142], and the fact that the SSVEP (HMD) condition only stimulated one eye [90]. These results show the potential of SSVEP as an input mechanism for HMDs and demonstrate that such inputs can be obtained using an existing hardware platform.

One limitation of the current study is that the SSVEP (desktop) and SSVEP (HMD) conditions were classified offline while the speech recognition and touch gestures conditions were classified in real-time. This could have affected the results in two ways. First, offline classification may predict better performance than what is achieved online. A recent SSVEP-based BCI paper, however, demonstrated that online performance was better than offline performance [38]. Second, the classifier requires computation time. An analysis of the classifier used for both the SSVEP (desktop) and the SSVEP (HMD) conditions showed that the computation time was only 0.01s per trial. If 0.01s were added to each of the SSVEP trials, the bitrate of the SSVEP (desktop) condition would be reduced by less than 0.01 bits/second. For the speech recognition condition, the audio trigger collected clear audio data from some participants, enabling an analysis of classification time. Speech offset times (Figure 5.2a) were determined for three subjects (S1,S2,S3). By computing the difference between the speech offset time and the task completion time, an estimate of "classification time" was obtained. After subtracting this estimate from every subject's task completion time, performance of the speech recognition condition would rise from 0.61 bits/second to 0.84 bits/second. Even in this case, however, the speech recognition condition would not have a significantly higher bitrate than the SSVEP (desktop) condition ($p > 0.9$) or the touch gestures condition ($p > 0.75$).

While this study chose to focus on input performance, future investigations

should also consider the advantages and disadvantages of SSVEP-based inputs from a user experience perspective [193]. SSVEP-based inputs may be advantageous because they provide confidentiality, can be used in cases where the users hands are occupied [4], and are not adversely affected by noisy environments. SSVEP stimuli, however, can be annoying to the user [220]. Some researchers have found high frequency stimuli (over 30 Hz) to be more comfortable for users, but less performant [197]. In addition, SSVEP-based input systems require cumbersome EEG recording hardware.

If one were to conduct a user experience study, it would be important to consider whether SSVEP-based input performance matches the user's perception of SSVEP-based input performance. For example, it is known that delays in feedback between one tenth of a second and one second are noticed by users and cause them to lose the feeling that they are directly interacting with the data [144]. In the case of speech recognition and touch gestures, the user orients their gaze, performs a motor action (speaking or gesturing), and (assuming a negligible classification time) immediately receives feedback. When using an overt SSVEP-based BCI, on the other hand, the cessation of gaze orientation is followed by a period in which the user generates an SSVEP. Since no other motor action is being performed during this time, it could be perceived by the user as a delay even when there isn't one.

This work represents the first direct comparison between existing input mechanisms for HMDs and SSEVP-based BCI. The results of the comparison study do not support the hypothesis that speech recognition or touch gestures enable a higher ITR than SSEVP-based BCI for the binary selection task tested here. A supplemental analysis also suggests that the differences in performance may be small enough that the SSVEP-based BCI could be considered non-inferior. While additional tests are necessary to confirm this new hypothesis, the current results are important because they provide estimates of performance for each of these input mechanisms that can be used in later studies. More broadly, the experiments describe one scenario—the binary selection of targets for HMDs—where SSVEP-based BCI may perform as well as existing input mechanisms. This is surprising as the general perception, for healthy populations, is that BCIs are uniformly slower than existing input mechanisms [161, 117]. The results in this chapter show that BCI-based input for HMDs represents an exciting opportunity for the BCI community and encourage future studies to directly compare the performance of these

systems with existing input mechanisms.

5.6 Acknowledgments

This work was funded by the University of Illinois Graduate College Focal Point and SURGE program.

CHAPTER 6

AN SSVEP-BASED BRAIN-COMPUTER INTERFACE FOR TEXT SPELLING WITH ADAPTIVE QUERIES THAT MAXIMIZE INFORMATION GAIN RATES[1]

6.1 Abstract

In this chapter, we present an adaptive user interface for text-entry using a steady-state visually evoked potential (SSVEP)-based brain-computer interface (BCI). Like other SSVEP-based spellers, ours identifies the desired input character by posing questions (or queries) to users through a visual interface. Each query defines a mapping from possible characters to steady-state stimuli. The user responds by attending to one of these stimuli. Unlike other SSVEP-based spellers, ours chooses from a much larger pool of possible queries—on the order of ten thousand instead of ten. The larger query pool allows our speller to adapt more effectively to the inherent structure of what is being typed and to the input performance of the user, both of which make certain queries provide more information than others. In particular, our speller chooses queries from this pool that maximize the amount of information to be received per unit of time, a measure of mutual information that we call information gain rate. To validate our interface, we compared it with two other state-of-the-art SSVEP-based spellers, which were re-implemented to use the same input mechanism. Results showed that our interface, with the larger query pool, allowed users to spell multiple-word texts nearly twice as fast as they could with the compared spellers.

[1]This work has been previously published as [3] and is co-authored by A. Akce and T. Bretl; ©2015 IEEE.

6.2 Introduction

The development of electroencephalogram (EEG)-based brain-computer interfaces (BCI) for text-entry has exploded over the past decade [37]. These interfaces create a direct neural link between a human user and a computer, allowing the user to type without a keyboard or physical movements. One common input mechanism, which we consider in this chapter, is the steady-state visually evoked potential (SSVEP). In an SSVEP-based speller, users are presented with a set of visual targets that are associated with possible characters. These targets blink on and off at slightly different but fixed frequencies. By attending to a particular target, the user elicits phase-locked EEG activity at the corresponding frequency. Measurement of this activity allows the computer to detect the target to which the user is attending, hence the user's desired character. While it is not within our scope to discuss the relative merits of BCI and non-BCI text-entry, we note that SSVEP may remain applicable even when users have no control over gaze (e.g., as with "locked-in" syndrome). Attentional focus that is independent of visual focus, also elicits SSVEPs [7].

Most existing SSVEP-based spellers have fewer visual targets than possible characters. As a consequence, the user must attend to a sequence of targets in order to type a single character. For example, the SSVEP-based spellers of both Volosyak [197] and Cecotti [36] allow 28 possible characters—the standard alphabet, space, and delete—but have only five targets. The interface of Volosyak [197] arranges characters in a grid, associates four targets with cardinal directions (left, right, up, down) in which to move a cursor in this grid, and interprets the fifth target as selecting the character at the current location of the cursor. The interface of Cecotti [36] arranges all characters except delete in a static hierarchical menu with a decision between three groups at each level of the hierarchy (three groups of 9 characters, then of 3 characters, and finally of 1 character), associates a target with each group, associates the fourth target with delete, and interprets the fifth target as moving up in the hierarchy.

When discussing these two interfaces, we find it helpful to regard each presentation of visual targets as a question or *query* posed to the human user. Each query defines a mapping from possible characters to visual targets, in the sense that there is a correct choice of target to which the user must attend

in order to specify a given character most quickly. The queries of Volosyak [197] ask which direction the desired character is with respect to the cursor. The queries of Cecotti [36] ask which of three groups contains the desired character.

In this chapter, we present a new SSVEP-based speller that is similar to the ones of Volosyak [197] and Cecotti [36] but that poses a different set of queries. These queries are of two types. A *range query* (Figure 6.1a) asks which of five ordered groups of characters (e.g., "delete" through B, C through K, L through M, N through T, and U through "space") contains the desired character, by associating a target with each group. A *character query* (Figure 6.1b) asks which of four ordered characters (e.g., C, F, G, and S)—if any—is the desired character, by associating a target with each one and by interpreting the fifth target as "none of them."

What is important about these two new types of queries is their variety. There are 2925 distinct range queries and 20475 distinct character queries, meaning that our interface has a total of 23400 queries from which to choose. You might say that our interface has a *query pool* of size 23400. In contrast, the interface of Volosyak [197] has a much smaller query pool of size 28, equal to the number of characters in the grid. Similarly, the interface of Cecotti [36] has a query pool only of size 13, equal to the number of possible groupings of characters in the static hierarchical menu.

The reason that variety is important is that not all queries are equally informative. Language has an inherent structure that—depending on context—makes certain characters much more likely than others. In principle, larger query pools allow better adaptation to this structure. They give an interface the freedom to pick "the right question."

Indeed, our SSVEP-based speller chooses queries that explicitly maximize the amount of information to be received per unit of time about the desired character, a measure of mutual information that we call *information gain rate (IGR)*. IGR is similar to other measures of mutual information like the commonly used information transfer rate (ITR) [210, 6, 217] and the less well known Nykopp bit rate [149]. The reason we use a new measure in this chapter is that IGR—unlike ITR, for example—does not assume that each visual target is equally likely to be selected within a given time window. Instead, IGR takes into account the expected input performance of each user (characterized by selection accuracy and selection latency) as well as

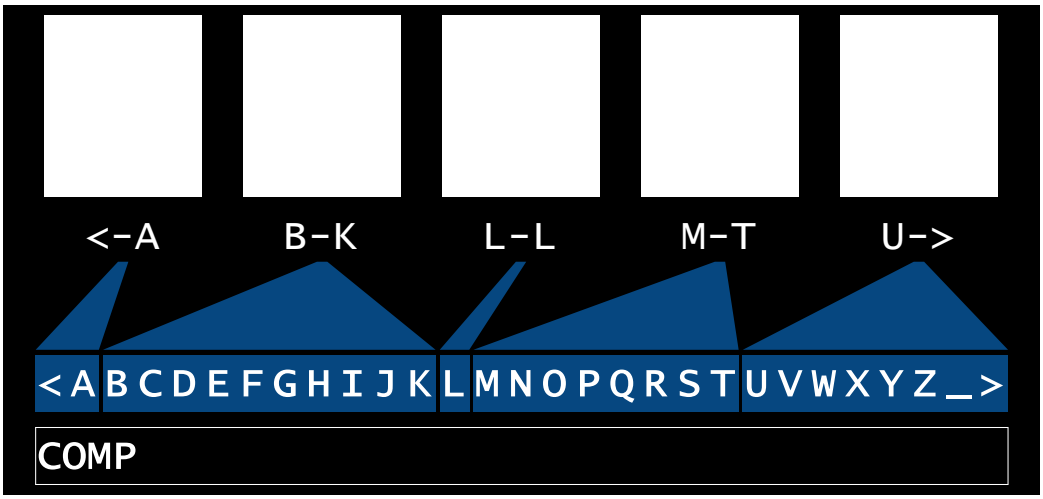

(a) A range query posed after spelling "COMP"

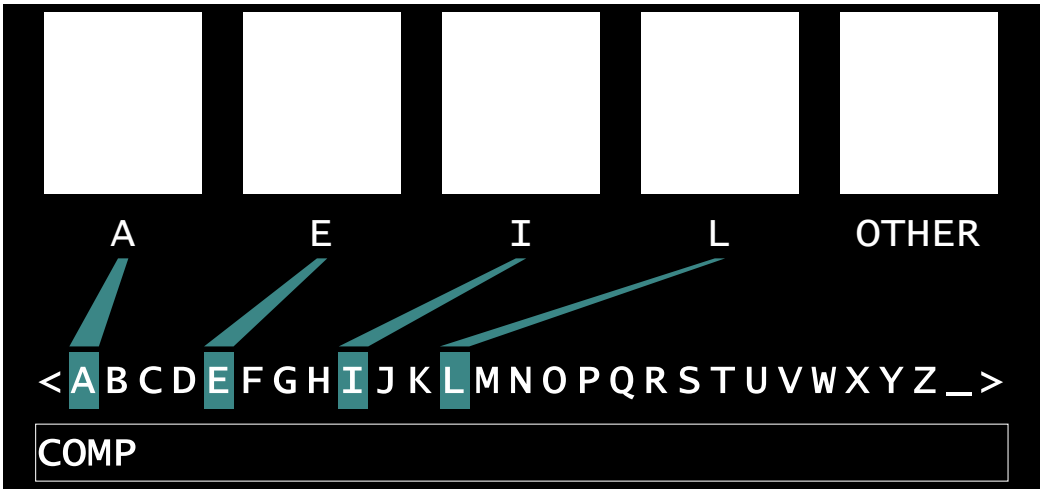

(b) A character query posed after spelling "COMP"

Figure 6.1: Examples of the two types of queries posed by our speller, range queries (a) and character queries (b). In each case, targets are arranged horizontally at the top of the screen (the white boxes) and text appears along the bottom.

a probabilistic language model. We emphasize that IGR and the models that it takes into account are not in direct competition with the query pool. Rather, if the query pool gives us the freedom to pick the right query, IGR offers our interface the means to select that query. This choice of measure distinguishes our interface from others that also have larger query pools, like the motor-imagery-based speller of Blankertz et al. [24] and the P300-based speller of Ma et al. [121]—although, these other interfaces are harder to compare directly due to their use of input mechanisms other than SSVEP.

We acknowledge that many factors affect the performance of an SSVEP-based speller (e.g., the classification rate [122, 62], the stimulus design [40, 220, 86], and the layout of the interface [208, 83]). Larger query pools may also necessitate the use of serial visual search strategies by the participant, resulting in prolonged selection latencies. Nonetheless, empirical results with six qualified subjects showed that our SSVEP-based speller—with the larger query pool and with IGR as the performance measure to be maximized—allowed users to spell multiple-word texts nearly twice as fast as they would with the SSVEP-based spellers of Volosyak [197] and Cecotti [36].

In what follows, we first present our new speller (Section 6.3). Next, we describe the experimental comparison to existing spellers (Section 6.4) and give the results of this comparison (Section 6.5). Finally, we conclude by discussing the importance of these results with respect to the design of BCI text-entry systems (Section 6.6).

6.3 Design of Our Speller

Our SSVEP-based speller allows a user to type a string of text that consists of the standard alphabet ('A' to 'Z'), space ('_'), and delete ('<'). In order to type each individual character, the user must respond to a sequence of queries. Each query associates possible characters with one of five visual targets (i.e., five blinking SSVEP stimuli). Our speller poses two types of queries (Figure 6.1):

1. A *range query* asks which of five ordered groups of characters contains the desired character, by associating a target with each group. In the example of Figure 6.1a, the five groups are '<' to 'A', 'B' to 'K', 'L' (i.e., a group with only one character), 'M' to 'T', and 'U' to '_'.

2. A *character query* asks which of four ordered characters—if any—is the desired character, by associating a target with each one and by interpreting the fifth target as "none of them." In the example of Figure 6.1b, the four characters are 'A', 'E', 'I', and 'L'.

Each query reduces our speller's uncertainty about the user's desired character. Once the speller is confident enough, it makes a "guess" at the desired

character, appends this guess to the string of text at the bottom of the screen, and proceeds with a new sequence of queries to obtain the next character.

In Section 6.3.1, we define a formal model of our speller. In Section 6.3.2, we use this model to derive algorithms that say how to choose each query (based on maximizing a measure of mutual information that we call IGR) and how to guess the desired character (based on maximizing likelihood with respect to a language model).

6.3.1 Models

In what follows, we denote the set of possible characters by $\mathcal{C} = \{\text{`<'}, \text{`A'}, \ldots, \text{`Z'}, \text{`\_'}\}$ and the set of possible targets, numbered from left to right, by $\mathcal{U} = \{1, \ldots, 5\}$.

Queries

We can describe any range or character query as a map $f \colon \mathcal{C} \to \mathcal{U}$. For example, the range query in Figure 6.1a is given by

$$f(c) = \begin{cases} 1 & \text{if } c \in \{\text{`<'}, \text{`A'}\} \\ 2 & \text{if } c \in \{\text{`B'}, \ldots, \text{`K'}\} \\ 3 & \text{if } c \in \{\text{`L'}\} \\ 4 & \text{if } c \in \{\text{`M'}, \ldots, \text{`T'}\} \\ 5 & \text{otherwise.} \end{cases} \tag{6.1}$$

Suppose that the user in this example were trying to spell the word "COMPILE." Having already spelled "COMP," the current desired character would be 'I'. The formal definition (6.1) of the range query in Figure 6.1a makes clear that the correct choice of target would be $f(\text{`I'}) = 2$—i.e., that the user should attend to the second target from the left in order to specify their desired character most quickly. Similarly, the character query in Figure 6.1b

is given by

$$f(c) = \begin{cases} 1 & \text{if } c = \text{`A'} \\ 2 & \text{if } c = \text{`E'} \\ 3 & \text{if } c = \text{`I'} \\ 4 & \text{if } c = \text{`L'} \\ 5 & \text{otherwise.} \end{cases} \tag{6.2}$$

Continuing with our example, the correct choice of target in this case would be $f(\text{`I'}) = 3$. As can easily be derived, we have 2925 distinct range queries and 20475 distinct character queries from which to choose, for a total of $n = 23400$. We index the corresponding maps by $f_1, \ldots, f_n$.

Accuracy and Latency

As we have seen, there is a single correct choice of target—call it the *intended target*—to which the user should attend in response to a query. Because of uncertainty in the measurement and interpretation of SSVEP, the target that is actually selected—call it the *observed target*—may differ from the intended target. To capture this difference, we model the intended target as a discrete random variable X and the observed target as a discrete random variable Y, both taking values in $\mathcal{U}$. We also model the amount of time taken for the user to respond to a query as a continuous random variable T, taking values in the set of positive real numbers $\mathbb{R}^+$. Two statistical quantities then suffice to describe the input performance of a user:

- the conditional probability mass function $p_{Y|X}(y|x)$, which specifies the likelihood that the observed target is y given that the intended target is x;
- the conditional expectation $\mathbb{E}(T|X = x, Y = y)$, which specifies the average time taken for the user to respond to a query given that the intended target is x and the observed target is y.

We will refer to $p_{Y|X}(y|x)$ as the *accuracy model* and to $\mathbb{E}(T|X = x, Y = y)$ as the *latency model*. Although these two models may differ from one user to another, we assume that they remain the same over time—in other words, that input performance is the same when typing the first character in a string

of text as when typing the last character. Accuracy and latency models can be computed from experimental data (e.g., during user training)—we will say how in Section 6.4.3. For now, we assume both models are given.

Language

We model the desired character as a discrete random variable C, taking values in $\mathcal{C}$. The probability mass function $p_C(c)$ then completely describes the speller's uncertainty about the user's desired character. We will refer to $p_C(c)$ as the *language model*. There are standard ways to derive this language model from a database of English text—we will say how in Section 6.4.4. For now, we assume that the language model is given.

Unlike the accuracy and latency models, the language model changes over time—indeed, the purpose of each query is to steer this change in a way that reduces uncertainty about the desired character. In particular, by application of Bayes' theorem (see Appendix 6.8), it is possible to show that

$$p_{C|Y}(c|y) = \frac{p_{Y|X}(y|f_i(c))p_C(c)}{\sum_{s\in\mathcal{C}} p_{Y|X}(y|f_i(s))p_C(s)} \tag{6.3}$$

for all $c \in \mathcal{C}$. Equation (6.3) provides a recursive update rule: start with the current language model p_C, observe a target y in response to a query f_i, compute a new language model $p_{C|Y}$ using (6.3), and replace p_C with $p_{C|Y}$.

6.3.2 Algorithms

How to choose each query

We can use the models defined in Section 6.3.1 to measure the amount of information to be received per unit of time about the desired character. We call this quantity IGR and define it as follows:

$$\text{IGR} = \frac{I(X;Y)}{\mathbb{E}(T)}. \tag{6.4}$$

The numerator in (6.4) is the mutual information between the intended target and the observed target. It is defined as

$$I(X;Y) = \sum_{x \in \mathcal{U}} \sum_{y \in \mathcal{U}} p_{X,Y}(x,y) \log \left(\frac{p_{X,Y}(x,y)}{p_X(x) p_Y(y)} \right) \tag{6.5}$$

and is a commonly used measure of information gain [50]. The denominator in (6.4) is the average time taken for the user to respond to a query. It is defined as

$$\mathbb{E}(T) = \sum_{x \in \mathcal{U}} \sum_{y \in \mathcal{U}} p_{X,Y}(x,y) \mathbb{E}(T|X=x, Y=y). \tag{6.6}$$

It is possible to show (see Appendix 6.9) that

$$p_{X,Y}(x,y) = p_{Y|X}(y|x) p_X(x) \tag{6.7}$$

$$p_Y(y) = \sum_{x \in \mathcal{U}} p_{Y|X}(y|x) p_X(x) \tag{6.8}$$

and

$$p_X(x) = \sum_{\{c \in \mathcal{C}:\ f_i(c) = x\}} p_C(c), \tag{6.9}$$

so IGR (6.4) can be computed with knowledge of the accuracy model $p_{Y|X}(y|x)$, the latency model $\mathbb{E}(T|X=x, Y=y)$, the language model $p_C(c)$, and the query $f_i(c)$, all of which we defined in the previous section. Note that IGR is an explicit function of the query index i—we can make this dependence clear by writing $\mathrm{IGR}(i)$. Our speller chooses the query with index that maximizes IGR:

$$i_{\max} = \arg\max_{i \in \{1,\ldots,n\}} \mathrm{IGR}(i).$$

How and when to guess the desired character

Our speller's best guess at the desired character given an observed target y in response to a query f_i is the character of maximum likelihood with respect to the updated language model:

$$c_{\max} = \arg\max_{c \in \mathcal{C}} p_{C|Y}(c|y),$$

where $p_{C|Y}(c|y)$ is computed as in (6.3). The only remaining question is if our speller is confident enough about this guess to append $c_{\max}$ to the string of text, or if it should continue posing queries. To answer this question, our speller compares the maximum likelihood

$$p_{\max} = p_{C|Y}(c_{\max}|y)$$

to the likelihood of certain other possible characters. In particular, we define the set

$$\mathcal{C}_{\text{inner}} = \{c \in \mathcal{C} \colon f(c) = y \text{ and } c \neq c_{\max}\}$$

of characters other than $c_{\max}$ that are associated with the same observed target y, and the set

$$\mathcal{C}_{\text{outer}} = \{c \in \mathcal{C} \colon f(c) \neq y\}$$

of characters not associated with this target. Next, we compute

$$p_{\text{inner}} = \begin{cases} 0 & \text{if } \mathcal{C}_{\text{inner}} = \emptyset \\ \max\left\{p_{C|Y}(c|y) \colon c \in \mathcal{C}_{\text{inner}}\right\} & \text{otherwise} \end{cases}$$

and

$$p_{\text{outer}} = \begin{cases} 0 & \text{if } \mathcal{C}_{\text{outer}} = \emptyset \\ \max\left\{p_{C|Y}(c|y) \colon c \in \mathcal{C}_{\text{outer}}\right\} & \text{otherwise,} \end{cases}$$

i.e., the maximum likelihood over characters in $\mathcal{C}_{\text{inner}}$ and $\mathcal{C}_{\text{outer}}$, respectively (or zero if either set is empty). Our speller stops posing queries when both

$$\frac{p_{\max}}{p_{\text{inner}}} > \alpha \qquad \text{and} \qquad \frac{p_{\max}}{p_{\text{outer}}} > \beta,$$

where the thresholds α and β are parameters.

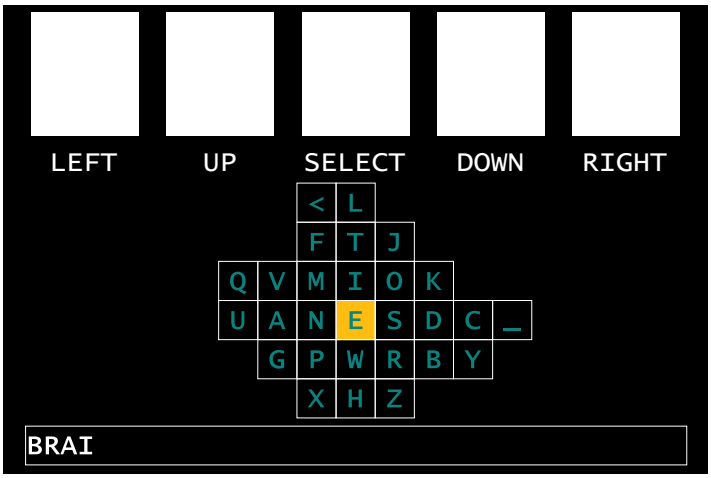

(a) Speller of Volosyak

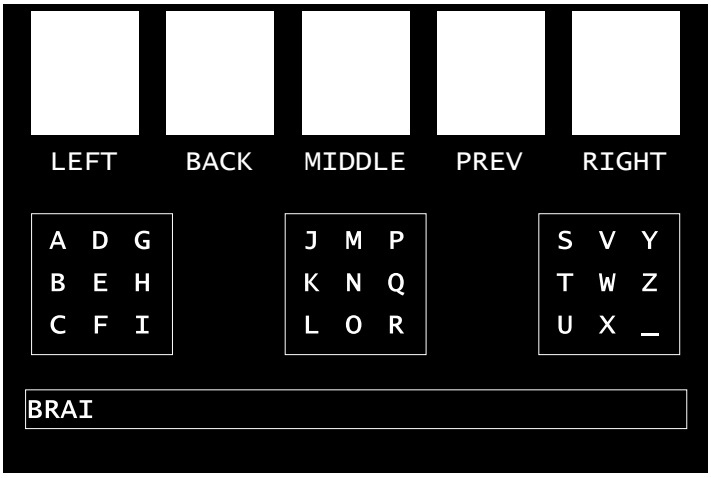

(b) Speller of Cecotti

Figure 6.2: Sample screenshots of the spellers re-implemented for comparison to our speller: speller of Volosyak [shown in (a)] and speller of Cecotti [shown in (b)].

6.4 Method

6.4.1 Participants

We performed experiments with 11 able-bodied participants between the ages of twenty and thirty who had normal or corrected-to-normal vision. All experiments were approved by the Institutional Review Board of the University of Illinois.

6.4.2 Signal Recording and Classification

The steady-state stimuli were 5 targets presented on an LCD monitor, ordered from left to right, at 7.50, 10.0, 6.67, 12.0, and 8.57Hz. These stimuli appear as white squares across the top of Figure 6.1. EEG signals were extracted from seven electrode sites across the occipital region of the scalp (PO7, PO3, PO4, PO8, O1, OZ, O2) at impedances not exceeding 10kΩ. All electrodes were referenced to electrode location PZA [88]. EEG signals were acquired using a 128-channel bioamplifier at 256Hz, bandpass-filtered from 1Hz to 30Hz, and analyzed using a 1.5 second sliding window with an overlap of 1.375 seconds. A classifier, based on the traditional power spectral density analysis (PSDA) method [192], was used to determine user selections. In our implementation of this classifier, multi-electrode EEG data were filtered into four different spatial representations using bipolar and Laplacian combinations (see [65] for a description). The specific combinations, taken from Prueckl [160], were as follows:

$$CH_1 = 4 * OZ - (O1 + O2 + PO7 + PO8)$$
$$CH_2 = 2 * OZ - (O1 + O2)$$
$$CH_3 = 4 * OZ - (O1 + O2 + PO3 + PO4)$$
$$CH_4 = 2 * OZ - (PO7 + PO8)$$

The Fast Fourier Transform (FFT) with a rectangular window and zero-padded to 1024 points, was computed for each combination using MATLAB's 'fft' function. The result was then multiplied by its complex conjugate to obtain power spectra. A signal-to-noise ratio (SNR) was obtained for each combination and each frequency by dividing the power of the signal (average power at the frequency of interest $\pm$ 0.2Hz) by the average power of the noise (average power in the frequency band of 6.25-12.5Hz excluding the frequency of interest $\pm$ 0.2Hz). The highest and lowest SNR values for each frequency were discarded. The two remaining SNR values were averaged to obtain a single value for each frequency. If any of these five averaged values exceeded a pre-determined threshold, the corresponding target was selected as the observed target. If more than one frequency exceeded the threshold during the same window of time, the lowest frequency was selected as the observed target.

6.4.3 Training Phase

The accuracy model and the latency model (Section 6.3.1) for each user were derived from data collected during a training phase. In this training phase, 100 queries were presented to each user. An arrow specified the intended target for each query. Users were asked to respond by attending to that target. In total, each of the five targets was specified as the intended target twenty times, in random order. For each query, the intended target, the observed target, and the user response time were recorded. The conditional probability $p_{Y|X}(y|x)$ was computed as the ratio of the number of times y was the observed target given that x was the intended target over the number of times x was the intended target. If y was never observed, in other words if the empirical value of $p_{Y|X}(y|x) = 0$, a small number (0.01) was added. These values were then normalized to obtain a probability measure. The conditional expectation $\mathbb{E}(T|X = x, Y = y)$ was computed as the average user response time over all queries in which the intended target was x and the observed target was y. If y was never observed, in other words if the empirical value of $\mathbb{E}(T|X = x, Y = y) = 0$, then this empirical value was replaced with the average user response time over all queries (over all intended and observed targets).

6.4.4 Spelling Phase

Following training, participants completed a three-part spelling phase. The purpose of this spelling phase was to evaluate the performance of participants using our speller with their performance using two existing SSVEP spellers, the one of Volosyak [197] and the one of Cecotti [36], that were highlighted in a review of BCI text-entry [37]. All three spellers presented the same number of visual targets (five) and allowed users to type a string of text consisting of the same standard alphabet ('A' to 'Z'), space ('_'), and delete ('<'). These spellers were implemented as follows:

- Our interface (Figure 6.1) was implemented exactly as described in Section 6.3. The accuracy and latency models were derived from data collected during training as described in Section 6.4.3. The language model was constructed with prediction by partial matching (PPM) [42] applied to the English corpus provided with the Dasher text-entry in-

Table 6.1: Target texts and their negative log-likelihoods (NLL)

Text	Text	NLL (bits/char)
Txt1	BCI	7.19
Txt2	BRAIN	3.04
Txt3	SIREN	5.31
Txt4	BRAIN_COMPUTER_INTERFACE	1.98
Txt5	PLEASE_GET_ME_A_BLANKET	2.64

terface [207]. The conditional probability of the delete ('<') character, which was not included in the PPM model, was fixed at 0.05.

- The interface of Volosyak [197] arranges characters in a grid according to their frequency in English text, associates four targets with cardinal directions (left, right, up, down) in which to move a cursor in this grid, and interprets the fifth target as selecting the character at the current location of the cursor (Figure 6.2a). As an example, a user might try to select 'B' with the following sequence of intended targets: *right*, *right*, *down*, and then *select*. There were differences between our implementation and the original implementation of [197], both in the location of targets on the screen and in the arrangement of characters in the grid. These differences are potential sources of error and will be discussed further in Section 3.5.

- The interface of Cecotti [36] arranges all characters except delete ('<') in a static hierarchical menu with a decision between three groups at each level of the hierarchy (three groups of 9 characters, then of 3 characters, and finally of 1 character), associates a target with each group, associates the fourth target with delete ('<'), and interprets the fifth target as moving up in the hierarchy (Figure 6.2b). For example, a user might try to select 'B' with the following sequence of intended targets: *left*, *left*, and *middle*. Our implementation and the original implementation of [36] differ only with respect to the location of targets on the screen.

During the evaluation of each speller, subjects were asked to specify the texts in Table 6.1. The first three (Txt1, Txt2, Txt3) were single-words texts and the last two (Txt4 and Txt5) were multiple-word texts. Table 6.1 also

lists the likelihood of each text with respect to our language model as measured by the average number of bits necessary per character, a quantity that is called the *negative log-likelihood per character* (NLL). The multiple-word texts (Txt4, Txt5) had NLL comparable to the average NLL of English texts, which is about 2 bits per character [14, 124]. Participants completed all five texts, in order, for a single speller before moving on to the next speller. There was a short (one minute) break between each speller. To reduce possible bias, the order in which the spellers were evaluated was randomized. Experimentation was halted at the request of the user or if user performance was lower than one character per minute (cpm).

6.4.5 Simulation Study

As we acknowledged in Section 6.4.4, there were small differences between our implementation and the original implementation of the spellers of Volosyak [197] and Cecotti [36]. In our implementation of the speller of Volosyak, the fifth row of the character grid was shifted one cell to the right of the original implementation. To quantify the effect of this layout change we performed Monte-Carlo simulations using two versions of the speller of Volosyak: the one utilized in the present study, and the one in [197] with the original layout. A total of 1000 simulations were conducted with each text (listed in Table 6.1) and participant (S1-S6, S8, S9). In each query, recall that there is a single correct choice of intended target, the simulation assumes that the human subject always makes the correct choice of intended target. The observed targets and the target selection latencies were randomly sampled according to the accuracy and latency models of each participant. In particular, given an intended target x the observed target y was sampled according to the probability distribution $p_{Y|X}(y|x)$. The selection latency was sampled from a normal distribution with mean $\mathbb{E}(T|X = x, Y = y)$ and with standard deviation computed from the participant's training trials. Results were obtained for our speller, the two versions of the speller of Volosyak, and the speller of Cecotti.

6.5 Results

Of the 11 subjects who participated in our study, six (S1, S2, S3, S4, S5, S6) were able to complete the entire experiment. Three of the participants (S7, S8, S9) completed the training phase, but were unable to complete all three parts of the spelling phase. The remaining two participants were unable to complete the training phase with at least 50% accuracy on all of the targets. Their data have been excluded from further analysis. All subjects were naïve to EEG-based BCIs with the exception of subjects S1 and S2, who had extensive experience. Specifically, subjects S1 and S2 had previously participated in greater than 20 hours of experiments with SSVEP-based BCIs. The following performance measures were used:

- *input error* (ϵ), the fraction of the number of incorrect queries—in which the observed target did not match the intended target—to the number of all queries;
- *input latency* ($\mathbb{E}(T)$), the mean latency—the time it takes to obtain a user response after the onset of a stimulus—across all queries;
- *input/character ratio* (C), the average number of user responses required to spell a single character of the target text, i.e., the ratio of the total number of queries to the number of characters in the target text;
- *spelling rate* (R), the average number of characters spelled per minute (cpm), without counting any instances of delete, i.e., the ratio of the number of characters in the target text to the total time elapsed in spelling.

We note that it was indeed possible to compute the input error during the spelling phase, since—under the assumption that errors are derived from incorrect classification of SSVEP response and not from incorrect user behavior—the intended target (either a singleton or a finite set) was always known.

6.5.1 Training Phase

Table 6.2 shows the training data obtained from each participant. Across the six subjects who completed the entire experiment, the input error was 2%,

Table 6.2: Training Phase

(a) Average input accuracy (%) of each subject for each target

Subject	Target 1	Target 2	Target 3	Target 4	Target 5	Avg
S1	100	100	100	100	100	100
S2	100	95	100	100	100	99
S3	100	100	80	100	100	96
S4	100	100	100	100	95	99
S5	100	100	100	100	95	99
S6	100	95	100	95	100	98
Avg	100	98	96	99	98	98.5
S7	100	100	95	100	100	99
S8	90	95	100	55	95	87
S9	75	75	80	95	75	80
Avg	88.3	90	91.7	83.3	90	88.7

(b) Average input latency (seconds) of each subject for each target

Subject	Target 1	Target 2	Target 3	Target 4	Target 5	Avg
S1	2.66	2.63	3.07	3.54	2.64	2.91
S2	6.07	3.45	3.77	3.84	2.85	3.99
S3	2.76	2.79	3.94	2.27	2.25	2.80
S4	2.65	1.77	1.88	2.85	2.10	2.25
S5	1.44	1.38	1.98	1.74	1.53	1.61
S6	4.80	4.04	3.90	3.50	3.61	3.97
Avg	3.40	2.68	3.09	2.96	2.50	2.92
S7	1.97	2.57	1.84	3.73	2.40	2.50
S8	3.37	3.65	2.65	8.17	2.40	4.05
S9	7.65	9.93	5.23	3.82	8.22	6.97
Avg	4.33	5.38	3.24	5.24	4.34	4.51

and the input latency was about 3 seconds. For subjects S8 and S9, who only completed the training phase, error was higher, 13% for S8 and 20% for S9. Average input latency for subjects S7 and S8 was comparable to those who completed the entire study. Input latency for S9, however, was considerably higher at 6.97 seconds.

6.5.2 Spelling Phase

Table 6.3 shows the spelling rates obtained for each speller and text during the three-part spelling phase. We applied the Friedman Test—a common non-parametric statistical test for repeated measures experiments—to determine any significant differences in spelling rate due to the speller interface across all of the texts (Txt1, Txt2, Txt3, Txt4, and Txt5). The Friedman Test revealed a significant main effect of speller interface ($\chi^2 = 10.17$, $p < 0.01$) on spelling rate. Post-hoc tests with Bonferroni correction revealed that our speller was significantly faster than the speller of Volosyak ($p < 0.05$) and the speller of Cecotti ($p < 0.05$), but our implementations of the spellers of Volosyak and Cecotti did not differ significantly in performance from one another ($p > 0.5$). For single-word texts (Txt1, Txt2 and Txt3) average spelling rates obtained with all three spellers were similar, averaging 7.33 cpm for our speller, 6.32 cpm for the speller of Volosyak, and 6.25 cpm for the speller of Cecotti. For multiple-word texts (Txt4 and Txt5), the average spelling rate obtained with our speller (11.93 cpm) was nearly twice as fast as those obtained with the spellers of Volosyak (5.69 cpm) and Cecotti (6.22 cpm). Notably, using our speller subject S2 achieved more than 17 cpm by spelling Txt5 with zero input error and with 2.5 seconds of mean input latency.

Table 6.4 shows the average input error, input latency, and input per character ratio for each of the three spellers and five texts. Input errors (Table 6.4a) increased compared to training, but were similar across both single-word and multiple-word texts at about 5%. Input latencies (Table 6.4b) also increased compared to training from 2.92 seconds to 3.38 seconds for the speller of Cecotti, 3.60 seconds for our speller, and 3.91 seconds for the speller of Volosyak. During the spelling of multiple-word texts our speller required less than half (1.60) the number of the inputs as the spellers of Volosyak

Table 6.3: Spelling Phase Results - Spelling Rate

(a) Average spelling rates (by subject and text) for our speller

Subject	Txt1	Txt2	Txt3	Single Words	Txt4	Txt5	Multiple Words
S1	6.75	9.93	4.31	7.00	10.96	11.09	11.03
S2	7.89	10.00	11.11	9.67	15.05	17.12	16.09
S3	2.31	10.33	8.90	7.18	12.23	13.44	12.84
S4	3.93	10.15	4.76	6.28	10.41	8.97	9.69
S5	4.82	14.74	11.16	10.24	15.67	15.53	15.60
S6	1.95	2.26	6.63	3.61	6.95	5.72	6.34
Avg	4.61	9.57	7.81	7.33	11.88	11.98	11.93

(b) Average spelling rates (by subject and text) for speller of Volosyak [197]

Subject	Txt1	Txt2	Txt3	Single Words	Txt4	Txt5	Multiple Words
S1	4.52	5.35	5.16	5.01	4.27	4.55	4.41
S2	5.61	6.10	10.67	7.46	5.96	5.61	5.79
S3	4.67	7.75	9.62	7.35	7.43	8.15	7.79
S4	4.45	4.78	8.72	5.98	5.92	6.52	6.22
S5	7.48	7.24	12.18	8.97	7.55	8.18	7.87
S6	2.09	2.77	4.65	3.17	2.75	1.38	2.07
Avg	4.80	5.67	8.50	6.32	5.65	5.73	5.69

(c) Average spelling rates (by subject and text) for speller of Cecotti [36]

Subject	Txt1	Txt2	Txt3	Single Words	Txt4	Txt5	Multiple Words
S1	3.52	4.56	3.59	3.89	3.95	4.75	4.35
S2	5.59	8.95	6.14	6.89	7.35	6.80	7.08
S3	8.25	9.15	7.53	8.31	9.03	4.22	6.63
S4	5.65	8.39	8.82	7.62	6.16	7.35	6.76
S5	3.44	10.51	9.34	7.76	8.12	9.87	9.00
S6	2.67	3.42	2.90	3.00	3.17	3.87	3.52
Avg	4.85	7.50	6.39	6.25	6.30	6.14	6.22

Table 6.4: Spelling Phase Results - Input Error, Input Latency, and Input per Character Ratio

(a) % Input Error (ϵ) for each target, averaged across subjects

Speller	Txt1	Txt2	Txt3	Single Words	Txt4	Txt5	Multiple Words
Ours	0.09	0.04	0.02	0.05	0.02	0.04	0.03
Volosyak	0	0.03	0.11	0.05	0.04	0.05	0.05
Cecotti	0.03	0.02	0.05	0.03	0.04	0.09	0.07

(b) Input latency ($\mathbb{E}(T)$) in seconds for each target, averaged across subjects

Speller	Txt1	Txt2	Txt3	Single Words	Txt4	Txt5	Multiple Words
Ours	3.66	3.40	3.63	3.60	3.44	3.45	3.45
Volosyak	4.35	3.46	3.93	3.91	3.55	3.31	3.43
Cecotti	3.98	2.95	3.22	3.38	3.25	2.95	3.10

(c) Input/character ratio (C) for each target, averaged across subjects

Speller	Txt1	Txt2	Txt3	Single Words	Txt4	Txt5	Multiple Words
Ours	4.44	2.40	2.40	3.08	1.58	1.62	1.60
Volosyak	3.33	3.40	2.07	2.93	3.35	4.13	3.74
Cecotti	3.56	3.13	3.43	3.37	3.38	3.84	3.61

Table 6.5: Simulation Study

(a) Average simulated spelling rates (R) of single-word texts (Txt1, Txt2, Txt3) for an average of subjects S1-S6, subject S8, and subject S9. Simulations that failed to produce the target text are denoted "-".

Speller	Average (S1-S6)	S8	S9
Ours	9.45	6.15	3.99
Volosyak	7.26	3.32	-
Volosyak (original)	8.18	3.60	-
Cecotti	6.17	4.40	1.22

(b) Average simulated spelling rates (R) of multiple-word texts (Txt4, Txt5) for an average of subjects S1-S6, subject S8, and subject S9. Simulations that failed to produce the target text are denoted "-".

Speller	Average (S1-S6)	S8	S9
Ours	15.1	10.38	1.78
Volosyak	6.29	3.52	-
Volosyak (original)	6.38	3.58	-
Cecotti	6.03	4.49	1.21

(3.74) or Cecotti (3.61) to specify the same characters (Table 6.4c).

6.5.3 Simulation Study

Table 6.5 shows the results of Monte-Carlo simulations. For single-word texts, the original layout for the speller of Volosyak [197] was, on average, 0.92 cpm faster for S1-S6 than the layout we used in our implementation of this speller. For multiple-word texts, the original layout of the speller of Volosyak [197] was 0.09 cpm faster for S1-S6 than the layout we used in our implementation of this speller.

6.6 Discussion

When asked to specify multiple-word texts, participant performance with our speller (11.93 cpm) was nearly double that with the compared spellers (5.69 cpm for the speller of Volosyak [197] and 6.22 cpm for the speller

of Cecotti [36]). This increase in performance was not due to differences in input error (Table 6.4a), in input latency (Table 6.4b), or in the size and shape of visual targets, which were identical. Instead, the performance increase can be attributed to the reduction in the number of queries required to determine the desired input character. In particular, when evaluated on multiple-word texts, our speller required less than half the number of queries as the spellers of Cecotti [36] or Volosyak [200] to specify a character, on average (Table 6.4c). Our use of a larger query pool and of IGR as a measure of performance to be maximized when choosing queries from this pool was what led to this reduction in the number of required queries.

Despite the fact that users specified texts faster with our speller, results show that the spelling rate for single-word texts was comparable for all three interfaces: 7.33 cpm with our speller, 6.32 cpm with the speller of Volosyak [197], and 6.25 with the speller of Cecotti [36]. We attribute the lower spelling rate of our interface under these conditions to the higher NLL values of the single-word texts (Table 6.1). In particular, we observe a clear inverse relationship between NLL and spelling rate in Table 6.3a: Txt1 had an NLL of 7.19 and was spelled at a rate of 4.61 cpm, Txt3 had an NLL of 5.31 and was spelled at a rate of 7.81 cpm, and Txt2 had an NLL of 3.04 and was spelled at a rate of 9.57 cpm. Both multiple-word texts had lower NLLs—closer to the average of English text, which is 2 bits per character [14, 124]—and consequently higher average spelling rates. The reason for this trend is that, by using a language model, our speller tries to take advantage of the fact that text with high NLL (e.g., "BCI" as in Txt1) is rare in everyday conversation.

Results from the simulation studies suggest that the increase in performance with our speller as compared to the speller of Volosyak [197] was not due to the small difference in character layout. The fifth row of the character grid in our implementation was shifted one character to the right of the original implementation described in [197]. We simulated performance with our implementation and compared it with the performance of the original implementation. These simulations showed no difference between our implementation (6.38 cpm) and the original (6.29 cpm) for multiple-word texts. For single-word texts, the original implementation was slightly faster (8.18 cpm) than our implementation (7.26 cpm). We note that the original versions of the spellers of Volosyak [197] and Cecotti [36] also differed from our implementations in the locations of the targets. The effect of this change has

not been investigated further, may have increased overall input latency, and represents a potential source of error.

One interesting trend that emerged from our study is that the average input latency of users with our speller (3.60 seconds) was higher than the average input latency for the speller of Cecotti [36] (3.38 seconds). The input latency of all three spellers was slower than the average input latency during training (2.92 seconds). Since the layout of characters in our speller changes for each query, the user needs to visually search the layout in order to locate their desired character, slowing target selection in our speller as opposed to the speller of Cecotti [36]. Our speller was designed to minimize this issue by displaying characters in a single, alphabetically ordered, row. There may be conditions, however, when smaller query pools are actually preferable. Another possible drawback of our speller is that it requires training. This requirement is a limitation of the design, but it may be possible to either minimize this training step or to use an online training paradigm. Some more advanced classifier designs also require training data [87]—it may be possible to train both the speller and the classifier simultaneously. With respect to our use of multiple query types, further work would be needed to characterize the impact of each type of query on overall performance.

6.7 Conclusion

In this chapter, we presented a steady-state visually evoked potential based brain-computer interface that allowed users to input text by responding to a sequence of queries. These queries were chosen from a large query pool to maximize IGR, the expected amount of information to be received per unit of time about the desired character. The computation of IGR was based on three models, a language model (that predicted likely characters based on context) and two models of user performance (input accuracy and input latency). Experimental results demonstrated that six subjects were able to use our interface to input multiple-word text at an average of 11.93 cpm, with one subject achieving an average spelling rate of 16.09 cpm.

There are several ways in which the interface described here could be improved. Input response times could be reduced through the use of different classifiers (such as those by Lin [112] or Johnson [87]), the shape and size of

the stimuli could be changed, the number of input classes could be increased, word completion [196] could be implemented, and different frequencies could be assigned to the targets. As an example of how these changes might improve the interface, consider the assignment of frequencies to targets. It is clear from our training data (Table 6.2) that this association matters. For example, during training subject S2 selected Target 5 (8.57Hz) more than twice as fast (2.85s) as Target 1 (7.5Hz, 6.07s). In other words, for subject S2, Target 5 was easier to select than Target 1. If we switch the assignment of frequencies to targets, we would expect Target 1 (8.57Hz) to be easier to select than Target 5 (7.5Hz). In our interface, the set of characters with which Target 1 and Target 5 are associated are different. Thus, when we change the assignment of frequencies to targets, we expect a specific set of characters to be easier to select. IGR could be used to determine the best assignment of frequencies to targets. This could improve the maximum spelling rate of participants and represents a topic of future work.

6.8 Derivation of Language Model Update Rule

We will proceed to derive Equation (6.3), which says how to update the language model given an observed target y in response to a query f_i. Bayes' theorem tells us that

$$p_{C|Y}(c|y) = \frac{p_{Y|C}(y|c)p_C(c)}{\sum_{s\in\mathcal{C}} p_{Y|C}(y|s)p_C(s)} \tag{6.10}$$

for all $c \in \mathcal{C}$. Note that

$$\begin{aligned} p_{Y|C}(y|c) &= \sum_{x\in\mathcal{U}} p_{Y|X,C}(y|x,c)p_{X|C}(x|c) && (6.11)\\ &= \sum_{x\in\mathcal{U}} p_{Y|X}(y|x)p_{X|C}(x|c) && (6.12)\\ &= p_{Y|X}(y|f_i(c)), && (6.13) \end{aligned}$$

where (6.11) follows from the law of total probability, (6.12) follows by assumption that the observed target and the desired character are conditionally independent given knowledge of the desired target, and (6.13) follows by as-

sumption of zero user error in response to a query, since in this case

$$p_{X|C}(x|c) = \begin{cases} 1 & \text{if } f_i(c) = x \\ 0 & \text{otherwise.} \end{cases}$$

After substitution of (6.13) into (6.10), we arrive at (6.3).

6.9 Derivation of Information Gain Rate

We will proceed to derive Equations (6.7)-(6.9), which are used to compute the IGR. Equation (6.7) follows from the definition of conditional probability. Equation (6.8) follows from the law of total probability. Equation (6.9) follows from the law of total probability

$$p_X(x) = \sum_{c \in \mathcal{C}} p_{X|C}(x|c) p_C(c)$$

and by assumption of zero user error in response to a query, since in this case

$$p_{X|C}(x|c) = \begin{cases} 1 & \text{if } f_i(c) = x \\ 0 & \text{otherwise.} \end{cases}$$

CHAPTER 7

CONCLUSION

This dissertation described five fundamental contributions to the design of SSVEP-based BCIs.

- In Chapter 2, we described a new method for investigating how SSVEPs are generated in the brain, one that is based on the elicitation of SSVEPs during sleep. This study provided a theoretical motivation for eliciting SSVEPs during sleep, experimental evidence that SSVEPs can be elicited during sleep, and supplemental data that suggests that SSVEPs elicited during sleep are larger in amplitude than those elicited during waking.

- In Chapter 3, the performance of children using an SSVEP-based BCI for target selection was reported, and this data was compared to data from adults using the same SSVEP-based BCI. The data showed that children were able to use an SSVEP-based BCI with an accuracy that is much greater than previously believed. Furthermore, the target selection accuracy of the 11 children who completed the experimental phase of our study was very similar to the target selection accuracy of the adults. This work was only the second study to investigate SSVEP-based BCIs for children.

- In Chapter 4, a new epidermal electronic system electrode was presented. The electrode can record EEG from non-hair bearing regions without electrolyte gel or a mechanical fastener. In addition, this new electrode has the appearance of a second skin, conforming to the wearer. These properties increase the likelihood that a user would wear this system outside of the research laboratory.

- In Chapter 5, a potential application for SSVEP-based BCIs in those without disabilities was discussed. In this chapter, we also reported one

of the only comparisons between SSVEP-based BCIs and traditional input mechanisms. There is a perception within the field of brain-computer interfacing that, when targeting users without disabilities, BCIs are low performing replacements for existing input mechanisms. The experiments reported in Chapter 5 challenged that perception. They showed that inputs obtained from an SSVEP-based BCI on a desktop were non-inferior to those obtained through speech recognition or touch gestures. In the very specific case of a binary selection task, SSVEP-based BCIs may provide performance that is as good, or better than other methodologies. One potential application for such a BCI would be in augmented or virtual reality systems.

- Finally, in Chapter 6, the design of an SSVEP-based BCI for text-entry is presented. This system enabled users to input character selections nearly twice as fast as two existing SSVEP-based BCI interfaces implemented for the purpose of comparison. While a more recent SSVEP-based BCI for text-entry has achieved even higher performance [38], the system we described only used five stimuli to make selections, while Chen et al. [38] used 40. The use of fewer stimuli may be particularly applicable in the case of those with disabilities, such as LIS, who have limited ability to move their eyes.

7.1 Future Work

Each of the five studies presented in this dissertation raised new questions that could be the focus of future research.

- SSVEPs can be elicited during sleep (Chapter 2). Experimental evidence from our study as well as a study by Sharon and Nir [181] suggest that SSVEPs elicited during sleep are different than those elicited during waking. Neither our study nor the study by Sharon and Nir [181] accounted for dark adaptation. This makes it difficult to determine whether the differences in SSVEPs observed were due to sleep or dark adaptation. In addition, the combined data from two studies only considered a few of the variables (e.g. frequency and color) that are known to impact the amplitude of SSVEPs. Therefore, it remains unclear

how exactly the morphology of SSVEPs change with sleep. Further research that shows how sleep affects SSVEPs may then allow us to test hypotheses about how these signals are generated in the brain.

- Data reported in Chapter 3 show that 9-11 year old children can use an SSVEP-based BCI for target selection. Of the 14 children who participated, 3 were unable to exceed the threshold for inclusion into the experimental phase. We posed several possible explanations for this result. First, it is possible that the children were not engaged with the task. Another explanation is that developmental differences between children and adults explain the differences observed in the experiments. It is also possible that random chance is the reason that all of the adults met the criteria for inclusion while three children were excluded. Resolving which of these hypotheses (or others) to explain why some children performed poorly during the training phase would contribute greatly to the development of BCIs for children.

  Given the overall performance of the children included in the experimental phase of our study, it is also of interest to determine how well younger children perform when using an SSVEP-based BCI. Investigating a younger age group could simultaneously extend our understanding of who can use an SSVEP-based BCI and may help us to understand why some children performed poorly during the training session. If younger children can also use the SSVEP-based BCI, this may enable new applications for these systems for children with or without physical disabilities.

- The EES electrodes presented in Chapter 4 have the potential to enable unobtrusive long-term EEG recording outside of the laboratory. There are many ways, however, that the current design could be improved. For example, different metals (instead of gold) could reduce cost or increase signal quality, a conductive coating might improve contact, or better connectors could ease electrode placement and longevity.

- The experiments described in Chapter 5 require careful consideration. Our data show that the SSVEP-based BCI on a desktop computer was non-inferior to two traditional input mechanisms for augmented and virtual reality applications. Non-inferiority tests, however, should be

based on an *a priori* hypothesis, not a *post hoc* analysis. Therefore, at a minimum, our experiments should be replicated. If SSVEP-based BCIs are non-inferior to the two input mechanisms that we tested, they may be slower or less accurate than other untested input mechanisms. Non-inferiority tests are implicitly designed to answer the question of whether two systems are close enough in performance that any differences are not important. This evokes the question of how much of a difference in performance matter. Even more interestingly, are perceptions of differences in performance between two input mechanisms the same as the actual performance differences? It is intriguing to consider that maybe SSVEP-based BCIs are perceived as being slow, when in fact, their performance is as good or better than other input mechanisms.

- Building on our work on the SSVEP-based BCI user interface. There are many ways that our text-entry system could be improved. A larger pool of queries could be considered, models of user performance could be updated in real-time, and the dictionary could be vastly reduced to consider only words that an SSVEP-based BCI user may want to input. Perhaps the more important question to ask is why SSVEP-based BCIs for text-entry merit further development? These systems are often purported to be for those with physical disabilities, but are always tested on people without physical disabilities.

Taken together, the five contributions described in this dissertation each move a step toward solving the challenges facing the design of SSVEP-based BCIs. As a result, these challenges can be more clearly defined and the potential uses of SSVEP-based BCIs can be better understood. Through continued research, the long-term goal of a useful BCI for those with or without disabilities will be achieved, and Vidal's vision of a genuine prosthetic for the brain will be realized.

REFERENCES

[1] E. D. Adrian and B. H. C. Matthews. The interpretation of potential waves in the cortex. *The Journal of Physiology*, 81(4):440–471, Jul 1934.

[2] A. Akce, J. Norton, and T. Bretl. A brain-machine interface to navigate mobile robots along human-like paths amidst obstacles. In *2012 IEEE/RSJ International Conference on Intelligent Robots and Systems*. Institute of Electrical & Electronics Engineers (IEEE), Oct 2012.

[3] A. Akce, J. J. S. Norton, and T. Bretl. An SSVEP-based brain computer interface for text spelling with adaptive queries that maximize information gain rates. *IEEE Transactions on Neural Systems and Rehabilitation Engineering*, 23(5):857–866, Sep 2015.

[4] B. Allison, B. Graimann, and A. Gräser. Why use a BCI if you are healthy? In *BrainPlay'07 Brain-Computer Interfaces and Games Workshop at ACE (Advances in Computer Entertainment)*, pages 7–11, 2007.

[5] B. Allison, T. Lüth, D. Valbuena, A. Teymourian, I. Volosyak, and A. Gräser. BCI demographics: How many (and what kinds of) people can use an SSVEP BCI? *IEEE Transactions on Neural Systems and Rehabilitation Engineering*, 18(2):107–116, Apr 2010.

[6] B. Z. Allison, S. Dunne, R. Leeb, J. d. R. Millán, and A. Nijholt, editors. *Towards practical brain-computer interfaces: bridging the gap from research to real-world applications*. Springer Science & Business Media, Aug 2012.

[7] B. Z. Allison, D. J. McFarland, G. Schalk, S. D. Zheng, M. M. Jackson, and J. R. Wolpaw. Towards an independent brain–computer interface using steady state visual evoked potentials. *Clinical Neurophysiology*, 119(2):399–408, Feb 2008.

[8] S. Amiri, A. Rabbi, L. Azinfar, and R. Fazel-Rezai. A review of p300, SSVEP, and hybrid p300/SSVEP brain-computer interface systems. In *Brain-Computer Interface Systems - Recent Progress and Future Prospects*. InTech, Jun 2013.

[9] S. K. Andersen and M. M. Mller. Behavioral performance follows the time course of neural facilitation and suppression during cued shifts of feature-selective attention. *Proceedings of the National Academy of Sciences*, 107(31):13878–13882, 2010.

[10] P. Apkarian, M. Mirmiran, and R. Tijssen. Effects of behavioural state on visual processing in neonates. *Neuropediatrics*, 22(2):85–91, May 1991.

[11] C. Babiloni, C. Del Percio, L. Arendt-Nielsen, A. Soricelli, G. L. Romani, P. M. Rossini, and P. Capotosto. Cortical EEG alpha rhythms reflect task-specific somatosensory and motor interactions in humans. *Clinical Neurophysiology*, 125(10):1936–1945, Oct 2014.

[12] D.-H. Baek, J. Lee, H. jin Byeon, H. Choi, I. Y. Kim, K.-M. Lee, J. J. Pak, D. P. Jang, and S.-H. Lee. A thin film polyimide mesh microelectrode for chronic epidural electrocorticography recording with enhanced contactability. *Journal of Neural Engineering*, 11(4):046023, Jul 2014.

[13] S. W. Baertschi, D. Clapham, C. Foti, P. J. Jansen, S. Kristensen, R. A. Reed, A. C. Templeton, and H. H. Tnnesen. Implications of in-use photostability: proposed guidance for photostability testing and labeling to support the administration of photosensitive pharmaceutical products, part 1: drug products administered by injection. *Journal of Pharmaceutical Sciences*, 102(11):3888–3899, Nov 2013.

[14] R. Begleiter, R. El-Yaniv, and G. Yona. On prediction using variable order Markov models. *Journal of Artificial Intelligence Research*, 22:385–421, Dec 2004.

[15] H. Berger. Psyche, 1940. *Jena: Gustav Fischer*.

[16] H. Berger. Über das elektrenkephalogramm des menschen. *Archiv für Psychiatrie und Nervenkrankheiten*, 87(1):527–570, Dec 1929.

[17] R. B. Berry, R. Brooks, C. E. Gamaldo, S. M. Hardling, C. L. Marcus, and B. V. Vaughn. *The AASM manual for the scoring of sleep and associated events: rules, terminology and technical specifications*. American Academy of Sleep Medicine, Darien, Illinois, version 2.0.2 edition, 2012.

[18] N. Bigdely-Shamlo, A. Vankov, R. R. Ramirez, and S. Makeig. Brain activity-based image classification from rapid serial visual presentation. *IEEE Transactions on Neural Systems and Rehabilitation Engineering*, 16(5):432–441, Oct 2008.

[19] G. Bin, X. Gao, Z. Yan, B. Hong, and S. Gao. An online multi-channel SSVEP-based braincomputer interface using a canonical correlation analysis method. *Journal of Neural Engineering*, 6(4):046002, Jun 2009.

[20] A. Birca, L. Carmant, A. Lortie, and M. Lassonde. Interaction between the flash evoked SSVEPs and the spontaneous EEG activity in children and adults. *Clinical Neurophysiology*, 117(2):279–288, Feb 2006.

[21] A. Birca, L. Carmant, A. Lortie, P. Vannasing, H. Sauerwein, M. Robert, L. Lemay, X.-P. Wang, D. Piper, V. Donici, et al. Maturational changes of 5hz SSVEPs elicited by intermittent photic stimulation. *International Journal of Psychophysiology*, 78(3):295–298, Dec 2010.

[22] G. E. Birch, Z. Bozorgzadeh, and S. G. Mason. Initial on-line evaluations of the LF-ASD brain-computer interface with able-bodied and spinal-cord subjects using imagined voluntary motor potentials. *IEEE Transactions on Neural Systems and Rehabilitation Engineering*, 10(4):219–224, Dec 2002.

[23] B. Blankertz, G. Dornhege, M. Krauledat, M. Schröder, J. Williamson, R. Murray-Smith, and K.-R. Müller. The berlin brain-computer interface presents the novel mental typewriter hex-o-spell. 2006.

[24] B. Blankertz, M. Krauledat, G. Dornhege, J. Williamson, R. Murray-Smith, and K.-R. Müller. A note on brain actuated spelling with the Berlin brain-computer interface. In C. Stephanidis, editor, *Universal Access in Human-Computer Interaction. Ambient Interaction*, volume 4555, pages 759–768. Springer-Verlag Berlin Heidelberg, 2007.

[25] A. P. Born, I. Law, T. E. Lund, E. Rostrup, L. G. Hanson, G. Wildschidtz, H. C. Lou, and O. B. Paulson. Cortical deactivation induced by visual stimulation in human slow-wave sleep. *NeuroImage*, 17(3):1325–1335, Nov 2002.

[26] D. A. Bowman, E. Kruijff, J. J. LaViola Jr, and I. Poupyrev. *3D User Interfaces: Theory and Practice*. Addison-Wesley, 2004.

[27] D. H. Brainard. The psychophysics toolbox. *Spatial Vision*, 10(4):433–436, Jan 1997.

[28] M.-A. Bruno, J. L. Bernheim, D. Ledoux, F. Pellas, A. Demertzi, and S. Laureys. A survey on self-assessed well-being in a cohort of chronic locked-in syndrome patients: happy majority, miserable minority. *BMJ open*, 1(1):e000039–e000039, Feb 2011.

[29] M.-A. Bruno, C. Schnakers, F. Damas, F. Pellas, I. Lutte, J. Bernheim, S. Majerus, G. Moonen, S. Goldman, and S. Laureys. Locked-in syndrome in children: report of five cases and review of the literature. *Pediatric Neurology*, 41(4):237–246, Oct 2009.

[30] D. T. Bundy and E. C. Leuthardt. An ipsilateral, contralesional BCI in chronic stroke patients. In *SpringerBriefs in Electrical and Computer Engineering*, pages 19–29. Springer International Publishing, 2014.

[31] G. L. Calhoun and G. R. McMillan. EEG-based control for human-computer interaction. In *Proceedings Third Annual Symposium on Human Interaction with Complex Systems. HICS'96*, pages 4–9. IEEE, IEEE Comput Soc Press, 1996.

[32] F. W. Campbell and J. J. Kulikowski. The visual evoked potential as a function of contrast of a grating pattern. *The Journal of Physiology*, 222(2):345–356, Apr 1972.

[33] A. Capilla, P. Pazo-Alvarez, A. Darriba, P. Campo, and J. Gross. Steady-state visual evoked potentials can be explained by temporal superposition of transient event-related responses. *PLoS ONE*, 6(1):e14543, Jan 2011.

[34] R. Caton. Electrical currents of the brain. *The Journal of Nervous and Mental Disease*, 2(4):610, 1875.

[35] R. Cecere, G. Rees, and V. Romei. Individual differences in alpha frequency drive crossmodal illusory perception. *Current Biology*, 25(2):231–235, Jan 2015.

[36] H. Cecotti. A self-paced and calibration-less SSVEP-based brain-computer interface speller. *IEEE Transactions on Neural Systems and Rehabilitation Engineering*, 18(2):127–133, Apr 2010.

[37] H. Cecotti. Spelling with non-invasive brain–computer interfaces – current and future trends. *Journal of Physiology-Paris*, 105(1–3):106–114, July 2011.

[38] X. Chen, Y. Wang, M. Nakanishi, X. Gao, T.-P. Jung, and S. Gao. High-speed spelling with a noninvasive brain-computer interface. *Proceedings of the National Academy of Sciences*, 112(44):E6058–E6067, Oct 2015.

[39] M. Cheng and S. Gao. An EEG-based cursor control system. In *[Engineering in Medicine and Biology, 1999. 21st Annual Conference and the 1999 Annual Fall Meetring of the Biomedical Engineering Society] BMES/EMBS Conference, 1999. Proceedings of the First Joint*,

volume 1, pages 669–vol. IEEE, Institute of Electrical & Electronics Engineers (IEEE), 1999.

[40] M. Cheng, X. Gao, S. Gao, and D. Xu. Multiple color stimulus induced steady state visual evoked potentials. In *2001 Conference Proceedings of the 23rd Annual International Conference of the IEEE Engineering in Medicine and Biology Society*, volume 2, pages 1012–1014. IEEE, Institute of Electrical & Electronics Engineers (IEEE), 2001.

[41] Y. M. Chi, T.-P. Jung, and G. Cauwenberghs. Dry-contact and non-contact biopotential electrodes: methodological review. *IEEE Reviews in Biomedical Engineering*, 3:106–119, 2010.

[42] J. Cleary and I. Witten. Data compression using adaptive coding and partial string matching. *IEEE Transactions on Communications*, 32(4):396–402, Apr 1984.

[43] L. T. Cohen, F. W. Rickards, and G. M. Clark. A comparison of steady-state evoked potentials to modulated tones in awake and sleeping humans. *The Journal of the Acoustical Society of America*, 90(5):2467–2479, Nov 1991.

[44] T. F. Collura. History and evolution of electroencephalographic instruments and techniques. *Journal of Clinical Neurophysiology*, 10(4):476–504, 1993.

[45] E. Colon, V. Legrain, and A. Mouraux. Steady-state evoked potentials to study the processing of tactile and nociceptive somatosensory input in the human brain. *Neurophysiologie Clinique/Clinical Neurophysiology*, 42(5):315–323, Oct 2012.

[46] I. M. Colrain and K. B. Campbell. The use of evoked potentials in sleep research. *Sleep Medicine Reviews*, 11(4):277–293, Aug 2007.

[47] A. Compston. The berger rhythm: potential changes from the occipital lobes in man, by e.d. adrian and b.h.c. matthews (from the physiological laboratory, cambridge). brain 1934: 57: 355-385. *Brain*, 133(1):3–6, Jan 2010.

[48] J. C. G. Costa, P. J. G. Da-Silva, R. M. V. Almeida, and A. F. C. Infantosi. Validation in principal components analysis applied to EEG data. *Computational and Mathematical Methods in Medicine*, 2014:1–10, 2014.

[49] K. A. Cote. Probing awareness during sleep with the auditory odd-ball paradigm. *International Journal of Psychophysiology*, 46(3):227–241, Dec 2002.

[50] T. M. Cover and J. A. Thomas. *Elements of Information Theory*. John Wiley & Sons, Inc., New York, NY, 2nd edition, Apr 2005.

[51] A. Delorme and S. Makeig. EEGLAB: an open source toolbox for analysis of single-trial EEG dynamics including independent component analysis. *Journal of Neuroscience Methods*, 134(1):9–21, Mar 2004.

[52] M. Dencheva, M. Lyapina, A. Kisselova-Yaneva, S. Garov, S. Hristova, M. Konstantinova, and D. Majlekov. Thermovision in dental allergology. *Journal of IMAB–Annual Proceeding (Scientific Papers)*, 20(3):558–562, Aug 2014.

[53] F. Di Russo, S. Pitzalis, T. Aprile, G. Spitoni, F. Patria, A. Stella, D. Spinelli, and S. A. Hillyard. Spatiotemporal analysis of the cortical sources of the steady-state visual evoked potential. *Human Brain Mapping*, 28(4):323–334, 2007.

[54] A. J. Doud, J. P. Lucas, M. T. Pisansky, and B. He. Continuous three-dimensional control of a virtual helicopter using a motor imagery based brain-computer interface. *PLoS ONE*, 6(10):e26322, Oct 2011.

[55] A. Duszyk, M. Bierzyńska, Z. Radzikowska, P. Milanowski, R. Kuś, P. Suffczyński, M. Michalska, M. Łabecki, P. Zwoliński, and P. Durka. Towards an optimization of stimulus parameters for brain-computer interfaces based on steady state visual evoked potentials. *PLoS ONE*, 9(11):e112099, Nov 2014.

[56] F. Ebrahimi, M. Mikaeili, E. Estrada, and H. Nazeran. Automatic sleep stage classification based on EEG signals by using neural networks and wavelet packet coefficients. In *2008 30th Annual International Conference of the IEEE Engineering in Medicine and Biology Society*, volume 2008, pages 1151–1154. Institute of Electrical & Electronics Engineers (IEEE), Aug 2008.

[57] J. Ehlers, D. Valbuena, A. Stiller, and A. Gräser. Age-specific mechanisms in an SSVEP-based BCI scenario: evidences from spontaneous rhythms and neuronal oscillators. *Computational Intelligence and Neuroscience*, 2012:1–9, 2012.

[58] J. Faller, R. Leeb, G. Pfurtscheller, and R. Scherer. Avatar navigation in virtual and augmented reality environments using an SSVEP BCI. In *International Conference on Applied Bionics and Biomechanics (ICABB)*, 2010.

[59] J. Faller, G. Müller-Putz, D. Schmalstieg, and G. Pfurtscheller. An application framework for controlling an avatar in a desktop-based virtual environment via a software SSVEP brain–computer interface. *Presence: Teleoperators and Virtual Environments*, 19(1):25–34, Feb 2010.

[60] L. Farwell and E. Donchin. Talking off the top of your head: toward a mental prosthesis utilizing event-related brain potentials. *Electroencephalography and Clinical Neurophysiology*, 70(6):510–523, Dec 1988.

[61] I. P. Fawcett, G. R. Barnes, A. Hillebrand, and K. D. Singh. The temporal frequency tuning of human visual cortex investigated using synthetic aperture magnetometry. *NeuroImage*, 21(4):1542–1553, Apr 2004.

[62] R. Fazel-Rezai, B. Z. Allison, C. Guger, E. W. Sellers, S. C. Kleih, and A. Kbler. P300 brain computer interface: current challenges and emerging trends. *Frontiers in Neuroengineering*, 5(14), Jul 2012.

[63] T. C. Ferree, P. Luu, G. S. Russell, and D. M. Tucker. Scalp electrode impedance, infection risk, and EEG data quality. *Clinical Neurophysiology*, 112(3):536–544, Mar 2001.

[64] R. S. Fisher, G. Harding, G. Erba, G. L. Barkley, and A. Wilkins. Photic- and pattern-induced seizures: A review for the epilepsy foundation of america working group. *Epilepsia*, 46(9):1426–1441, Sep 2005.

[65] O. Friman, I. Volosyak, and A. Gräser. Multiple channel detection of steady–state visual evoked potentials for brain–computer interfaces. *IEEE Transactions on Biomedical Engineering*, 54(4):742–750, Apr 2007.

[66] L. Genzel, M. C. W. Kroes, M. Dresler, and F. P. Battaglia. Light sleep versus slow wave sleep in memory consolidation: a question of global versus local processes? *Trends in Neurosciences*, 37(1):10–19, Jan 2014.

[67] S. Giselbrecht, B. E. Rapp, and C. M. Niemeyer. The chemistry of cyborgsinterfacing technical devices with organisms. *Angewandte Chemie International Edition*, 52(52):13942–13957, 2013.

[68] M. Gray, A. H. Kemp, R. B. Silberstein, and P. J. Nathan. Cortical neurophysiology of anticipatory anxiety: an investigation utilizing steady state probe topography (SSPT). *NeuroImage*, 20(2):975–986, Oct 2003.

[69] C. Guger, B. Z. Allison, B. Großwindhager, R. Prückl, C. Hintermüller, C. Kapeller, M. Bruckner, G. Krausz, and G. Edlinger. How many people could use an SSVEP BCI? *Frontiers in Neuroscience*, 6:169, 2012.

[70] C. Guger, S. Daban, E. Sellers, C. Holzner, G. Krausz, R. Carabalona, F. Gramatica, and G. Edlinger. How many people are able to control

a P300-based brain–computer interface (BCI)? *Neuroscience Letters*, 462(1):94–98, Sep 2009.

[71] C. Guger, G. Edlinger, W. Harkam, I. Niedermayer, and G. Pfurtscheller. How many people are able to operate an EEG-based brain-computer interface (bci)? *IEEE Transactions on Nural Systems and Rehabilitation Engineering*, 11(2):145–147, Jun 2003.

[72] L. F. Haas. Hans berger (1873–1941), richard caton (1842–1926), and electroencephalography. *Journal of Neurology, Neurosurgery & Psychiatry*, 74(1):9–9, Jan 2003.

[73] W. D. Hairston, K. W. Whitaker, A. J. Ries, J. M. Vettel, J. C. Bradford, S. E. Kerick, and K. McDowell. Usability of four commercially-oriented EEG systems. *Journal of Neural Engineering*, 11(4):046018, Jul 2014.

[74] B. Hamadicharef. Brain-computer interface (BCI) literature-a bibliometric study. In *10th International Conference on Information Science, Signal Processing and their Applications (ISSPA 2010)*, pages 626–629. Institute of Electrical & Electronics Engineers (IEEE), Institute of Electrical & Electronics Engineers (IEEE), May 2010.

[75] M. L. Hammock, A. Chortos, B. C. K. Tee, J. B. H. Tok, and Z. Bao. 25th anniversary article: The evolution of electronic skin (e-skin): A brief history, design considerations, and recent progress. *Advanced Materials*, 25(42):5997–6038, 2013.

[76] Y. Hattori, L. Falgout, W. Lee, S.-Y. Jung, E. Poon, J. W. Lee, I. Na, A. Geisler, D. Sadhwani, Y. Zhang, Y. Su, X. Wang, Z. Liu, J. Xia, H. Cheng, R. C. Webb, A. P. Bonifas, P. Won, J.-W. Jeong, K.-I. Jang, Y. M. Song, B. Nardone, M. Nodzenski, J. A. Fan, Y. Huang, D. P. West, A. S. Paller, M. Alam, W.-H. Yeo, and J. A. Rogers. Multifunctional skin-like electronics for quantitative, clinical monitoring of cutaneous wound healing. *Advanced Healthcare Materials*, 3(10):1597–1607, Mar 2014.

[77] C. S. Herrmann. Human EEG responses to 100hz flicker: resonance phenomena in visual cortex and their potential correlation to cognitive phenomena. *Experimental Brain Research*, 137(3-4):346–353, Apr 2001.

[78] J. D. Hincapié-Ramos, K. Ozacar, P. P. Irani, and Y. Kitamura. Gyrowand: IMU-based raycasting for augmented reality head-mounted displays. In *Proceedings of the 3rd ACM Symposium on Spatial User Interaction - SUI '15*, pages 89–98. Association for Computing Machinery (ACM), 2015.

[79] J. A. Hobson. Sleep is of the brain, by the brain and for the brain. *Nature*, 437(7063):1254–1256, Oct 2005.

[80] J. Höhne, M. Schreuder, B. Blankertz, and M. Tangermann. A novel 9-class auditory ERP paradigm driving a predictive text entry system. *Frontiers in Neuroscience*, 5:99, 2011.

[81] P. Horki, T. Solis-Escalante, C. Neuper, and G. Müller-Putz. Combined motor imagery and SSVEP based BCI control of a 2 DoF artificial upper limb. *Medical & Biological Engineering & Computing*, 49(5):567–577, 2011.

[82] H.-T. Hsu, I.-H. Lee, H.-T. Tsai, H.-C. Chang, K.-K. Shyu, C.-C. Hsu, H.-H. Chang, T.-K. Yeh, C.-Y. Chang, and P.-L. Lee. Evaluate the feasibility of using frontal SSVEP to implement an SSVEP-based BCI in young, elderly and ALS groups. *IEEE Transactions on Neural Systems and Rehabilitation Engineering*, 24(5):603–615, May 2016.

[83] H.-J. Hwang, J.-H. Lim, Y.-J. Jung, H. Choi, S. W. Lee, and C.-H. Im. Development of an SSVEP-based BCI spelling system adopting a QWERTY-style LED keyboard. *Journal of Neuroscience Methods*, 208(1):59–65, 2012.

[84] J.-W. Jeong, M. K. Kim, H. Cheng, W.-H. Yeo, X. Huang, Y. Liu, Y. Zhang, Y. Huang, and J. A. Rogers. Capacitive epidermal electronics for electrically safe, long-term electrophysiological measurements. *Advanced Healthcare Materials*, 3(5):642–648, Oct 2013.

[85] J.-W. Jeong, W.-H. Yeo, A. Akhtar, J. J. S. Norton, Y.-J. Kwack, S. Li, S.-Y. Jung, Y. Su, W. Lee, J. Xia, et al. Materials and optimized designs for human-machine interfaces via epidermal electronics. *Advanced Materials*, 25(47):6839–6846, Sep 2013.

[86] C. Jia, X. Gao, B. Hong, and S. Gao. Frequency and phase mixed coding in SSVEP–based brain–computer interface. *IEEE Transactions on Biomedical Engineering*, 58(1):200–206, Jan 2011.

[87] E. C. Johnson, J. J. S. Norton, D. Jun, T. Bretl, and D. L. Jones. Sequential selection of window length for improved SSVEP-based BCI classification. In *Engineering in Medicine and Biology Society (EMBC), 2013 35th Annual International Conference of the IEEE*, pages 7060–7063. Institute of Electrical & Electronics Engineers (IEEE), Jul 2013.

[88] V. Jurcak, D. Tsuzuki, and I. Dan. 10/20, 10/10, and 10/5 systems revisited: their validity as relative head-surface-based positioning systems. *NeuroImage*, 34(4):1600–1611, Feb 2007.

[89] R. Kakigi, D. Naka, T. Okusa, X. Wang, K. Inui, Y. Qiu, T. D. Tran, K. Miki, Y. Tamura, T. B. Nguyen, S. Watanabe, and M. Hoshiyama. Sensory perception during sleep in humans: a magnetoencephalograhic study. *Sleep Medicine*, 4(6):493–507, Nov 2003.

[90] Y. Kim, N. Kaongoen, and S. Jo. Hybrid-BCI smart glasses for controlling electrical devices. In *2015 54th Annual Conference of the Society of Instrument and Control Engineers of Japan (SICE)*, pages 1162–1166. Institute of Electrical & Electronics Engineers (IEEE), Institute of Electrical & Electronics Engineers (IEEE), Jul 2015.

[91] Y.-J. Kim, M. Grabowecky, K. A. Paller, and S. Suzuki. Differential roles of frequency-following and frequency-doubling visual responses revealed by evoked neural harmonics. *Journal of Cognitive Neuroscience*, 23(8):1875–1886, Aug 2011.

[92] E. Kinney-Lang, B. Auyeung, and J. Escudero. Expanding the (kaleido) scope: exploring current literature trends for translating electroencephalography (EEG) based brain–computer interfaces for motor rehabilitation in children. *Journal of Neural Engineering*, 13(6):061002, Oct 2016.

[93] S. C. Kleih, F. Nijboer, S. Halder, and A. Kübler. Motivation modulates the P300 amplitude during brain–computer interface use. *Clinical Neurophysiology*, 121(7):1023–1031, 2010.

[94] B. Koo and S. Choi. SSVEP response on oculus rift. In *The 3rd International Winter Conference on Brain-Computer Interface*, pages 1–4. Institute of Electrical & Electronics Engineers (IEEE), Jan 2015.

[95] J. Kronegg, S. Voloshynovskyy, and T. Pun. Analysis of bit-rate definitions for brain-computer interfaces. 2005.

[96] A. Kübler, F. Nijboer, J. Mellinger, T. M. Vaughan, H. Pawelzik, G. Schalk, D. J. McFarland, N. Birbaumer, and J. R. Wolpaw. Patients with ALS can use sensorimotor rhythms to operate a brain-computer interface. *Neurology*, 64(10):1775–1777, May 2005.

[97] M. Kutas and K. D. Federmeier. Electrophysiology reveals semantic memory use in language comprehension. *Trends in Cognitive Sciences*, 4(12):463–470, Dec 2000.

[98] E. C. Lalor, S. P. Kelly, C. Finucane, R. Burke, R. Smith, R. B. Reilly, and G. Mcdarby. Steady-state VEP-based brain-computer interface control in an immersive 3D gaming environment. *EURASIP Journal on Applied Signal Processing*, 2005:3156–3164, 2005.

[99] G. Lantz, R. G. de Peralta, L. Spinelli, M. Seeck, and C. M. Michel. Epileptic source localization with high density EEG: how many electrodes are needed? *Clinical Neurophysiology*, 114(1):63–69, 2003.

[100] J. H. Lee, S. M. Lee, H. J. Byeon, J. S. Hong, K. S. Park, and S.-H. Lee. CNT/PDMS-based canal-typed ear electrodes for inconspicuous EEG recording. *Journal of Neural Engineering*, 11(4):046014, Jun 2014.

[101] S. M. Lee, H. J. Byeon, J. H. Lee, D. H. Baek, K. H. Lee, J. S. Hong, and S.-H. Lee. Self-adhesive epidermal carbon nanotube electronics for tether-free long-term continuous recording of biosignals. *Scientific Reports*, 4(1), Aug 2014.

[102] S. M. Lee, J. H. Kim, H. J. Byeon, Y. Y. Choi, K. S. Park, and S.-H. Lee. A capacitive, biocompatible and adhesive electrode for long-term and cap-free monitoring of EEG signals. *Journal of Neural Engineering*, 10(3):036006, Apr 2013.

[103] R. Leeb, F. Lee, C. Keinrath, R. Scherer, H. Bischof, and G. Pfurtscheller. Brain–computer communication: motivation, aim, and impact of exploring a virtual apartment. *IEEE Transactions on Neural Systems and Rehabilitation Engineering*, 15(4):473–482, Dec 2007.

[104] J. Legény, R. V. Abad, and A. Lécuyer. Navigating in virtual worlds using a self-paced SSVEP-based brain–computer interface with integrated stimulation and real-time feedback. *Presence: Teleoperators and Virtual Environments*, 20(6):529–544, Dec 2011.

[105] W. H. Leschey and B. Hall. Photic stimulation in sleep. *Clinical EEG and Neuroscience*, 8(3):125–134, Jul 1977.

[106] D. Lesenfants, D. Habbal, Z. Lugo, M. Lebeau, P. Horki, E. Amico, C. Pokorny, F. Gómez, A. Soddu, G. Müller-Putz, et al. An independent SSVEP-based brain–computer interface in locked-in syndrome. *Journal of Neural Engineering*, 11(3):035002, May 2014.

[107] L.-D. Liao, C.-Y. Chen, I.-J. Wang, S.-F. Chen, S.-Y. Li, B.-W. Chen, J.-Y. Chang, and C.-T. Lin. Gaming control using a wearable and wireless EEG-based brain-computer interface device with novel dry foam-based sensors. *Journal of NeuroEngineering and Rehabilitation*, 9(1):1, 2012.

[108] J.-H. Lim, H.-J. Hwang, C.-H. Han, K.-Y. Jung, and C.-H. Im. Classification of binary intentions for individuals with impaired oculomotor function:'eyes-closed' SSVEP-based braincomputer interface (BCI). *Journal of Neural Engineering*, 10(2):026021, Feb 2013.

[109] C.-T. Lin, Y.-C. Chen, T.-Y. Huang, T.-T. Chiu, L.-W. Ko, S.-F. Liang, H.-Y. Hsieh, S.-H. Hsu, and J.-R. Duann. Development of wireless brain computer interface with embedded multitask scheduling and its application on real-time driver's drowsiness detection and warning. *IEEE Transactions on Biomedical Engineering*, 55(5):1582–1591, 2008.

[110] C.-T. Lin, L.-D. Liao, Y.-H. Liu, I.-J. Wang, B.-S. Lin, and J.-Y. Chang. Novel dry polymer foam electrodes for long-term EEG measurement. *IEEE Transactions on Biomedical Engineering*, 58(5):1200–1207, May 2011.

[111] F.-C. Lin, J. K. Zao, K.-C. Tu, Y. Wang, Y.-P. Huang, C.-W. Chuang, H.-Y. Kuo, Y.-Y. Chien, C.-C. Chou, and T.-P. Jung. SNR analysis of high-frequency steady-state visual evoked potentials from the foveal and extrafoveal regions of human retina. In *2012 Annual International Conference of the IEEE Engineering in Medicine and Biology Society*, pages 1810–1814. Institute of Electrical & Electronics Engineers (IEEE), Aug 2012.

[112] Z. Lin, C. Zhang, W. Wu, and X. Gao. Frequency recognition based on canonical correlation analysis for SSVEP-based BCIs. *IEEE Transactions on Biomedical Engineering*, 54(6):1172–1176, Jun 2007.

[113] R. D. Linden, K. B. Campbell, G. Hamel, and T. W. Picton. Human auditory steady state evoked potentials during sleep. *Ear and Hearing*, 6(3):167–174, 1985.

[114] S. E. Lindley, J. Le Couteur, and N. L. Berthouze. Stirring up experience through movement in game play: effects on engagement and social behaviour. In *Proceedings of the SIGCHI Conference on Human Factors in Computing Systems*, pages 511–514. Association for Computing Machinery (ACM), 2008.

[115] D. Looney, P. Kidmose, C. Park, M. Ungstrup, M. L. Rank, K. Rosenkranz, and D. P. Mandic. The in-the-ear recording concept: user-centered and wearable brain monitoring. *IEEE Pulse*, 3(6):32–42, Nov 2012.

[116] M. A. Lopez-Gordo, D. Sanchez-Morillo, and F. P. Valle. Dry EEG electrodes. *Sensors*, 14(7):12847–12870, Jul 2014.

[117] F. Lotte. Brain-computer interfaces for 3D games: hype or hope? In *Proceedings of the 6th International Conference on Foundations of Digital Games - FDG '11*, pages 325–327. Association for Computing Machinery (ACM), 2011.

[118] S. J. Luck. *An introduction to the event-related potential technique*. MIT press, Cambridge, MA, 2014.

[119] Z. R. Lugo, M.-A. Bruno, O. Gosseries, A. Demertzi, L. Heine, M. Thonnard, V. Blandin, F. Pellas, and S. Laureys. Beyond the gaze: communicating in chronic locked-in syndrome. *Brain Injury*, 29(9):1056–1061, 2015.

[120] N. Luo, J. Ding, N. Zhao, B. H. Leung, and C. C. Poon. Mobile health: Design of flexible and stretchable electrophysiological sensors for wearable healthcare systems. In *2014 11th International Conference on Wearable and Implantable Body Sensor Networks*, pages 87–91. Institute of Electrical & Electronics Engineers (IEEE), Institute of Electrical & Electronics Engineers (IEEE), Jun 2014.

[121] R. Ma, N. Aghasadeghi, J. Jarzebowski, T. Bretl, and T. Coleman. A stochastic control approach to optimally designing hierarchical flash sets in P300 communication prostheses. *IEEE Transactions on Neural Systems and Rehabilitation Engineering*, 20(1):102–112, Jan 2012.

[122] J. N. Mak, Y. Arbel, J. W. Minett, L. M. McCane, B. Yuksel, D. Ryan, D. Thompson, L. Bianchi, and D. Erdogmus. Optimizing the P300-based brain–computer interface: current status, limitations and future directions. *Journal of Neural Engineering*, 8(2):025003, Mar 2011.

[123] S. Makeig, M. Westerfield, T.-P. Jung, S. Enghoff, J. Townsend, E. Courchesne, and T. J. Sejnowski. Dynamic brain sources of visual evoked responses. *Science*, 295(5555):690–694, Jan 2002.

[124] C. D. Manning and H. Schütze. *Foundations of statistical natural language processing*. MIT Press, 2002.

[125] N. Marlow, D. Wolke, M. A. Bracewell, and M. Samara. Neurologic and developmental disability at six years of age after extremely preterm birth. *New England Journal of Medicine*, 352(1):9–19, Jan 2005.

[126] M. Massimini, F. Ferrarelli, R. Huber, S. K. Esser, H. Singh, and G. Tononi. Breakdown of cortical effective connectivity during sleep. *Science*, 309(5744):2228–2232, Sep 2005.

[127] B. H. C. Matthews. A new electrical recording system for physiological work. *The Journal of Physiology*, 65(3):225–242, Jun 1928.

[128] D. J. McFarland, L. A. Miner, T. M. Vaughan, and J. R. Wolpaw. Mu and beta rhythm topographies during motor imagery and actual movements. *Brain Topography*, 12(3):177–186, 2000.

[129] R. McNaney, I. Poliakov, J. Vines, M. Balaam, P. Zhang, and P. Olivier. LApp: a speech loudness application for people with parkinson's on google glass. In *Proceedings of the 33rd Annual ACM Conference on Human Factors in Computing Systems - CHI '15*, pages

497–500, New York, NY, USA, 2015. Association for Computing Machinery (ACM).

[130] K. Meier-Ewert and R. J. Broughton. Photomyoclonic response of epileltic and non-epileptic subjects during wakefulness, sleep and arousal. *Electroencephalography and Clinical Neurophysiology*, 23(2):142–151, Aug 1967.

[131] A. C. MettingVanRijn, A. P. Kuiper, T. E. Dankers, and C. A. Grimbergen. Low-cost active electrode improves the resolution in biopotential recordings. In *Proceedings of 18th Annual International Conference of the IEEE Engineering in Medicine and Biology Society*, volume 1, pages 101–102. Institute of Electrical & Electronics Engineers (IEEE), 1996.

[132] S. Miano, R. Donfrancesco, O. Bruni, R. Ferri, S. Galiffa, J. Pagani, E. Montemitro, L. Kheirandish, D. Gozal, and V. M. Pia. NREM sleep instability is reduced in children with attention-deficit/hyperactivity disorder. *Sleep*, 29(6):797–803, 2006.

[133] D. Millett. Hans berger: From psychic energy to the EEG. *Perspectives in Biology and Medicine*, 44(4):522–542, 2001.

[134] S. Moratti, B. A. Clementz, Y. Gao, T. Ortiz, and A. Keil. Neural mechanisms of evoked oscillations: stability and interaction with transient events. *Human Brain Mapping*, 28(12):1318–1333, 2007.

[135] S. T. Morgan, J. C. Hansen, and S. A. Hillyard. Selective attention to stimulus location modulates the steady-state visual evoked potential. *Proceedings of the National Academy of Sciences*, 93(10):4770–4774, May 1996.

[136] M. J. Moseley, S. C. Bayliss, and A. R. Fielder. Light transmission through the human eyelid: in vivo measurement. *Ophthalmic and Physiological Optics*, 8(2):229–230, Apr 1988.

[137] A. R. Mota, L. Duarte, D. Rodrigues, A. C. Martins, A. V. Machado, F. Vaz, P. Fiedler, J. Haueisen, J. M. Nóbrega, and C. Fonseca. Development of a quasi-dry electrode for EEG recording. *Sensors and Actuators A: Physical*, 199:310–317, Sep 2013.

[138] M. M. M uller and S. Hillyard. Concurrent recording of steady-state and transient event-related potentials as indices of visual-spatial selective attention. *Clinical Neurophysiology*, 111(9):1544–1552, Sep 2000.

[139] M. M. M uller, W. Teder-S alej arvi, and S. A. Hillyard. The time course of cortical facilitation during cued shifts of spatial attention. *Nature Neuroscience*, 1(7):631–634, Nov 1998.

[140] G. R. Müller-Putz, R. Scherer, C. Brauneis, and G. Pfurtscheller. Steady-state visual evoked potential (SSVEP)-based communication: impact of harmonic frequency components. *Journal of Neural Engineering*, 2(4):123–130, Oct 2005.

[141] A. C. Myers, H. Huang, and Y. Zhu. Wearable silver nanowire dry electrodes for electrophysiological sensing. *RSC Advances*, 5(15):11627–11632, 2015.

[142] K. B. Ng, A. P. Bradley, and R. Cunnington. Stimulus specificity of a steady-state visual-evoked potential-based brain–computer interface. *Journal of Neural Engineering*, 9(3):036008, May 2012.

[143] E. Nguyen, T. Modak, E. Dias, Y. Yu, and L. Huang. Fitnamo: using bodydata to encourage exercise through google glass™. In *Proceedings of the extended abstracts of the 32nd annual ACM conference on Human factors in computing systems - CHI EA '14*, pages 239–244, New York, NY, USA, 2014. Association for Computing Machinery (ACM).

[144] J. Nielsen. Elsevier BV, 1993.

[145] A. M. Norcia, L. G. Appelbaum, J. M. Ales, B. R. Cottereau, and B. Rossion. The steady-state visual evoked potential in vision research: a review. *Journal of Vision*, 15(6):4–4, May 2015.

[146] J. J. S. Norton, D. S. Lee, J. W. Lee, W. Lee, O. Kwon, P. Won, S.-Y. Jung, H. Cheng, J.-W. Jeong, A. Akce, S. Umunna, I. Na, Y. H. Kwon, X.-Q. Wang, Z. Liu, U. Paik, Y. Huang, T. Bretl, W.-H. Yeo, and J. A. Rogers. Soft, curved electrode systems capable of integration on the auricle as a persistent brain–computer interface. *Proceedings of the National Academy of Sciences*, 112(13):3920–3925, 2015.

[147] J. J. S. Norton, S. Umunna, and T. Bretl. The elicitation of steady-state visual evoked potentials during sleep. *Psychophysiology*, 54(4):496–507, Jan 2017.

[148] A. Notbohm, J. Kurths, and C. S. Herrmann. Modification of brain oscillations via rhythmic light stimulation provides evidence for entrainment but not for superposition of event-related responses. *Frontiers in Human Neuroscience*, 10, feb 2016.

[149] T. Nykopp. Statistical modelling issues for the adaptive brain interface. 2001.

[150] M. Oehler, P. Neumann, M. Becker, G. Curio, and M. Schilling. Extraction of SSVEP signals of a capacitive EEG helmet for human machine interface. In *2008 30th Annual International Conference of the*

IEEE Engineering in Medicine and Biology Society, pages 4495–4498. Institute of Electrical & Electronics Engineers (IEEE), Aug 2008.

[151] R. Oostenveld and P. Praamstra. The five percent electrode system for high-resolution EEG and ERP measurements. *Clinical Neurophysiology*, 112(4):713–719, Apr 2001.

[152] I. Oruç, O. Krigolson, K. Dalrymple, L. S. Nagamatsu, T. C. Handy, and J. J. S. Barton. Bootstrap analysis of the single subject with event related potentials. *Cognitive Neuropsychology*, 28(5):322–337, Jul 2011.

[153] J. A. Padilla-Medina, F. León-Ordoñez, J. Prado-Olivarez, N. Vela-Aguirre, A. Ramírez-Agundis, and J. Díaz-Carmona. Assessment technique for acne treatments based on statistical parameters of skin thermal images. *Journal of Biomedical Optics*, 19(4):046019–046019, 2014.

[154] J. Pan, X. Gao, F. Duan, Z. Yan, and S. Gao. Enhancing the classification accuracy of steady-state visual evoked potential-based brain–computer interfaces using phase constrained canonical correlation analysis. *Journal of Neural Engineering*, 8(3):036027, May 2011.

[155] C. Pang, J. H. Koo, A. Nguyen, J. M. Caves, M.-G. Kim, A. Chortos, K. Kim, P. J. Wang, J. B.-H. Tok, and Z. Bao. Highly skin-conformal microhairy sensor for pulse signal amplification. *Advanced Materials*, 27(4):634–640, Oct 2015.

[156] M. A. Pastor, M. Valencia, J. Artieda, M. Alegre, and J. C. Masdeu. Topography of cortical activation differs for fundamental and harmonic frequencies of the steady-state visual-evoked responses. An EEG and PET $H_2{}^{15}O$ study. *Cerebral Cortex*, 17(8):1899–1905, Oct 2007.

[157] T. Penzel, J. W. Kantelhardt, L. Grote, J.-H. Peter, and A. Bunde. Comparison of detrended fluctuation analysis and spectral analysis for heart rate variability in sleep and sleep apnea. *IEEE Transactions on Biomedical Engineering*, 50(10):1143–1151, Oct 2003.

[158] W. M. Perlstein, M. A. Cole, M. Larson, K. Kelly, P. Seignourel, and A. Keil. Steady-state visual evoked potentials reveal frontally-mediated working memory activity in humans. *Neuroscience Letters*, 342(3):191–195, 2003.

[159] G. Prats-Boluda, Y. Ye-Lin, E. Garcia-Breijo, J. Ibanez, and J. Garcia-Casado. Active flexible concentric ring electrode for non-invasive surface bioelectrical recordings. *Measurement Science and Technology*, 23(12):125703, Nov 2012.

[160] R. Prueckl and C. Guger. A brain-computer interface based on steady state visual evoked potentials for controlling a robot. In J. Cabestany, F. Sandoval, A. Prieto, and J. M. Corchado, editors, *Bio-Inspired Systems: Computational and Ambient Intelligence*, volume 5517 of *Lecture Notes in Computer Science*, pages 690–697. Springer, 2009.

[161] M. Quek, D. Boland, J. Williamson, R. Murray-Smith, M. Tavella, S. Perdikis, M. Schreuder, and M. Tangermann. Simulating the feel of brain-computer interfaces for design, development and social interaction. In *Proceedings of the 2011 annual conference on Human factors in computing systems - CHI '11*, pages 25–28, New York, NY, USA, 2011. Association for Computing Machinery (ACM).

[162] A. Rechtschaffen and A. Kales. A manual of standardized terminology, techniques and scoring system for sleep stages of human subjects. 1968.

[163] D. Regan. An effect of stimulus colour on average steady-state potentials evoked in man. *Nature*, 210(5040):1056–1057, Jun 1966.

[164] D. Regan. Chromatic adaptation and steady-state evoked potentials. *Vision Research*, 8(2):149–158, Feb 1968.

[165] D. Regan. *Human brain electrophysiology: evoked potentials and evoked magnetic fields in science and medicine*. Appleton & Lange, Norwalk, CT, 1989.

[166] J. K. Rice, C. Rorden, J. S. Little, and L. C. Parra. Subject position affects EEG magnitudes. *NeuroImage*, 64:476–484, Jan 2013.

[167] J. Robinson, S. C. Bayliss, and A. R. Fielder. Transmission of light across the adult and neonatal eyelid in vivo. *Vision Research*, 31(10):1837–1840, 1991.

[168] E. A. Rodin, D. D. Daly, and R. G. Bickford. Effects of photic stimulation during sleep a study of normal subjects and epileptic patients. *Neurology*, 5(3):149–149, Mar 1955.

[169] P. Salvo, R. Raedt, E. Carrette, D. Schaubroeck, J. Vanfleteren, and L. Cardon. A 3d printed dry electrode for ECG/EEG recording. *Sensors and Actuators A: Physical*, 174:96–102, Feb 2012.

[170] S. Sato, F. E. Dreifuss, and J. K. Penry. Photic sensitivity of children with absence seizures in slow wave sleep. *Electroencephalography and Clinical Neurophysiology*, 39(5):479–489, Nov 1975.

[171] G. Schalk, D. McFarland, T. Hinterberger, N. Birbaumer, and J. Wolpaw. BCI2000: A general-purpose brain-computer interface (BCI) system. *IEEE Transactions on Biomedical Engineering*, 51(6):1034–1043, Jun 2004.

[172] A. Schlogl, J. Kronegg, J. Huggins, and S. Mason. 19 evaluation criteria for BCI research. *Toward brain-computer interfacing*, 2007.

[173] A. Searle and L. Kirkup. A direct comparison of wet, dry and insulating bioelectric recording electrodes. *Physiological Measurement*, 21(2):271–283, May 2000.

[174] E. W. Sellers and E. Donchin. A P300-based brain–computer interface: initial tests by ALS patients. *Clinical Neurophysiology*, 117(3):538–548, mar 2006.

[175] E. W. Sellers, D. B. Ryan, and C. K. Hauser. Noninvasive brain-computer interface enables communication after brainstem stroke. *Science Translational Medicine*, 6(257):257re7–257re7, Oct 2014.

[176] E. W. Sellers, T. M. Vaughan, and J. R. Wolpaw. A brain-computer interface for long-term independent home use. *Amyotrophic Lateral Sclerosis*, 11(5):449–455, Jun 2010.

[177] S. C. Seow. *Designing and engineering time: the psychology of time perception in software*. Addison-Wesley Professional, Dec 2008.

[178] M. Serrano, B. M. Ens, and P. P. Irani. Exploring the use of hand-to-face input for interacting with head-worn displays. In *Proceedings of the 32nd annual ACM conference on Human factors in computing systems - CHI '14*, pages 3181–3190, New York, NY, USA, 2014. Association for Computing Machinery (ACM).

[179] A. S. Shah, S. L. Bressler, K. H. Knuth, M. Ding, A. D. Mehta, I. Ulbert, and C. E. Schroeder. Neural dynamics and the fundamental mechanisms of event-related brain potentials. *Cerebral Cortex*, 14(5):476–483, Mar 2004.

[180] F. Sharbrough, G. E. Chatrian, R. P. Lesser, H. Lders, M. Nuwer, and T. W. Picton. American electroencephalographic society guidelines for standard electrode position nomenclature. *Journal of Clinical Neurophysiology*, 8(2):200–202, Apr 1991.

[181] O. Sharon and Y. Nir. Attenuated fast steady-state visual evoked potentials during human sleep. *Cerebral Cortex*, pages 1–15, 2017.

[182] A. Shepherd, K. Saunders, and D. McCulloch. Effect of sleep state on the flash visual evoked potential. *Documenta Ophthalmologica*, 98(3):247–256, 1999.

[183] R. Sitaram, R. Veit, B. Stevens, A. Caria, C. Gerloff, N. Birbaumer, and F. Hummel. Acquired control of ventral premotor cortex activity by feedback training an exploratory real-time fMRI and TMS study. *Neurorehabilitation and Neural Repair*, 26(3):256–265, Sep 2012.

[184] W. Skrandies. The effect of stimulation frequency and retinal stimulus location on visual evoked potential topography. *Brain Topography*, 20(1):15–20, Apr 2007.

[185] S. J. M. Smith. EEG in the diagnosis, classification, and management of patients with epilepsy. *Journal of Neurology, Neurosurgery & Psychiatry*, 76(suppl 2):ii2–ii7, Jun 2005.

[186] A. C. N. Society et al. Guideline 9a: guidelines on evoked potentials. *American Journal of Electroneurodiagnostic Technology*, 23(2):125–137, Apr 2006.

[187] M. M. Spafford and S. L. Lu. Retinal adaptation effects on the patterned VEP and ERG. *Optometry & Vision Science*, 66(8):507–514, Aug 1989.

[188] W. Speier, C. Arnold, and N. Pouratian. Integrating language models into classifiers for BCI communication: a review. *Journal of Neural Engineering*, 13(3):031002, May 2016.

[189] P. Tallgren, S. Vanhatalo, K. Kaila, and J. Voipio. Evaluation of commercially available electrodes and gels for recording of slow EEG potentials. *Clinical Neurophysiology*, 116(4):799–806, Apr 2005.

[190] K. Tanaka, M. Iwata, K. Kunze, and K. Kise. Memory specs: An annotation system on google glass using document image retrieval. In *Proceedings of the 2014 ACM International Joint Conference on Pervasive and Ubiquitous Computing Adjunct Publication - UbiComp '14 Adjunct*, pages 267–270, New York, NY, USA, 2014. Association for Computing Machinery (ACM).

[191] T. Toyama, D. Sonntag, A. Dengel, T. Matsuda, M. Iwamura, and K. Kise. A mixed reality head-mounted text translation system using eye gaze input. In *Proceedings of the 19th international conference on Intelligent User Interfaces - IUI '14*, pages 329–334, New York, NY, USA, 2014. Association for Computing Machinery (ACM).

[192] L. J. Trejo, R. Rosipal, and B. Matthews. Brain-computer interfaces for 1–D and 2–D cursor control: Designs using volitional control of the EEG spectrum or steady-state visual evoked potentials. *IEEE Transactions on Neural Systems and Rehabilitation Engineering*, 14(2):225–229, Jun 2006.

[193] B. van de Laar, H. Gürkök, D. P.-O. Bos, F. Nijboer, and A. Nijholt. Perspectives on user experience evaluation of brain-computer interfaces. In *Universal Access in Human-Computer Interaction. Users Diversity*, pages 600–609. Springer Science, 2011.

[194] F.-B. Vialatte, M. Maurice, J. Dauwels, and A. Cichocki. Steady-state visually evoked potentials: focus on essential paradigms and future perspectives. *Progress in Neurobiology*, 90(4):418–438, Apr 2010.

[195] J. Vidal. Toward direct brain-computer communication. *Annual Review of Biophysics and Bioengineering*, 2(1):157–180, Jun 1973.

[196] A. Vilic, T. W. Kjaer, C. E. Thomsen, S. Puthusserypady, and H. B. D. Sorensen. DTU BCI speller: an SSVEP–based spelling system with dictionary support. In *Engineering in Medicine and Biology Society (EMBS) Annual Conference*, pages 2212–2215. Institute of Electrical & Electronics Engineers (IEEE), Jul 2013.

[197] I. Volosyak. SSVEP-based bremen–BCI interface—boosting information transfer rates. *Journal of Neural Engineering*, 8(3):036020, May 2011.

[198] I. Volosyak, H. Cecotti, D. Valbuena, and A. Graser. Evaluation of the bremen SSVEP based BCI in real world conditions. In *2009 IEEE International Conference on Rehabilitation Robotics*, pages 322–331. Institute of Electrical & Electronics Engineers (IEEE), Institute of Electrical & Electronics Engineers (IEEE), 2009.

[199] I. Volosyak, F. Gembler, and P. Stawicki. Age-related differences in SSVEP-based BCI performance. *Neurocomputing*, 250:57–64, aug 2017.

[200] I. Volosyak, A. Moor, and A. Gräser. A dictionary-driven SSVEP speller with a modified graphical user interface. volume 6691, pages 353–361. Springer, 2011.

[201] I. Volosyak, D. Valbuena, T. Lüth, T. Malechka, and A. Gräser. BCI demographics II: how many (and what kinds of) people can use a high-frequency SSVEP BCI? *IEEE Transactions on Neural Systems and Rehabilitation Engineering*, 19(3):232–239, Jun 2011.

[202] G. Voskerician, M. S. Shive, R. S. Shawgo, H. Von Recum, J. M. Anderson, M. J. Cima, and R. Langer. Biocompatibility and biofouling of MEMS drug delivery devices. *Biomaterials*, 24(11):1959–1967, May 2003.

[203] E. Walker and A. S. Nowacki. Understanding equivalence and noninferiority testing. *Journal of General Internal Medicine*, 26(2):192–196, 2011.

[204] L.-F. Wang, J.-Q. Liu, X.-X. Yan, B. Yang, and C.-S. Yang. A MEMS-based pyramid micro-needle electrode for long-term EEG measurement. *Microsystem Technologies*, 19(2):269–276, Aug 2013.

[205] L.-F. Wang, J.-Q. Liu, B. Yang, and C.-S. Yang. PDMS-based low cost flexible dry electrode for long-term EEG measurement. *IEEE Sensors Journal*, 12(9):2898–2904, 2012.

[206] Y.-T. Wang, Y. Wang, C.-K. Cheng, and T.-P. Jung. Measuring steady-state visual evoked potentials from non-hair-bearing areas. In *2012 Annual International Conference of the IEEE Engineering in Medicine and Biology Society*, pages 1806–1809. Institute of Electrical & Electronics Engineers (IEEE), Aug 2012.

[207] D. Ward, A. Blackwell, and D. MacKay. Dasher: A gesture-driven data entry interface for mobile computing. *Human-Computer Interaction*, 17(2):199–228, sep 2002.

[208] J. Williamson, R. Murray-Smith, B. Blankertz, M. Krauledat, and K.-R. Müller. Designing for uncertain, asymmetric control: Interaction design for brain–computer interfaces. *International Journal of Human-Computer Studies*, 67(10):827–841, Oct 2009.

[209] J. Wolpaw and E. W. Wolpaw. *Brain–computer interfaces: principles and practice*. Oxford University Press (OUP), Jan 2012.

[210] J. R. Wolpaw, N. Birbaumer, D. J. McFarland, G. Pfurtscheller, and T. M. Vaughan. Brain–computer interfaces for communication and control. *Clinical Neurophysiology*, 113(6):767–791, Jun 2002.

[211] J. R. Wolpaw, H. Ramoser, D. J. McFarland, and G. Pfurtscheller. EEG-based communication: improved accuracy by response verification. *IEEE Transactions on Rehabilitation Engineering*, 6(3):326–333, 1998.

[212] Z. Wu. The difference of SSVEP resulted by different pulse duty-cycle. In *2009 International Conference on Communications, Circuits and Systems (ICCCAS)*, pages 605–607. Institute of Electrical & Electronics Engineers (IEEE), Jul 2009.

[213] Z. Wu, Y. Lai, Y. Xia, D. Wu, and D. Yao. Stimulator selection in SSVEP-based BCI. *Medical Engineering & Physics*, 30(8):1079–1088, Oct 2008.

[214] J. Yamamoto, E. Furuya, H. Wakamatsu, and Y. Hishikawa. Modification of photosensitivity in epileptics during sleep. *Electroencephalography and Clinical Neurophysiology*, 31(5):509–513, Nov 1971.

[215] T. Yanagisawa, M. Hirata, Y. Saitoh, T. Goto, H. Kishima, R. Fukuma, H. Yokoi, Y. Kamitani, and T. Yoshimine. Real-time control of a prosthetic hand using human electrocorticography signals: technical note. *Journal of Neurosurgery*, 114(6):1715–1722, Jun 2011.

[216] W.-H. Yeo, Y.-S. Kim, J. Lee, A. Ameen, L. Shi, M. Li, S. Wang, R. Ma, S. H. Jin, Z. Kang, Y. Huang, and J. A. Rogers. Multifunctional epidermal electronics printed directly onto the skin. *Advanced Materials*, 25(20):2773–2778, 2013.

[217] P. Yuan, X. Gao, B. Allison, Y. Wang, G. Bin, and S. Gao. A study of the existing problems of estimating the information transfer rate in online brain–computer interfaces. *Journal of Neural Engineering*, 10(2):026014, Apr 2013.

[218] Y. Zhang, G. Zhou, J. Jin, X. Wang, and A. Cichocki. Frequency recognition in SSVEP-based BCI using multiset canonical correlation analysis. *International Journal of Neural Systems*, 24(04):1450013, Jun 2014.

[219] Y. Zhang, G. Zhou, Q. Zhao, A. Onishi, J. Jin, X. Wang, and A. Cichocki. Multiway canonical correlation analysis for frequency components recognition in SSVEP-based BCIs. In *International Conference on Neural Information Processing*, pages 287–295. Springer, 2011.

[220] D. Zhu, J. Bieger, G. G. Molina, and R. M. Aarts. A survey of stimulation methods used in SSVEP-based BCIs. *Computational Intelligence and Neuroscience*, 2010:1–12, 2010.